MIT

ATMOSPHERIC WATER VAPOR TRANSPORT: ESTIMATION OF CONTINENTAL PRECIPITATION RECYCLING AND PARAMETERIZATION OF A SIMPLE CLIMATE MODEL

by
KAYE L. BRUBAKER
DARA ENTEKHABI
and
PETER S. EAGLESON

DEPARTMENT
OF
CIVIL
ENGINEERING

RALPH M. PARSONS LABORATORY
HYDROLOGY AND WATER RESOURCE SYSTEMS

SCHOOL OF ENGINEERING
MASSACHUSETTS INSTITUTE OF TECHNOLOGY
Cambridge, Massachusetts 02139

Report Number 333

The Ralph M. Parsons Laboratory Technical Report Series
is supported in part by a grant from the Ralph M. Parsons Foundation

July, 1991

R91-18

ATMOSPHERIC WATER VAPOR TRANSPORT: ESTIMATION OF CONTINENTAL PRECIPITATION RECYCLING AND PARAMETERIZATION OF A SIMPLE CLIMATE MODEL

by

Kaye L. Brubaker
Dara Entekhabi
and
Peter S. Eagleson

RALPH M. PARSONS LABORATORY

HYDROLOGY AND WATER RESOURCE SYSTEMS

Report Number 333

Prepared under the support of a
National Science Foundation Graduate Fellowship
and the
National Aeronautics and Space Administration
Grant No. NAG 5-743

The Ralph M. Parsons Laboratory Technical Report Series
is supported in part by a grant from the Ralph M. Parsons Foundation

JULY 1991

Abstract

The advective transport of atmospheric water vapor and its role in global hydrology and the water balance of continental regions are discussed and explored. The data set consists of ten years of global wind and humidity observations interpolated onto a regular grid by objective analysis. Atmospheric water vapor fluxes across the boundaries of selected continental regions are displayed graphically.

The water vapor flux data are used to investigate the sources of continental precipitation.

The total amount of water that precipitates on large continental regions is supplied by two mechanisms: (1) advection from surrounding areas external to the region and (2) evaporation and transpiration from the land surface within the region. The latter supply mechanism is tantamount to the recycling of precipitation over the continental area. The degree to which regional precipitation is supplied by recycled moisture is a potentially significant climate feedback mechanism and land surface–atmosphere interaction, which may contribute to the persistence and intensification of droughts. A simplified model of the atmospheric moisture over continents and simultaneous estimates of regional precipitation are employed to estimate, for several large continental regions, the fraction of precipitation that is locally derived.

In a separate, but related, study estimates of ocean–to–land water vapor transport are used to parameterize an existing simple climate model, containing both land and ocean surfaces, that is intended to mimic the dynamics of continental climates.

Acknowledgments

This report is based upon work supported by a National Science Foundation Graduate Fellowship. Any opinions, findings, conclusions or recommendations expressed herein are those of the authors and do not necessarily reflect the views of the National Science Foundation. Additional support was provided by the National Aeronautics and Space Administration under Grant NAG 5–743. The work was performed by Kaye L. Brubaker and as presented here fulfills the thesis requirement for the degree of Master of Science in Civil Engineering at MIT. The work was supervised by Dr. Peter S. Eagleson, Edmund K. Turner Professor of Civil Engineering; and Dr. Dara Entekhabi, Visiting Assistant Professor, Department of Civil Engineering, at MIT.

The authors thank Dr. Abraham Oort of the National Oceanic and Atmospheric Administration Geophysical Fluid Dynamics Laboratory for providing the analyzed wind and humidity data.

TABLE OF CONTENTS

FIGURES

Figure 1.1: The horizontal divergence of the vertically–integrated water vapor flux, calculated from the original GFDL analysis. Units: 10 cm yr^{-1}. [Source: Peixoto and Oort (1983)]

Figure 1.2: The vertical integral of moisture flux divergence calculated from the modified GFDL data. Units: W m^{-2}. [Source: Savijärvi (1988)]

Figure 1.3: Map for each grid point of the lowest level used in vertical integration. A value of 1 indicates that the Earth's surface lies between 1000 and 950 mb, a value of 2 between 950 and 900 mb, a value of 3 between 900 and 850 mb, a value of 4 between 850 and 700 mb, and a value of 5 between 700 and 500 mb. [Source: Oort (1983)]

Figure 1.4: Continental regions selected for graphical analysis of the boundary flux of water vapor. The small crosses indicate the nodes of the GFDL data grid (5° longitude and 2.5° latitude).

Figure 1.5: A simple example illustrating the meaning of the bars in Figures 1.6 through 1.17. For constant $\vec{Q}$, the magnitude of f_k depends upon the normal component of $\vec{Q}$ and the length of the segment. The right–hand side shows how these results would appear in Figures such as 1.6 through 1.17.

Figure 1.6: The total moisture flux (mean motion plus transient eddies) across segments of horizontal regional boundaries, for North and South America. Values shown are the average of monthly average values for December, January and February, 1963–73.

Figure 1.7: The total moisture flux (mean motion plus transient eddies) across segments of horizontal regional boundaries, for North and South America. Values shown are the average of monthly average values for March, April and May, 1963–73.

Figure 1.8: The total moisture flux (mean motion plus transient eddies) across segments of horizontal regional boundaries, for North and South America. Values shown are the average of monthly average values for June, July and August, 1963–73.

Figure 1.9: The total moisture flux (mean motion plus transient eddies) across segments of horizontal regional boundaries, for North and South America. Values shown are the average of monthly average values for September, October and November, 1963–73.

Figure 1.10: The moisture flux by transient eddies across segments of horizontal regional boundaries, for North and South America. Values shown are the average of monthly average values for December, January and February, 1963–73.

Figure 2.5: Regions selected for precipitation recycling analysis. The analysis technique dictated a rectangular shape; otherwise, the regions were chosen on the basis of hydrological and historical interest.

Figure 2.6: Eurasian Region. The ratio of locally–evaporated to total precipitation, as estimated by the Modified 1–D and the 2–D method.

Figure 2.7: Eurasian Region. Terms used in estimating P_m/P by two methods. Atmospheric moisture convergence ($-\nabla\cdot\vec{Q}$), Precipitation (P) and Evaporation (E) are common to both methods; wu_{eff}/ℓ_{eff} is used in the Modified 1–D method, F^+/A in the 2–D method.

Figure 2.8: Eurasian Region. Bar graphs of the moisture flux across segments of the boundary. Each bar represents the integral of the normal component of $\vec{Q}$ along the segment at the base of the bar.

Figure 2.9: North American Region. The ratio of locally–evaporated to total precipitation, as estimated by the Modified 1–D and the 2–D method.

Figure 2.10: North American Region. Terms used in estimating P_m/P by two methods. Atmospheric moisture convergence ($-\nabla\cdot\vec{Q}$), Precipitation (P) and Evaporation (E) are common to both methods; wu_{eff}/ℓ_{eff} is used in the Modified 1–D method, F^+/A in the 2–D method.

Figure 2.11: North American Region. Bar graphs of the moisture flux across segments of the boundary. Each bar represents the integral of the normal component of $\vec{Q}$ along the segment at the base of the bar.

Figure 2.12: South American Region. The ratio of locally–evaporated to total precipitation, as estimated by the Modified 1–D and the 2–D method.

Figure 2.13: South American Region. Terms used in estimating P_m/P by two methods. Atmospheric moisture convergence ($-\nabla\cdot\vec{Q}$), Precipitation (P) and Evaporation (E) are common to both methods; wu_{eff}/ℓ_{eff} is used in the Modified 1–D method, F^+/A in the 2–D method.

Figure 2.14: South American Region. Bar graphs of the moisture flux across segments of the boundary. Each bar represents the integral of the normal component of $\vec{Q}$ along the segment at the base of the bar.

Figure 2.15: African Region. The ratio of locally–evaporated to total precipitation, as estimated by the Modified 1–D and the 2–D method.

Figure 2.16: African Region. Terms used in estimating P_m/P by two methods. Atmospheric moisture convergence ($-\nabla\cdot\vec{Q}$), Precipitation (P) and Evaporation (E) are common to both methods; wu_{eff}/ℓ_{eff} is used in the Modified 1–D method, F^+/A in the 2–D method.

Figure 2.17: African Region. Bar graphs of the moisture flux across segments of the boundary. Each bar represents the integral of the normal component of $\vec{Q}$ along the segment at the base of the bar.

Figure 2.18: a) Plan view of a region with convergent moisture flux, and with constant $\|\vec{Q}\|$ along the inflow boundaries. By symmetry, the average direction of moisture flux ($\hat{u}$) is due eastward.

b) The difference between the total boundary integral of influx (F^+) and the integral of boundary influx resolved parallel to $\hat{u}$ $[(wu)_{eff}\ \Delta y)]$.

Figure 3.1 Streamlines of the total aerial runoff, $\vec{Q}$; each barb represents 2 g kg^{-1} m s^{-1}: b, DJF; g, JJA; c, year. [Source: Peixóto and Oort, 1983]

Figure 3.2: The continent and ocean regions used to estimate the transport parameter, $\hat{\chi}$, from observations: Experiment 1.

Figure 3.3: The continent and ocean regions used to estimate the transport parameter, $\hat{\chi}$, from observations: Experiment 2.

Figure 3.4: χ and $-\nabla\cdot\vec{Q}$ for six different runs of the screening model. For each run, all other model parameters were held fixed while χ was varied; the model was integrated over 250 days for each ($-\nabla\cdot\vec{Q}$, χ) pair.

Figure 3.5: Estimates of $\hat{\chi}$ and $-\nabla\cdot\vec{Q}$ from the observational data for each of twelve months. The observations that do not satisfy model assumptions are labeled by month.

TABLES

Chapter 1

Atmospheric Water Vapor Transport

1.1 Introduction

Water vapor is a variable constituent of the atmosphere; it accounts for 0 to 4 percent by volume of tropospheric air. The saturation vapor pressure decreases with temperature; therefore the vapor content of the atmosphere decreases with height, with the result that atmospheric water vapor is concentrated in the lower troposphere and is negligible above the tropopause. The atmosphere contains about 12×10^3 km^3 equivalent of liquid water, enough to cover the Earth's surface to a depth of about 2.4 cm (assuming a smooth, spherical Earth). The average residence time of a water molecule in the atmospheric reservoir is on the order of ten days.

Water vapor is transported in the atmosphere by molecular and turbulent diffusion, convection, and advection. The vertical flux of evaporation from the oceans and the land surface into the atmosphere is accomplished by diffusion, and the vapor is vertically mixed by diffusion and convection. On the temporal and spatial scales of lateral transport, advection is the dominant mechanism. On these scales, water vapor can be treated as a scalar admixture advected by the horizontal wind.

The atmospheric water vapor transport vector has been an object of study, on both the global and the regional scale, since the availability (following World War II) of the aerological data required for vapor flux computations. Benton and Estoque (1954) used the vapor flux vector divergence field in computations of evapotranspiration over the North American continent for the calendar year 1949. In his 1956 Presidential Address to the

Royal Meteorological Society, Sutcliffe called for increased scientific inquiry into the problem of water balance and the general circulation of the atmosphere, and recommended wider application of the techniques introduced by Benton and Estoque. Starr and Peixoto (1958) found centers of divergence of atmospheric water vapor flux over many of the world's deserts, and inferred from mass balance considerations the existence of net subsurface inflow to these regions. Lufkin (1959) made the first estimate of water vapor transport from the oceans to the continents as a function of latitude. Hastenrath (1966) analyzed water vapor flux over the Central American seas as part of a more comprehensive study concerned with the general circulation and energetics in that area. Rasmusson (1967, 1968) investigated water vapor flux over North America and the Central American Sea as part of a continental water–balance study; this work was followed by a regional study of the hydrology of eastern North America (Rasmusson, 1971). Rasmusson (1977) recommended the application of vapor flux data in the routine computation of regional water balances over areas large enough to control the relative error of the resulting flux divergence estimates (he recommends 10^6 km^2 or more). He also provided guidelines for operational vapor flux computations within the context of the World Weather Watch. Peixoto and Oort (1983) used the divergence field to study connections between the atmospheric and surface branches of the hydrologic cycle. Chen (1985) analyzed water vapor transport and maintenance during the solstice seasons to explore how the high water vapor content of certain tropical areas is maintained by the large scale atmospheric circulation.

This thesis explores the role of the advective transport of atmospheric water vapor in two different aspects of global hydrology and the water balance of continental regions. This Chapter introduces some definitions and concepts

that are common to both investigations, and describes the observational data used in this study. Chapter Two addresses the question of the sources of precipitation water in selected land regions. Some of the water vapor that condenses into precipitation over a region is derived from vapor advected from the surrounding areas external to the region itself. The remainder is derived from surface evaporation within the region. The latter source is governed by regional surface hydrologic processes and it constitutes an important mechanism for land surface–atmosphere interaction. In Chapter Three, the aerological data are used to assess the validity of a parameterization for moisture advection in a spatially–averaged climate model. The simplified climate model represents the atmospheric branch of the hydrologic cycle over a land surface and an ocean region as exchange between two lumped reservoirs. The analysis in Chapter Three compares the parameter characterizing this exchange in the model with those derived from the aerological data.

1.2 Basic Concepts

The Vertically–Integrated Vapor Flux Vector

The atmosphere's specific humidity and the zonal and meridional components of the wind are variable in both space and time. In the geophysical coordinate system, the four–dimensional domain of these variables is defined by ϕ (latitude), λ (longitude), p (pressure), and t (time). Following Peixoto (1973) and Peixoto and Oort (1983), the dimensionality of the domain is reduced to two by defining a vertically–integrated, time–averaged vapor flux vector.

At a given point in space and time, a vector field of the advective transport of water vapor by the horizontal wind is defined:

$$q\vec{V}(\lambda,\phi,p,t) = (qu)\hat{i} + (qv)\hat{j} \qquad (1.1)$$

in which q is the specific humidity [g H_2O vapor per kg air]; $\vec{V}$ is the horizontal wind vector [m s^{-1}]; u is the zonal wind component (positive eastward); v is the meridional wind component (positive northward); and $\hat{i}$ and $\hat{j}$ are the unit vectors in the zonal and meridional directions, respectively. The horizontal transport vector $q\vec{V}$ has units g kg^{-1} m s^{-1}. As a product of terms, $q\vec{V}$ increases with either velocity or specific humidity; for example, slow–moving moist air may transport water vapor at the same rate as less moist but fast–moving air.

For a vertical atmospheric column with a unit base, the vertically–integrated horizontal vapor flux, $\vec{Q}$, is obtained by taking the mass–weighted vertical integral of (1.1):

$$\vec{Q}(\lambda,\phi,t) = \int_0^{p_0} q\vec{V}\,\frac{dp}{g} = Q_\lambda\hat{i} + Q_\phi\hat{j} \qquad (1.2)$$

in which p_0 is the surface pressure; g is the acceleration of gravity; and Q_λ and Q_ϕ are, respectively, the zonal (positive eastward) and meridional (positive northward) components of $\vec{Q}$. The vapor flux vector $\vec{Q}$ has units g s^{-1} m^{-1}. As a vertically–integrated quantity, $\vec{Q}$ expresses the magnitude and direction of the *net* transport of water vapor through the depth of the atmosphere above a point on the earth's surface; a small value of either component does not necessarily imply negligible transport at all levels in the atmosphere.

Equation (1.2) may be averaged over a time period τ to compute the

corresponding mean values $\overline{Q}_\lambda$ and $\overline{Q}_\phi$, where the overbar denotes the time–average operator:

$$\overline{Q}_\lambda(\lambda,\phi) \equiv \frac{1}{\tau}\int_0^\tau Q_\lambda(\lambda,\phi,t)\ dt \tag{1.3a}$$

and

$$\overline{Q}_\phi(\lambda,\phi) \equiv \frac{1}{\tau}\int_0^\tau Q_\phi(\lambda,\phi,t)\ dt\ . \tag{1.3b}$$

The time–averaged, vertically–integrated moisture flux vector $\overline{\vec{Q}}$ has units g s^{-1} m^{-1}; it is a function of two horizontal space variables, latitude and longitude.

The Role of $\vec{Q}$ in the Basic Equations of Hydrology

The mass conservation equation for water vapor in the atmosphere may be expressed as

$$\frac{\partial W}{\partial t} + \nabla\cdot\vec{Q} = E - P \tag{1.4}$$

in which W is the water vapor storage within the atmospheric column; E is the rate of evapotranspiration into the base of the column; P is the rate of precipitation from the column, also measured at the surface; and $\nabla\cdot\vec{Q}$ is the divergence of the lateral vapor flux, with $\vec{Q}$ as defined above. W, also known as the precipitable water in the column, may be expressed as either water vapor mass per unit surface area [kg m^{-2}] or equivalent depth of liquid water [m]. The use of the latter unit is more common in hydrologic practice; correspondingly, P, E, and $\nabla\cdot\vec{Q}$ have units m s^{-1}.

For an atmospheric control volume, bounded by a conceptual closed vertical wall and overlying a region of the Earth's surface having area A, (1.4) takes the form

$$\langle \frac{\partial W}{\partial t} \rangle + \langle \nabla \cdot \vec{Q} \rangle = \langle E - P \rangle \tag{1.5}$$

where the angled brackets denote a space average:

$$\langle h \rangle \equiv \frac{\iint h(x)\ dA}{\iint dA} = \frac{\iint h(x)\ dA}{A} \tag{1.6}$$

in which h(x) is any function of location. Applying Green's theorem allows (1.5) to be written

$$\langle \frac{\partial W}{\partial t} \rangle = \langle E - P \rangle - \frac{1}{A} \oint \vec{Q} \cdot \hat{n}_\gamma \, d\gamma \tag{1.7}$$

in which $\hat{n}_\gamma$ is the outward unit vector normal to the horizontal boundary (γ) of the region. Equation (1.7) states that the time rate of change in water vapor storage within the atmospheric volume is equal to evapotranspiration minus precipitation less the net lateral outflow through the vertical boundaries of the control volume.

Equations (1.5) and (1.7) express the mass balance of water in the atmospheric branch of the hydrological cycle. An excess of evapotranspiration over precipitation is balanced by the change in water content of the atmosphere and the net aerial runoff across the boundaries of the region. A region in which the mean divergence of $\vec{Q}$, $\langle \nabla \cdot \vec{Q} \rangle$, is positive is a source of water vapor to the rest of the atmosphere, while a region with negative $\langle \nabla \cdot \vec{Q} \rangle$, a region of convergence, is a sink of atmospheric water vapor.

The mean net transport of water *into* a region by horizontal atmospheric motion is equal to $-\langle \nabla \cdot \vec{Q} \rangle$ and the total transport into the region is the closed path integral $-\oint \vec{Q} \cdot \hat{n}_\gamma \, d\gamma$, with the normal to the boundary defined outward as in (1.7). In analyzing and modeling the atmospheric water balance, the

expression "divQ" (omitting the negative sign) is frequently used in reference to either of these quantities.

In the land surface branch of the hydrologic cycle, the mass balance can be written in the simplified form,

$$\langle \frac{\partial S}{\partial t} \rangle = \langle P - E \rangle + \langle R_{in} - R_{out} \rangle \qquad (1.8)$$

in which S is the mass of water stored in the surface and subsurface reservoirs of the region; R_{in} is the rate of water influx across the horizontal boundaries of the region by surface and subsurface lateral transport; and R_{out} is the rate of water efflux by these lateral processes. If the region's boundaries are surface drainage divides, and if the subsurface drainage corresponds to that on the surface, then $\langle R_{in} \rangle = 0$ and the term $\langle R_{in} - R_{out} \rangle$ is simply the rate of runoff per unit area; such a simplification is also the case when the study region is an entire continent. For smaller land regions that are not delineated along natural drainage divides, surface and subsurface lateral transport into a region may be significant.

Equation (1.8) may be rearranged as follows:

$$\langle P - E \rangle = - \langle E - P \rangle = \langle R_{out} - R_{in} \rangle + \langle \frac{\partial S}{\partial t} \rangle \qquad (1.9)$$

which states that an excess of precipitation over evapotranspiration is balanced by net surface and subsurface runoff and/or increased terrestrial storage in the region.

The term $\langle E - P \rangle$ is common to (1.7) and (1.9) and thus provides the link between the terrestrial and atmospheric branches of the hydrologic cycle:

$$\langle R_{out} - R_{in} \rangle + \langle \frac{\partial S}{\partial t} \rangle = - \langle \nabla \cdot \vec{Q} \rangle - \langle \frac{\partial W}{\partial t} \rangle \ . \qquad (1.10)$$

Therefore, if the aerological data are known, as well as runoff and precipitation, (1.10) and (1.7) may be used to estimate the average rate of change of groundwater storage and the average evaporation rate, two quantities that are difficult to measure. The accuracy of such an estimate is highly sensitive to the quality of the measurements. Typically, $\frac{\partial s}{\partial t}$ and $\frac{\partial w}{\partial t}$ are smaller than the other terms by at least one order of magnitude, and the smaller quantity is estimated from a difference of larger numbers. Accuracy is improved by enlarging the path of the boundary integral (1.7) which leads to the recommendation of Rasmusson (1977) that the region should have an area of at least 10^6 km^2

Modes of Transport

Any atmospheric variable, f, may be expressed in terms of a time mean and a perturbation from that mean:

$$f(\lambda,\phi,p,t) = \bar{f}(\lambda,\phi,p) + f'(\lambda,\phi,p,t) \tag{1.11}$$

in which the overbar denotes the mean value over a specified time interval. By definition, the mean value of the perturbations is zero ($f' \equiv 0$).

For example, expressing the zonal component of the horizontal wind and the specific humidity in this manner, the time mean of the zonal component of the horizontal vapor transport vector, $q\vec{V}$, contains cross–product terms:

$$\begin{aligned} \overline{qu}(\lambda,\phi,p) &= \overline{(\bar{q} + q')(\bar{u} + u')} \\ &= \overline{\bar{q}\,\bar{u}} + \overline{\bar{q}\,u'} + \overline{q'\bar{u}} + \overline{q'u'} \ . \end{aligned} \tag{1.12}$$

Because $\bar{q}$ and $\bar{u}$ are constants, and $\overline{u'}$ and $\overline{q'}$ vanish by definition,

$$\overline{qu} = \bar{q}\,\bar{u} + \overline{q'u'} \ . \tag{1.13}$$

The first term on the right–hand side of (1.13) represents the advection of mean specific humidity by mean zonal atmospheric motion. The second term is a correlation term; for example, $\overline{q'u'}$ is positive for a given location if winds that are more westerly (or less easterly) than the mean wind (positive u') are moister than average (positive q'), negative if winds that are more easterly (or less westerly) than the mean wind (negative u') tend to be moister than average, and zero if no correlation exists between the zonal wind and the specific humidity. Likewise, for the meridional component of vapor transport,

$$\overline{qv}(\lambda,\phi,p) = \bar{q}\,\bar{v} + \overline{q'v'} \ . \tag{1.14}$$

By convention, the terms on the right–hand sides of (1.13) and (1.14) are called, respectively, transport by *mean motion* and by *transient eddies.* The distinction between mean and eddy transport depends upon the averaging period.

The time–averaged vertically–integrated water vapor flux vector, $\vec{\bar{Q}}$, contains a mean and a transient eddy term in each of its components, i.e.,

$$\bar{Q}_\lambda \equiv \int_0^{p_s} \overline{qu}\ \frac{dp}{g} = \int_0^{p_s} \bar{q}\,\bar{u}\,\frac{dp}{g} + \int_0^{p_s} \overline{q'u'}\,\frac{dp}{g} \tag{1.15a}$$

and

$$\bar{Q}_\phi \equiv \int_0^{p_s} \overline{qv}\ \frac{dp}{g} = \int_0^{p_s} \bar{q}\,\bar{v}\ \frac{dp}{g} + \int_0^{p_s} \overline{q'v'}\,\frac{dp}{g} \ . \tag{1.15b}$$

Globally, the zonal component of $\overline{\vec{Q}}$ tends to exceed the meridional component by an order of magnitude. The mean motion dominates in Q_λ, whereas in Q_ϕ, the mean and transient eddy terms are of comparable magnitude. Transient eddy transport is particularly important at mid–latitudes and during the active winter season, where the eddies play a critical role in the poleward transport of sensible, as well as latent, heat (Peixoto and Oort, 1983).

A similar decomposition can be performed in the spatial dimension by averaging with respect to longitude around a belt of constant latitude. The resulting *zonal mean* and *standing eddy* terms are of great interest and value in studies of vapor transport over the globe as a whole. The present study focuses on the water balances of continental regions on a spatial scale that is too small to justify such spatial decomposition. However, the distinction between the time mean and transient eddy modes of transport will figure in the computation of $\overline{\vec{Q}}$ and the analysis of vapor flux into and out of regions.

1.3 Observational Data and Computational Method

Aerological Data

The humidity and wind data used in this study are from a data set provided by the Geophysical Fluid Dynamics Laboratory (GFDL) of NOAA at Princeton University through the courtesy of Dr. Abraham Oort. The GFDL data set consists of ten years of observations, transformed into a gridded form. The measurements were taken during the period May 1963 through April 1973. For the years 1963–1968, the observations were once daily, at 00 GMT, although a small number of 12 GMT observations were included. For the years 1968–1973 both 00 and 12 GMT data were used (Oort, 1983, pp. 5–8).

The aerological data were interpolated onto the regular grid by means of an objective analysis scheme, using the zonal average of data in a latitudinal belt as a first approximation. The objective analysis scheme, known as CRAM (Conditional Relaxation Analysis Method) is described by Harris et al. (1966) and Rosen et al. (1979).

Values of $\bar{q}$, $\bar{u}$, $\bar{v}$, $\overline{q'u'}$ and $\overline{q'v'}$ are given at each node of a 2.5° latitude by 5° longitude grid, and at each of 11 pressure levels; the overbars denote monthly averages, with $\overline{q'u'}$ and $\overline{q'v'}$ being the horizontal transient eddy fluxes in the zonal and meridional directions, respectively.

A known problem with the GFDL data set is the existence of suspicious divergences in the mean winds at mid–latitudes. Savijärvi (1988) used the vorticity equation and smoothing techniques to force a mass balance of the mean winds in the GFDL data. The effects of Savijärvi's correction on the water vapor flux divergence field are illustrated in Figures 1.1 and 1.2. Figure 1.1, taken from Peixoto and Oort (1983), shows $\nabla.\vec{Q}$ for the solstice seasons as calculated from the original data. Figure 1.2, from Savijärvi (1988) shows the corrected $\nabla\cdot\vec{Q}$ for the same seasons. (The figures are not given in the same units; multiplying values in Figure 1.1 [10 cm yr^{-1}] by 6.3 converts them to [W m^{-2}], compatible with Figure 1.2.) Over the continents, several changes are noteworthy, including the appearance in Fig. 1.2 of a tongue of convergence over Mexico and the U.S. Southwest in JJA, the narrower belt of convergence over Africa in JJA, and the disappearance of an irregularly–shaped zone of convergence over South America below 20° S. The "unexpected intense center of divergence" just west of India in JJA noted by Peixoto and Oort (1983) persists in the corrected divergence field. Unfortunately, Savijärvi's improvements to the GFDL data set were brought to the author's attention too late to be incorporated into the present study.

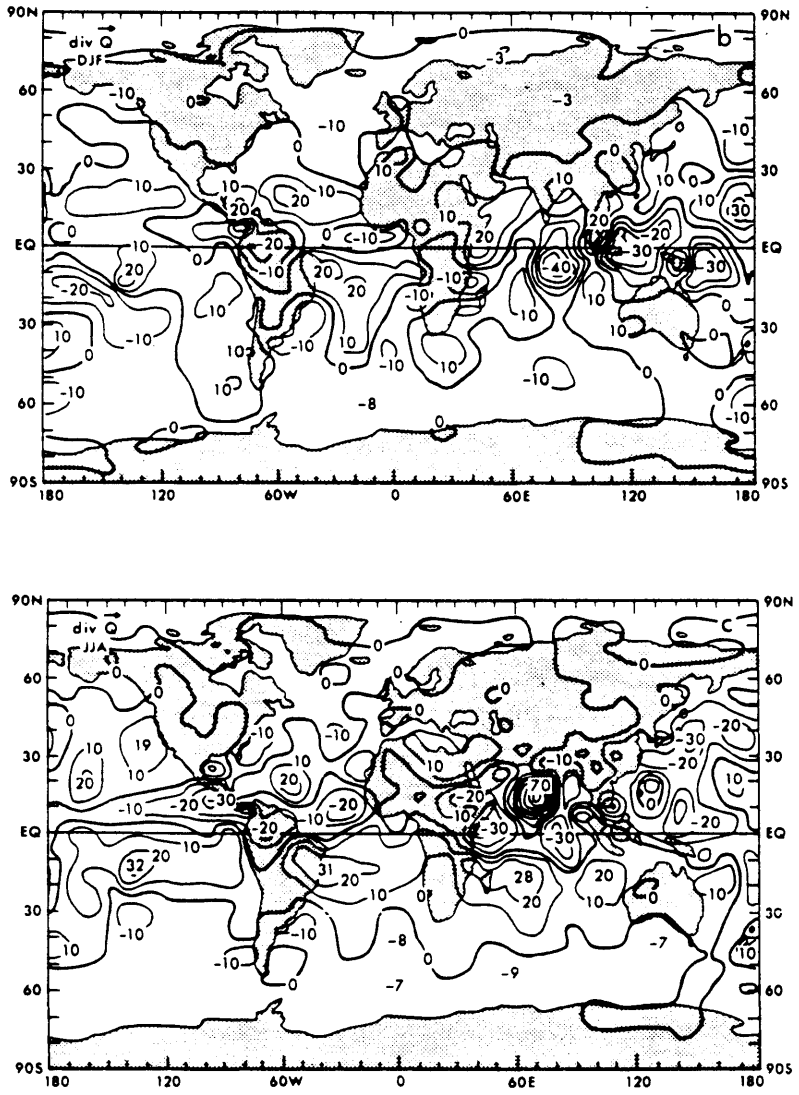

Figure 1.1: The horizontal divergence of the vertically–integrated water vapor flux, calculated from the original GFDL analysis. Units: 10 cm yr^{-1}. [Source: Peixóto and Oort (1983)]

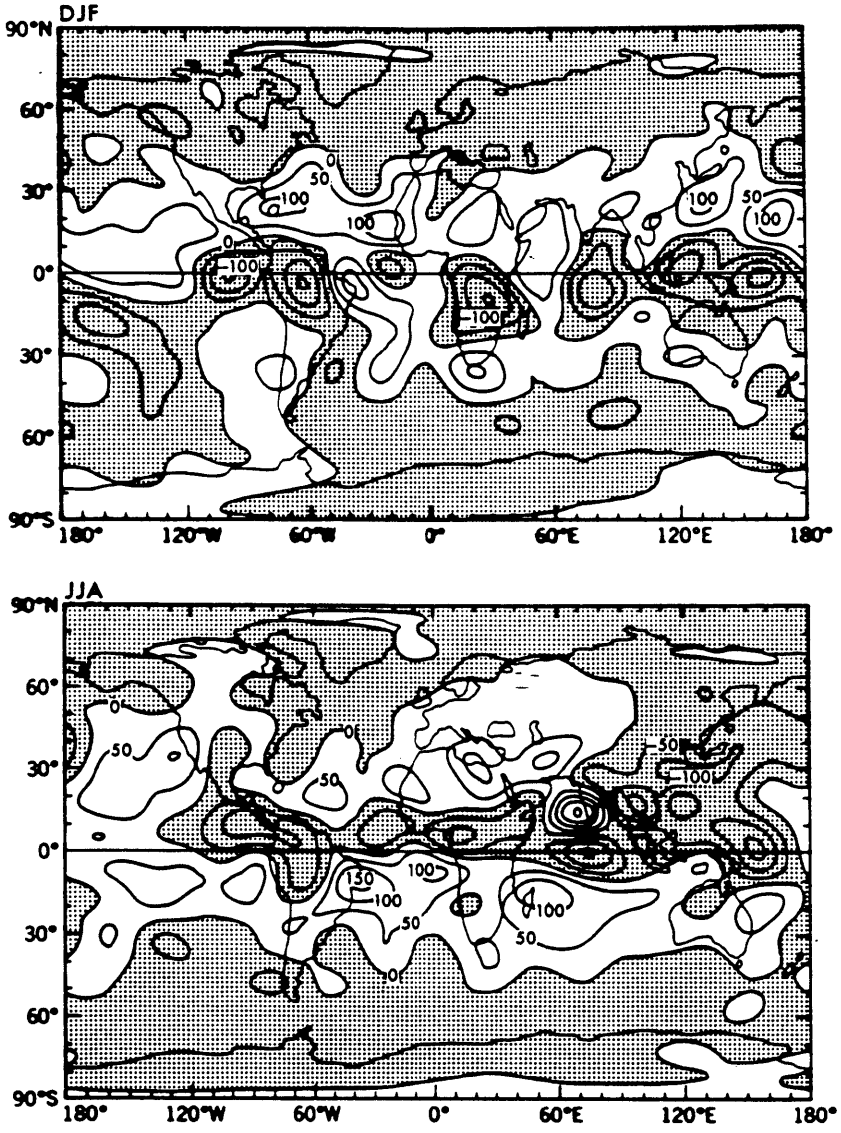

Figure 1.2 The vertical integral of moisture flux divergence calculated from the modified GFDL data. Units: W m^{-2}. [Source: Savijarvi (1988)]

Alestalo (1983) applied a constant error method to the station radiosonde data used in a study of the European water vapor budget. The following is a summary of Alestalo's correction techniques.

At a given pressure level, the divergence of the time mean water vapor transport vector can be expressed as

$$\nabla\cdot\ \overline{q\vec{V}} = \bar{q}(\nabla\cdot\bar{\vec{V}}) + \bar{\vec{V}}\cdot\nabla\bar{q} + \nabla\cdot\overline{q'\vec{V}'}\ . \tag{1.16}$$

The divergence of the time mean wind can be expressed as

$$\nabla\cdot\bar{\vec{V}} = \widehat{\nabla\cdot\bar{\vec{V}}} + (\nabla\cdot\bar{\vec{V}})'' \tag{1.17}$$

in which $\wedge$ denotes a vertical mean and $(\ )''$ a perturbation from that mean. Incorporating (1.17) into (1.16) and integrating vertically gives the result

$$\int_0^{p_s} \nabla\cdot\overline{q\vec{V}}\ = \widehat{\nabla\cdot\bar{\vec{V}}}\ \int_0^{p_s} \bar{q}\,\frac{dp}{g} + \int_0^{p_s} \bar{q}(\nabla\cdot\bar{\vec{V}})''\,\frac{dp}{g}$$

$$+\int_0^{p_s} \bar{\vec{V}}\cdot\nabla\bar{q}\,\frac{dp}{g} + \int_0^{p_s} \nabla\cdot\overline{q'\vec{V}'}\,\frac{dp}{g}\ . \tag{1.18}$$

Invoking the boundary condition that time mean vertical velocity vanishes at the upper and lower boundaries, and assuming no accumulation of air mass in the column, $\widehat{\nabla\cdot\bar{\vec{V}}}$ must vanish as required by mass conservation. However, this is not the case with real observations and analyzed data, due to sampling error, variability in the physical quantity being measured, and errors

introduced by interpolation and numerical integration. The non–zero divergence of the time–mean wind is eliminated by computing a corrected moisture flux divergence at each level, as follows:

$$\nabla\cdot\overline{q\vec{V}}\Big|_{\text{corrected}} = \nabla\cdot\overline{q\vec{V}}\Big|_{\text{computed}} - \bar{q}\,\widehat{\nabla\cdot\vec{V}}\ . \qquad (1.19)$$

The correction in (1.19) ensures that air mass is conserved for the column as a whole. However, at individual levels the divergence estimates may still be erroneous. Since water vapor advection is largely confined to the lower few atmospheric layers, the errors at individual levels may still be a problem, although the whole column is non–divergent in mass.

In the present study, no mass–balance corrections were applied to the aerological data. The nature of the analysis techniques applied herein would require corrections to the vapor flux components, and not only to the vapor flux divergence. The development of an appropriate correction method is of vital importance, as the results will show.

Computational Method

The components of the vertically–averaged water vapor flux vector, as defined in (1.15), were evaluated by trapezoidal rule integration. For each node, the surface pressure, p_s, was set equal to its mean annual value, with the beginning pressure level for integration selected according to Figure 1.3. Figure 1.3, taken from Oort (1983), indicates the annual mean surface pressure at the grid points in terms of the pressure levels of the analyzed data. A value of 1 indicates that the earth's surface lies between 1000 and 950 mb, a value of 2, between 950 and 900 mb, and so on. Vertical integration was

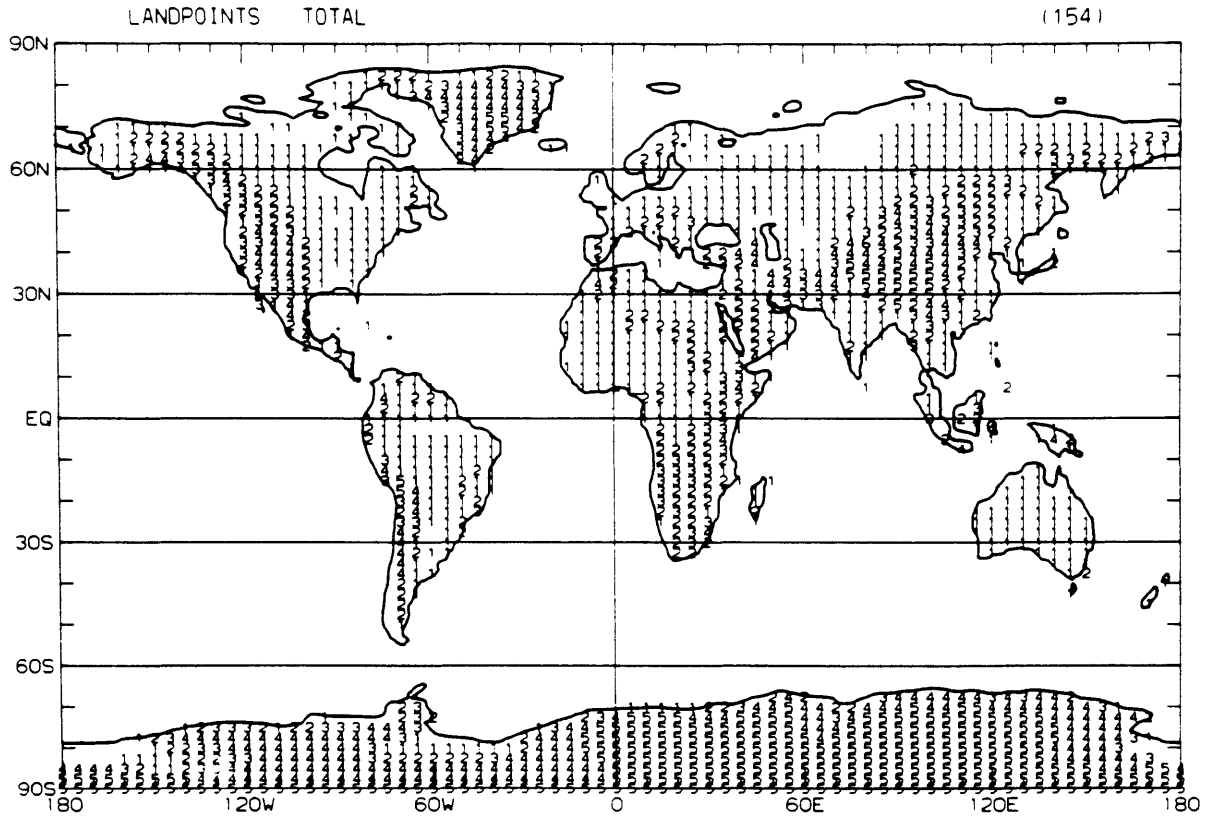

Figure 1.3: Map for each grid point of the lowest level used in vertical integration. A value of 1 indicates that the Earth's surface lies between 1000 and 950 mb, a value of 2 between 950 and 900 mb, a value of 3 between 900 and 850 mb, a value of 4 between 850 and 700 mb, and a value of 5 between 700 and 500 mb. [Source: Oort (1983)]

begun at the next standard pressure level above the surface pressure, i.e., at 1000 mb for a surface pressure greater than or equal to 1000, at 950 mb for surface pressure lying between 1000 and 950 mb, and so on.

Precipitation Data

The precipitation data used in this study are from the World Monthly Surface Station Climatology (and Associated Datasets) distributed by the National Center for Atmospheric Research (NCAR) in Boulder, Colorado. Monthly station precipitation data are given for over 3900 different World Meteorological Organization stations through 1987, with data for some stations going as far back as the mid–1700's. From this data set, the precipitation records for May 1963 through April 1973 were selected, in order to obtain precipitation data that are temporally compatible with the GFDL aerological data.

1.4 Boundary Flux Estimation

The closed–path line integral in (1.7) may be expressed as a sum of sub–integrals over segments of the boundary:

$$\oint \vec{Q}.\hat{n}_\gamma d\gamma = \sum_{k=1}^{m} \int_{x_k}^{x_{k+1}} \vec{Q}\cdot\hat{n}_\gamma d\gamma \qquad (1.20)$$

in which x_k and x_{k+1} are longitude–latitude points in sequence along the boundary, and m is the number of segments. For a closed path, x_{m+1} must be the same point as x_1. Each sub–integral has units kg s^{-1} and represents the time rate of moisture mass flux across that segment of the boundary.

For clarity in discussing the fluxes of moisture over the boundaries of regions, additional notation is introduced. The vertically–integrated moisture flux vector is decomposed into its mean motion and transient eddy terms,

$$\vec{Q} = \vec{Q}_M + \vec{Q}_{TE} \tag{1.21}$$

where

$$\vec{Q}_{TE}(\lambda,\phi) \equiv \int_0^{p_s} \overline{q'\vec{v}'} \frac{dp}{g} \tag{1.22a}$$

and

$$\vec{Q}_M(\lambda,\phi) \equiv \int_0^{p_s} \bar{q}\,\bar{\vec{v}} \frac{dp}{g} . \tag{1.22b}$$

The boundary sub–integrals in (1.20) are abbreviated as

$$f_k \equiv \oint_{x_k}^{x_{k+1}} \vec{Q}_M \cdot \hat{n}_\gamma d\gamma \tag{1.23}$$

and, analogous to (1.22),

$$f_{M,k} = \oint_{x_k}^{x_{k+1}} \vec{Q}_M \cdot \hat{n}_\gamma d\gamma \tag{1.24a}$$

and

$$f_{TE,k} \equiv \oint_{x_k}^{x_{k+1}} \vec{Q}_{TE} \cdot \hat{n}_\gamma d\gamma . \tag{1.24b}$$

By definition,

$$f_k = f_{M,k} + f_{TE,k} . \tag{1.25}$$

Consistent with the definition of $\hat{n}_\gamma$ as the outward unit vector, f_k is positive for moisture flux out of the region, and negative for flux into the region.

If a rectilinear boundary is defined by connecting nodes in the GFDL data grid, then each sub–integral, f_k, represents the moisture flux across either an east–west or a north–south line segment on the Earth's surface. Such rectilinear boundaries are well suited to graphical display of the moisture flux data; this technique is now introduced.

Figure 1.4 shows the rectilinear boundaries of North and South America superimposed on a cylindrical equidistant projection of the continents. The small crosses indicate the nodes of the GFDL grid (every 2.5° latitude and 5° longitude), and the solid lines the boundaries of the study regions. The nodes define the endpoints of the boundary segments, over which the sub–integrals in (1.24) were evaluated by trapezoidal rule integration for each of the twelve months of the year. The results are shown in a set of figures below. In these figures, the magnitude of the moisture flux, f_k, across segment k of the boundary is shown by a bar perpendicular to segment k, with its base at the segment. The length of the bar is proportional to f_k by the scale indicated, and the bar points into or out of the region according to the direction of net moisture flux across segment k. In addition, those bars representing flux into the region (negative f_k) are cross–hatched to further distinguish them from bars representing efflux (f_k positive). The total influx of atmospheric moisture into the region is proportional to the total length of cross–hatched bars, and the efflux is proportional to the total length of white bars.

It is important to note that the bars do not represent vector components; each represents the integral of the normal component of the flux vector over the length of the segment. The graphical scale, in units of kg s^{-1}, refers to the bars and has no relevance to the continental outlines, which are not drawn to scale and are in fact highly distorted by the cylindrical

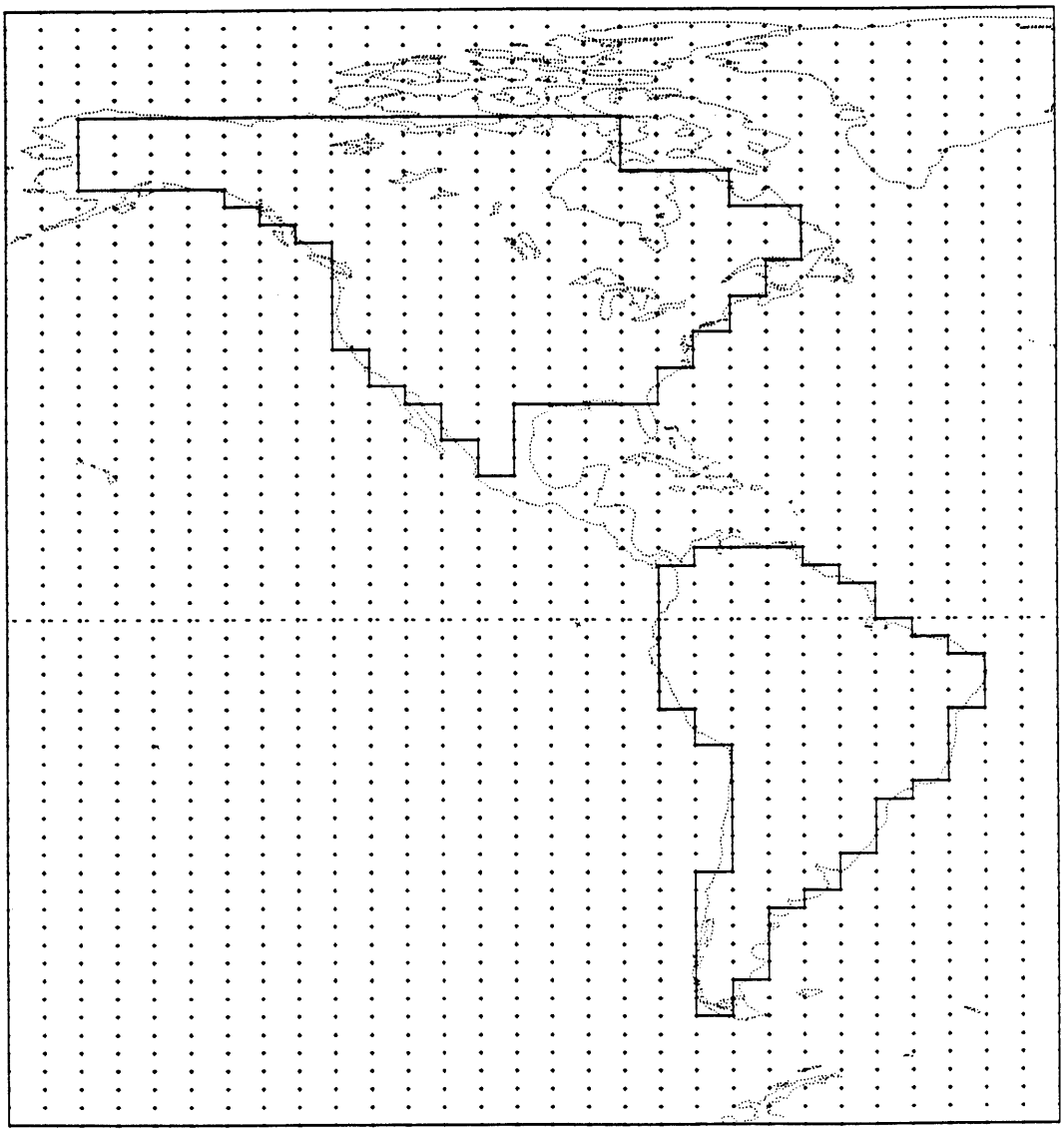

Figure 1.4: Continental regions selected for graphical analysis of the boundary flux of water vapor. The small crosses indicate the nodes of the GFDL data grid (5° longitude and 2.5° latitude).

equidistant projection. Figure 1.5 shows a simple example, illustrating the meaning of the bars in the set of figures to follow. Consider a constant $\vec{Q}$, directed at angle $\alpha = \tan^{-1}(0.5)$ (so that Q_λ is twice Q_ϕ) and two boundary segments, one of 5 degrees longitude, the other 2.5 degrees latitude. At the Equator (case a), the east–west boundary segment is twice as long as the north–south segment; however, the normal components of the flux vector across the boundaries have the inverse relationship; therefore, in this case, f_1 is equal to f_2. At 60° North (case b), the two segments have the same length, with the result that f_1 is equal to one–half of f_2. The right–hand side of Figure 1.5 shows how these results would be plotted in longitude–latitude space (equivalent to the cylindrical equidistant projection), in a figure such as 1.6 through 1.17.

Figures 1.6 through 1.9 show the total moisture flux (f) across the segments of the rectilinear continental regions defined in Fig. 1.4, for the months December, January and February (DJF); March, April and May (MAM); June, July and August (JJA); and September, October and November (SON). Figures 1.10 through 1.13 present the transient eddy moisture flux (f_{TE}) and Figures 1.14 through 1.17, the mean motion flux (f_M) for the same seasonal sequence. For Figures 1.14 through 1.17, values of $f_{TE,k}$ and $f_{M,k}$ were computed, then the values for three months were simply averaged. Therefore, the transient eddy values plotted in Figures 1.10–1.13 represent moisture transport by motions on time scales less than one month during the three month period, and the mean motion values plotted in Figures 1.14–1.17 represent transport on the time scale of one month.

The total flux of water vapor onto these continents reflects the circulation of the atmosphere and the distribution of temperature at the Earth's surface and in the lower troposphere. The pattern of the equatorial

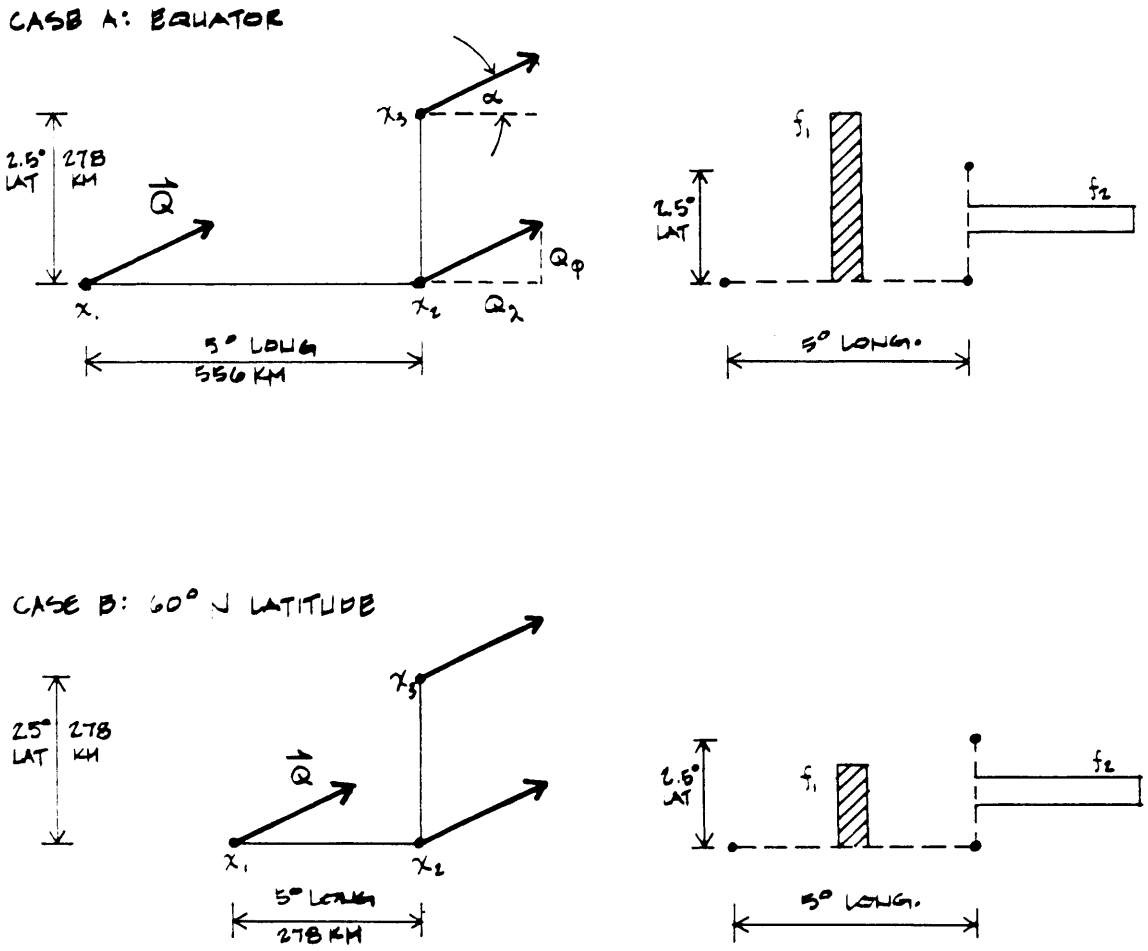

Figure 1.5: A simple example illustrating the meaning of the bars in Figures 1.6 through 1.17. For constant $\vec{Q}$, the magnitude of f_k depends upon the normal component of $\vec{Q}$ and the length of the segment. The right–hand side shows how these results would appear in Figures such as 1.6 through 1.17.

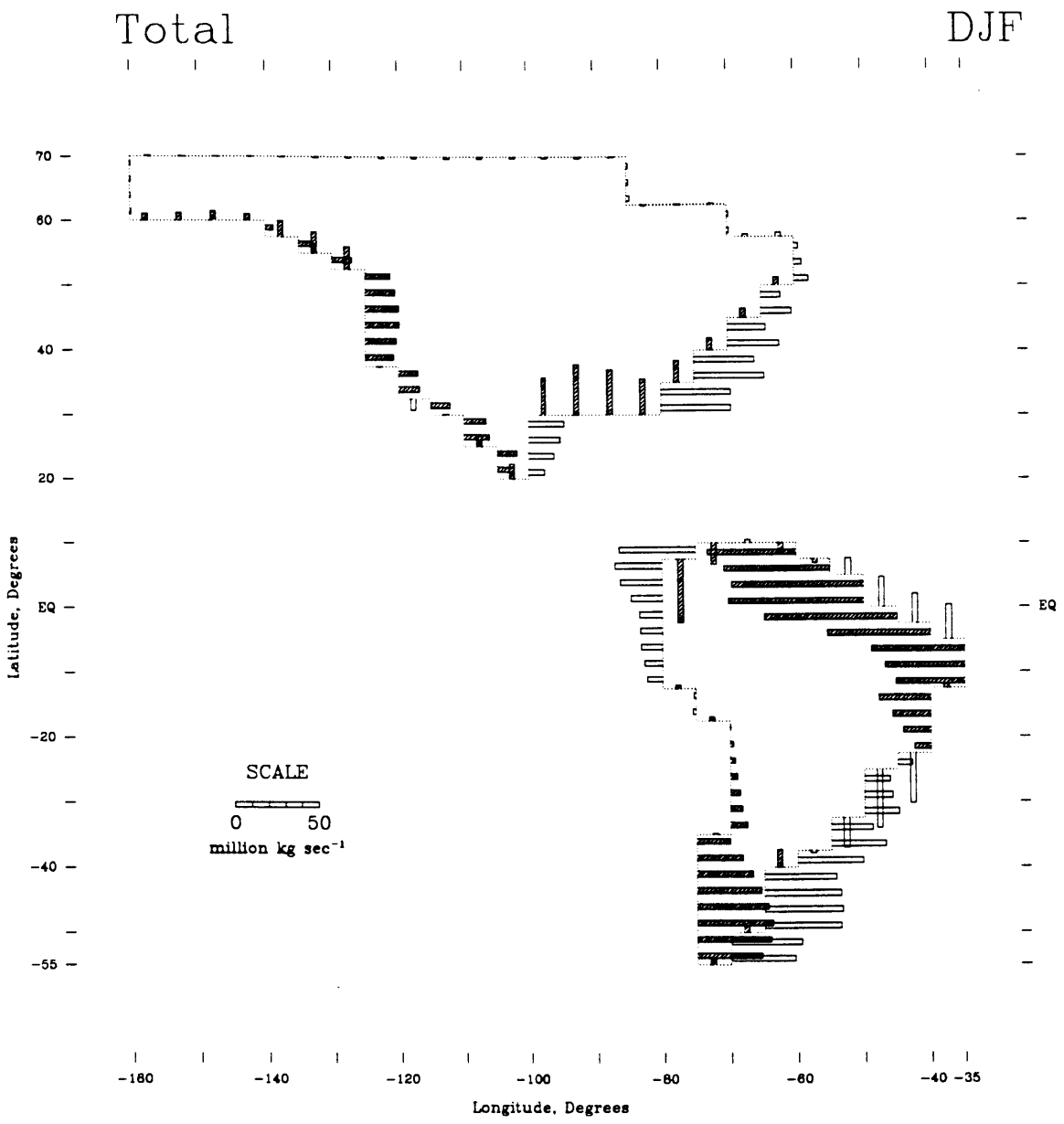

Figure 1.6: The total moisture flux (mean motion plus transient eddies) across segments of horizontal regional boundaries, for North and South America. Values shown are the average of monthly average values for December, January and February, 1963–73.

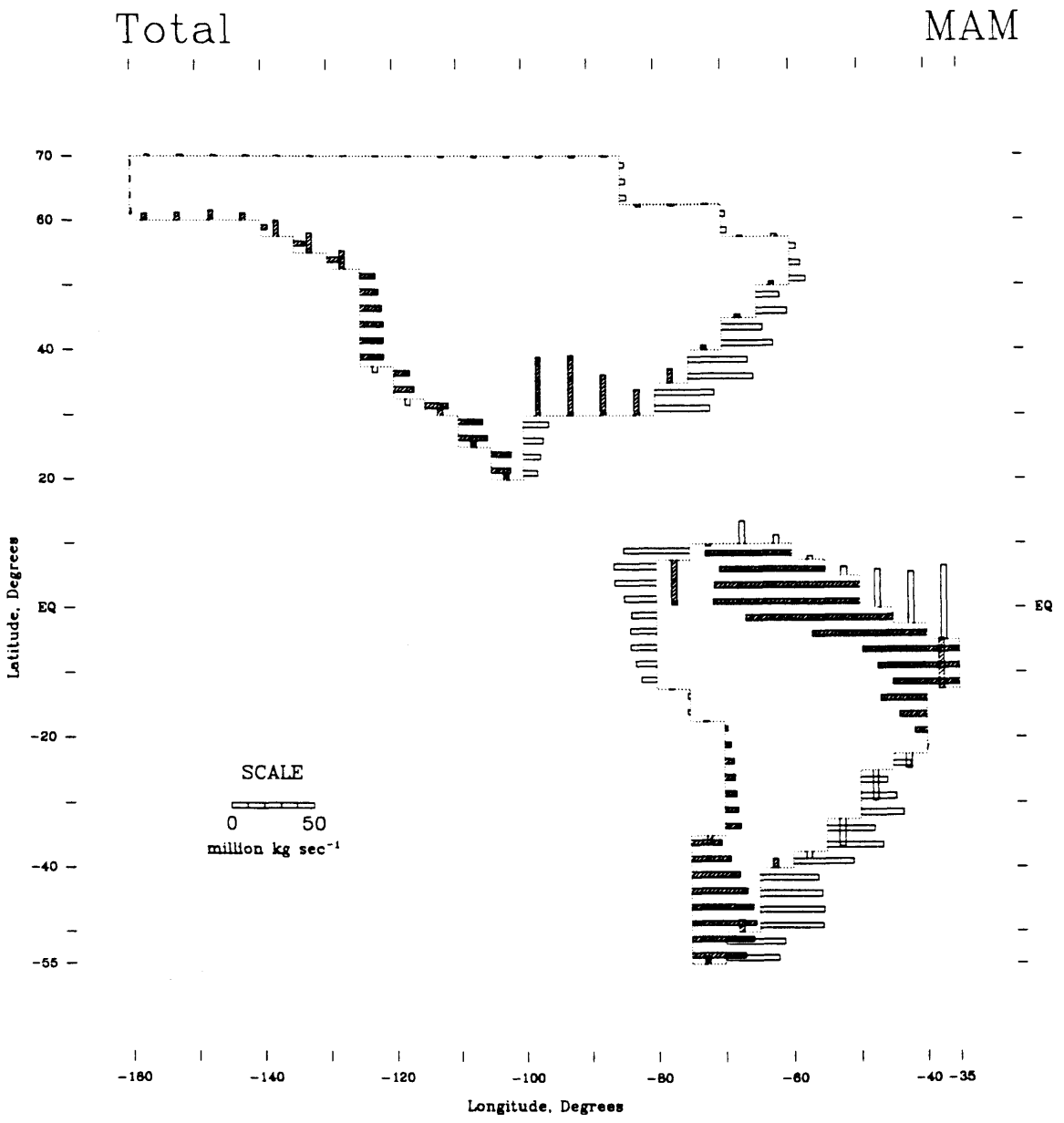

Figure 1.7: The total moisture flux (mean motion plus transient eddies) across segments of horizontal regional boundaries, for North and South America. Values shown are the average of monthly average values for March, April and May, 1963–73.

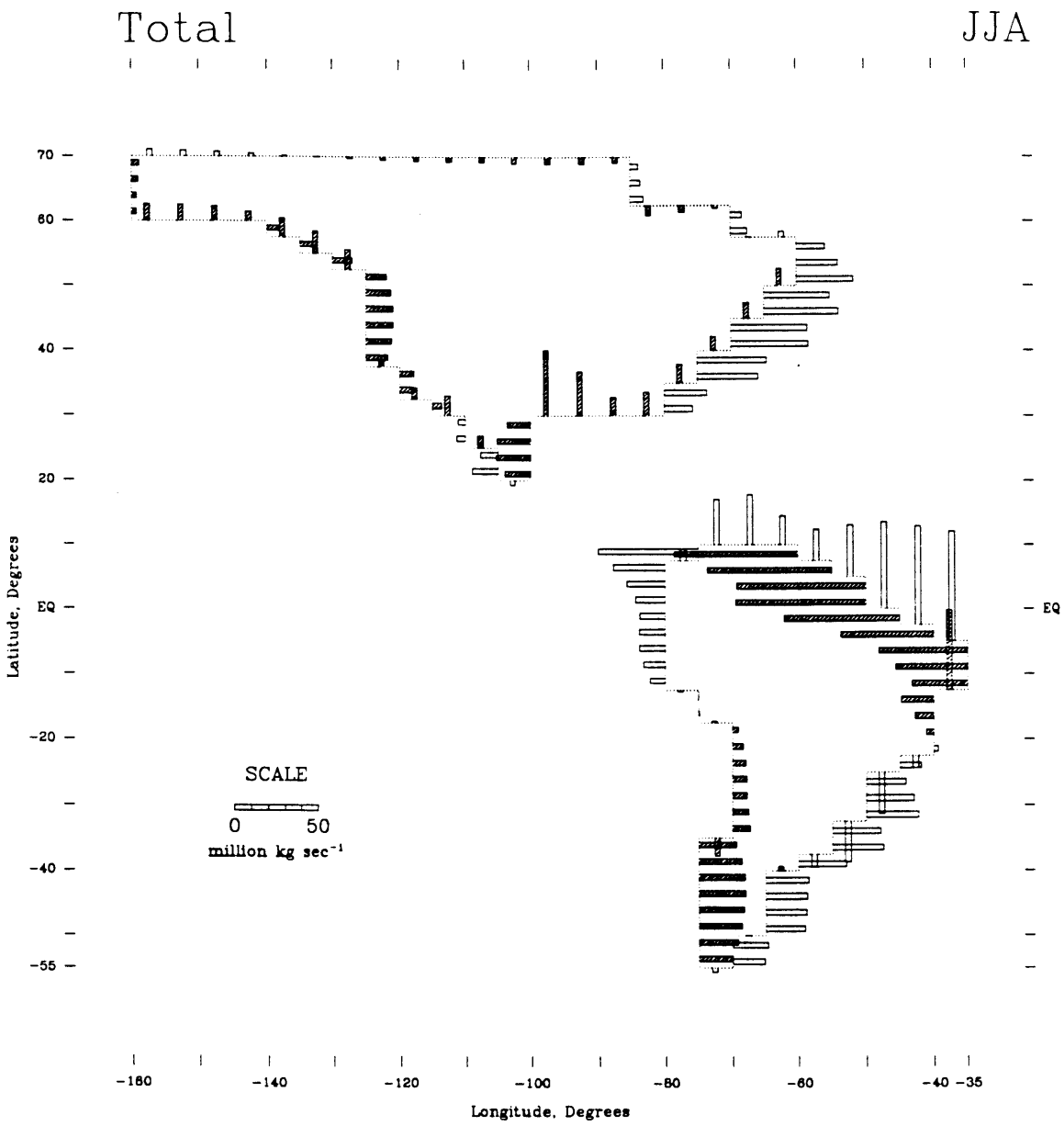

Figure 1.8: The total moisture flux (mean motion plus transient eddies) across segments of horizontal regional boundaries, for North and South America. Values shown are the average of monthly average values for June, July and August, 1963–73.

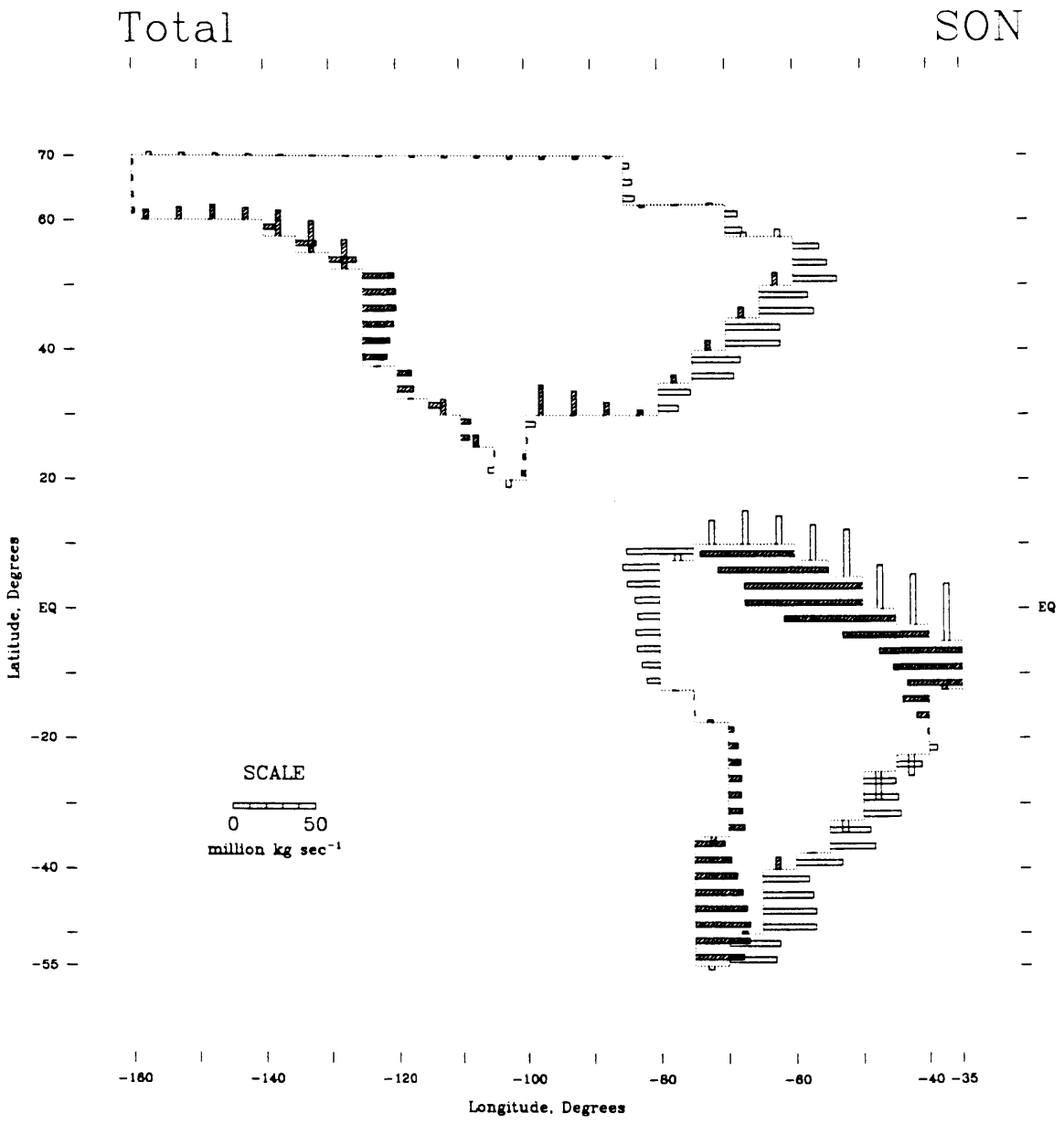

Figure 1.9: The total moisture flux (mean motion plus transient eddies) across segments of horizontal regional boundaries, for North and South America. Values shown are the average of monthly average values for September, October and November, 1963–73.

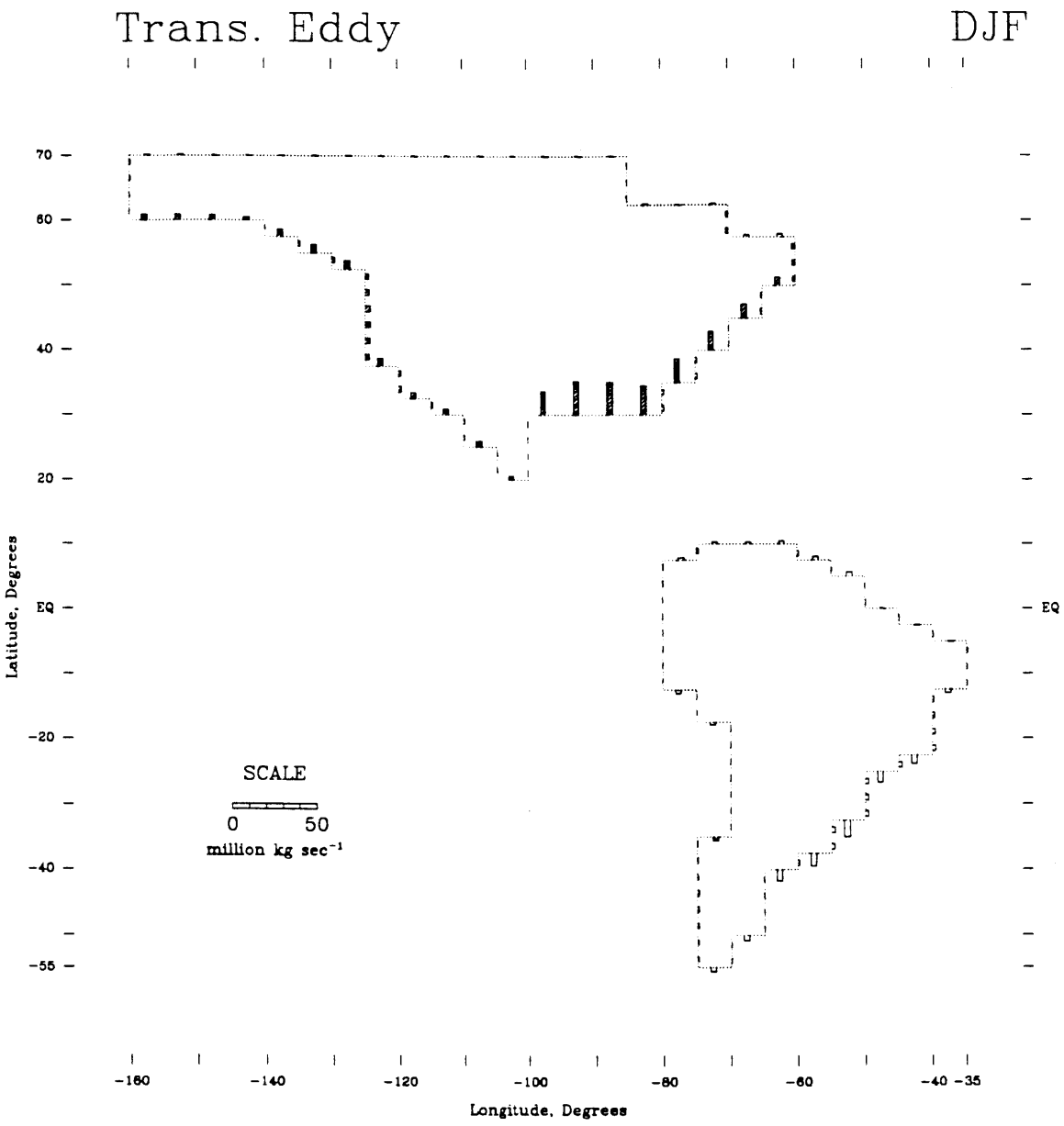

Figure 1.10: The moisture flux by transient eddies across segments of horizontal regional boundaries, for North and South America. Values shown are the average of monthly average values for December, January and February, 1963–73.

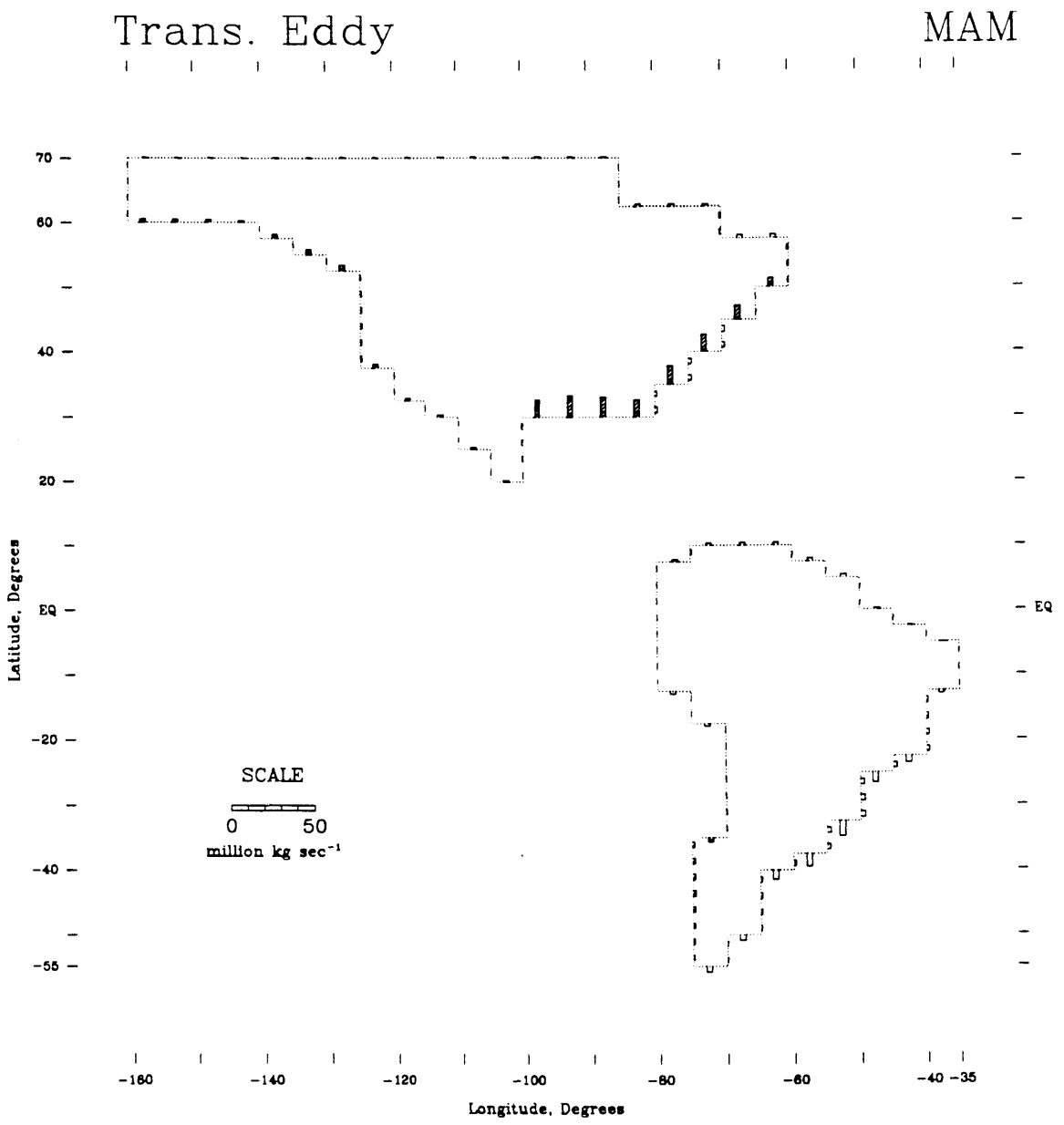

Figure 1.11: The moisture flux by transient eddies across segments of horizontal regional boundaries, for North and South America. Values shown are the average of monthly average values for March, April and May, 1963–73.

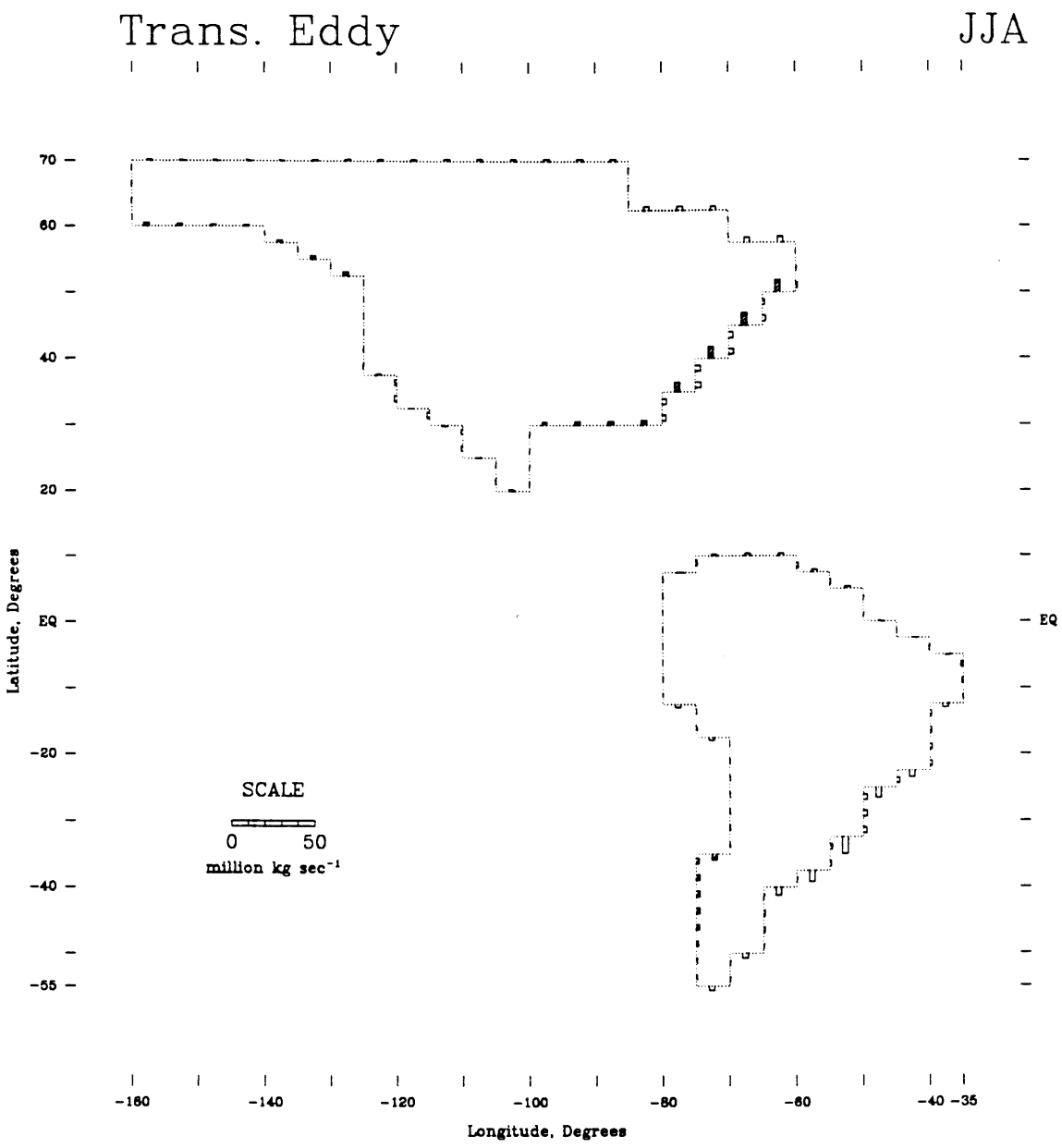

Figure 1.12: The moisture flux by transient eddies across segments of horizontal regional boundaries, for North and South America. Values shown are the average of monthly average values for June, July and August, 1963–73.

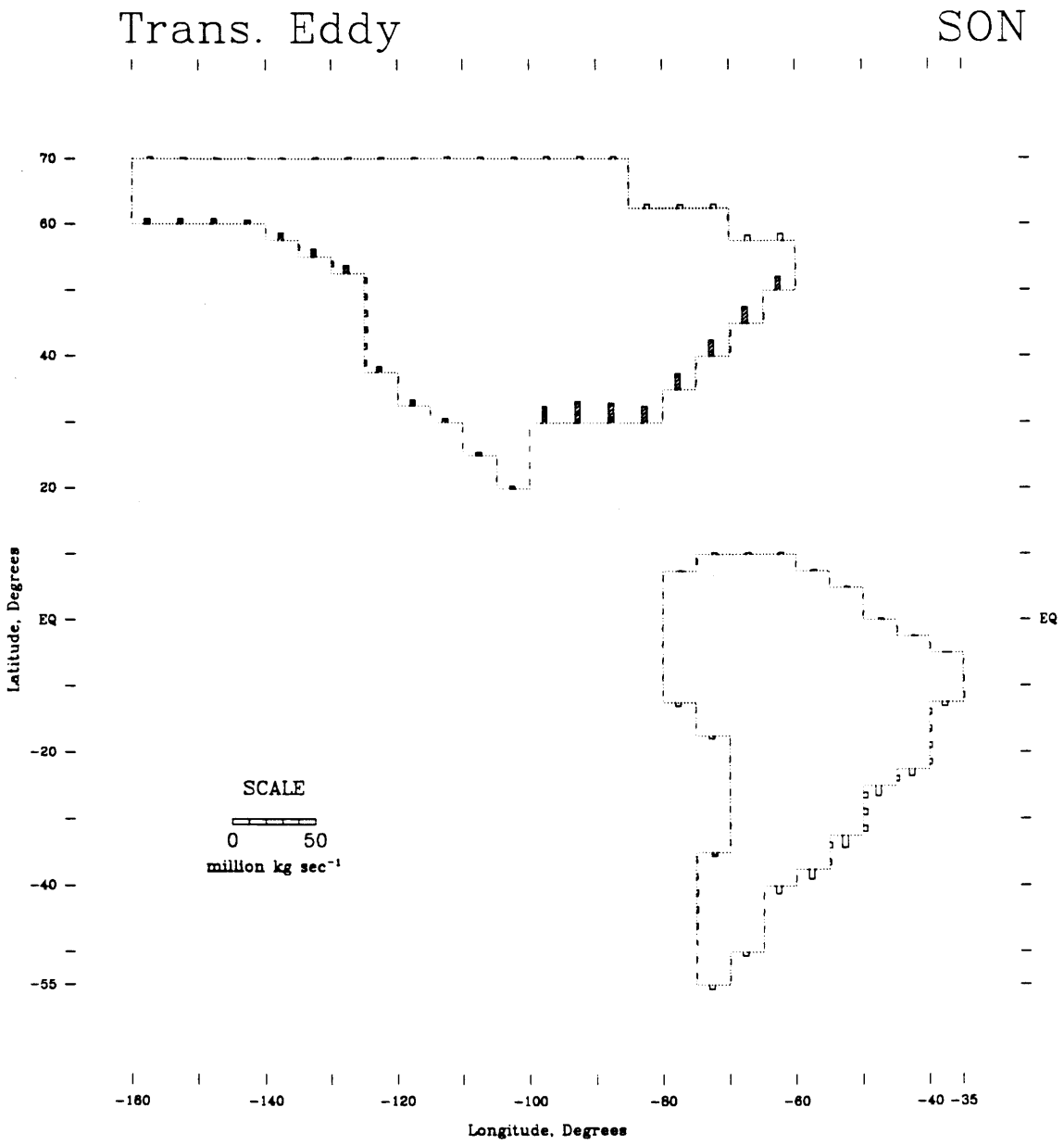

Figure 1.13: The moisture flux by transient eddies across segments of horizontal regional boundaries, for North and South America. Values shown are the average of monthly average values for September, October and November, 1963–73.

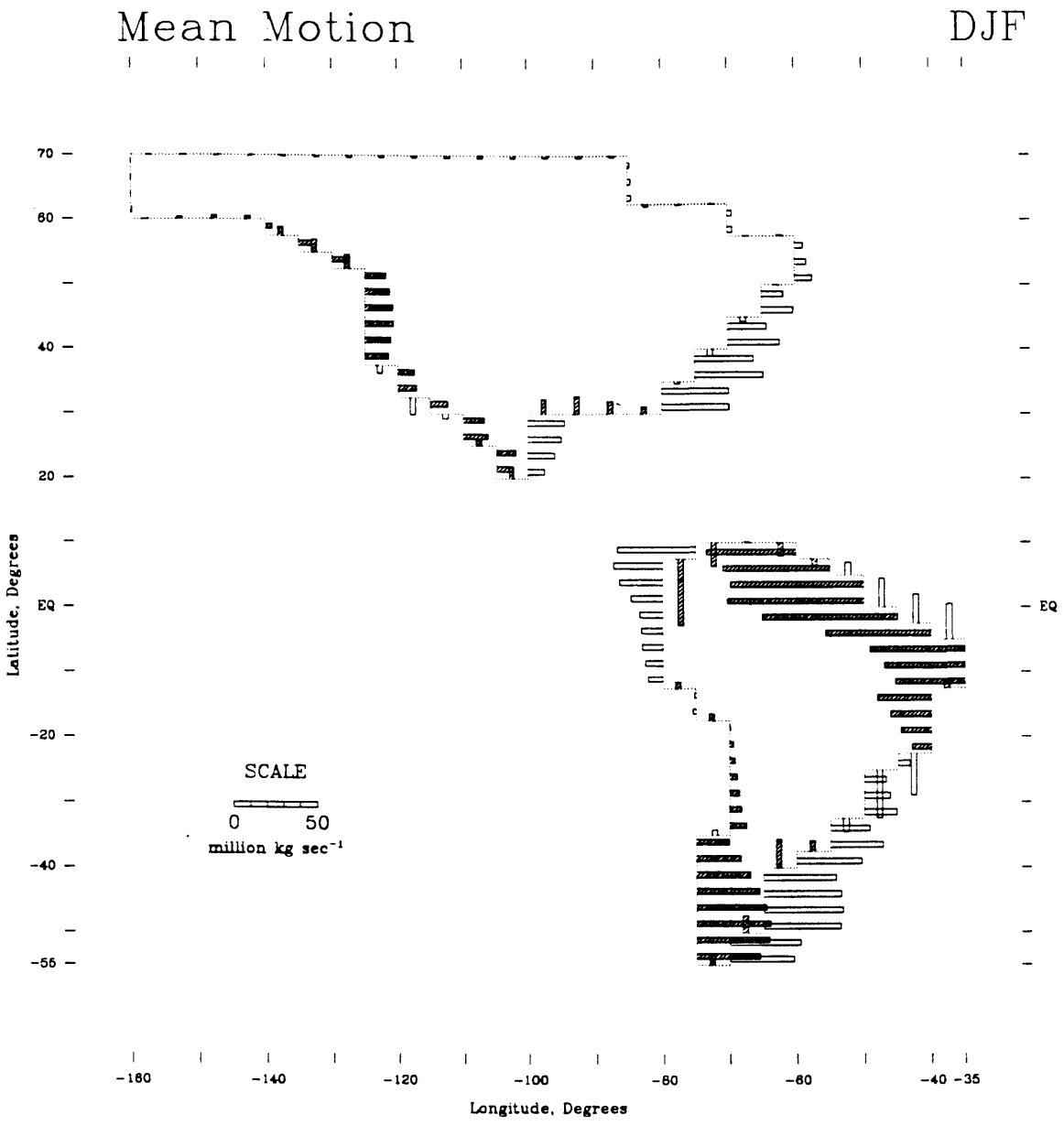

Figure 1.14: The moisture flux by monthly mean motion across segments of horizontal regional boundaries, for North and South America. Values shown are the average of monthly average values for December, January and February, 1963–1973.

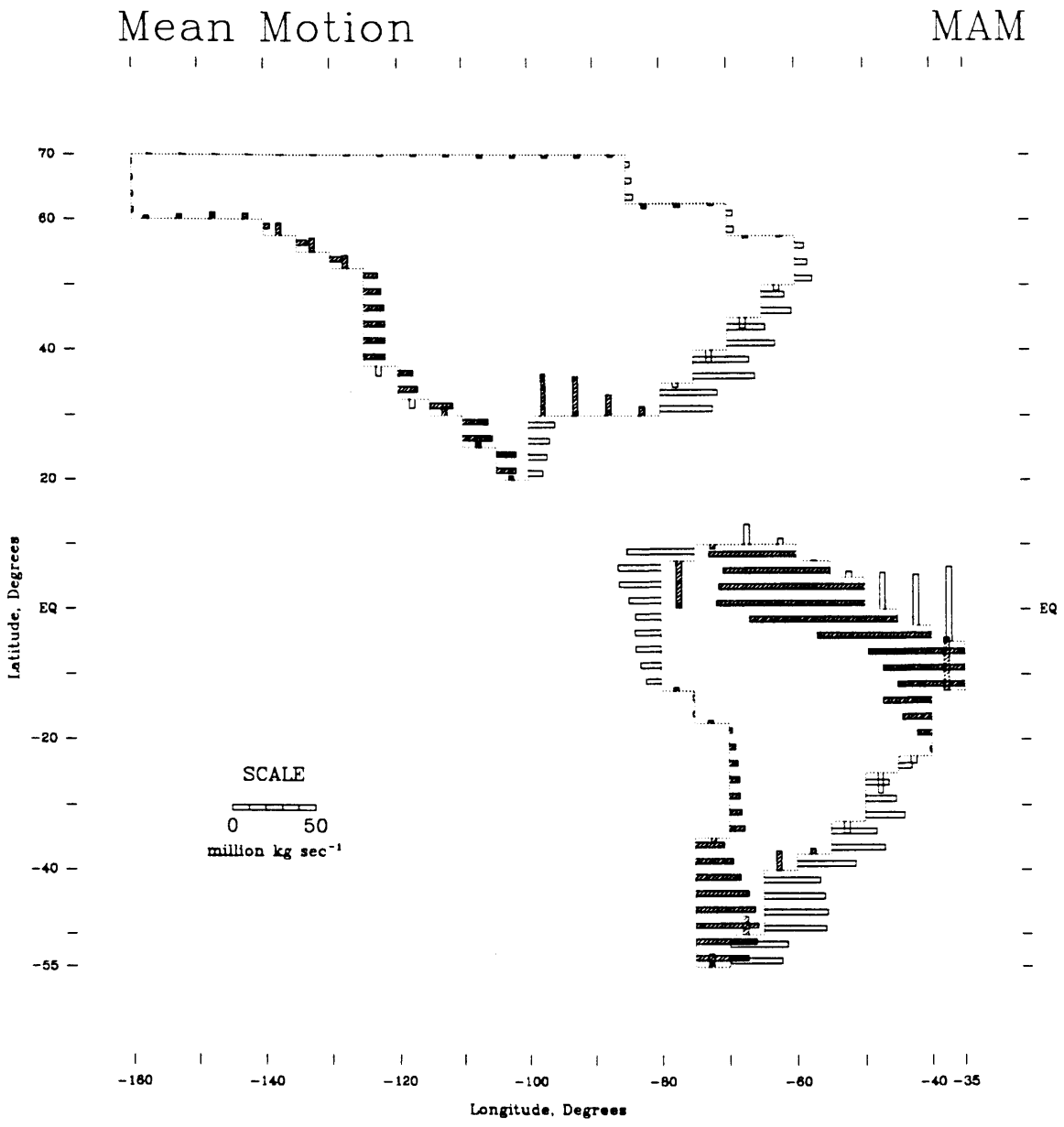

Figure 1.15: The moisture flux by monthly mean motion across segments of horizontal regional boundaries, for North and South America. Values shown are the average of monthly average values for March, April and May, 1963–1973.

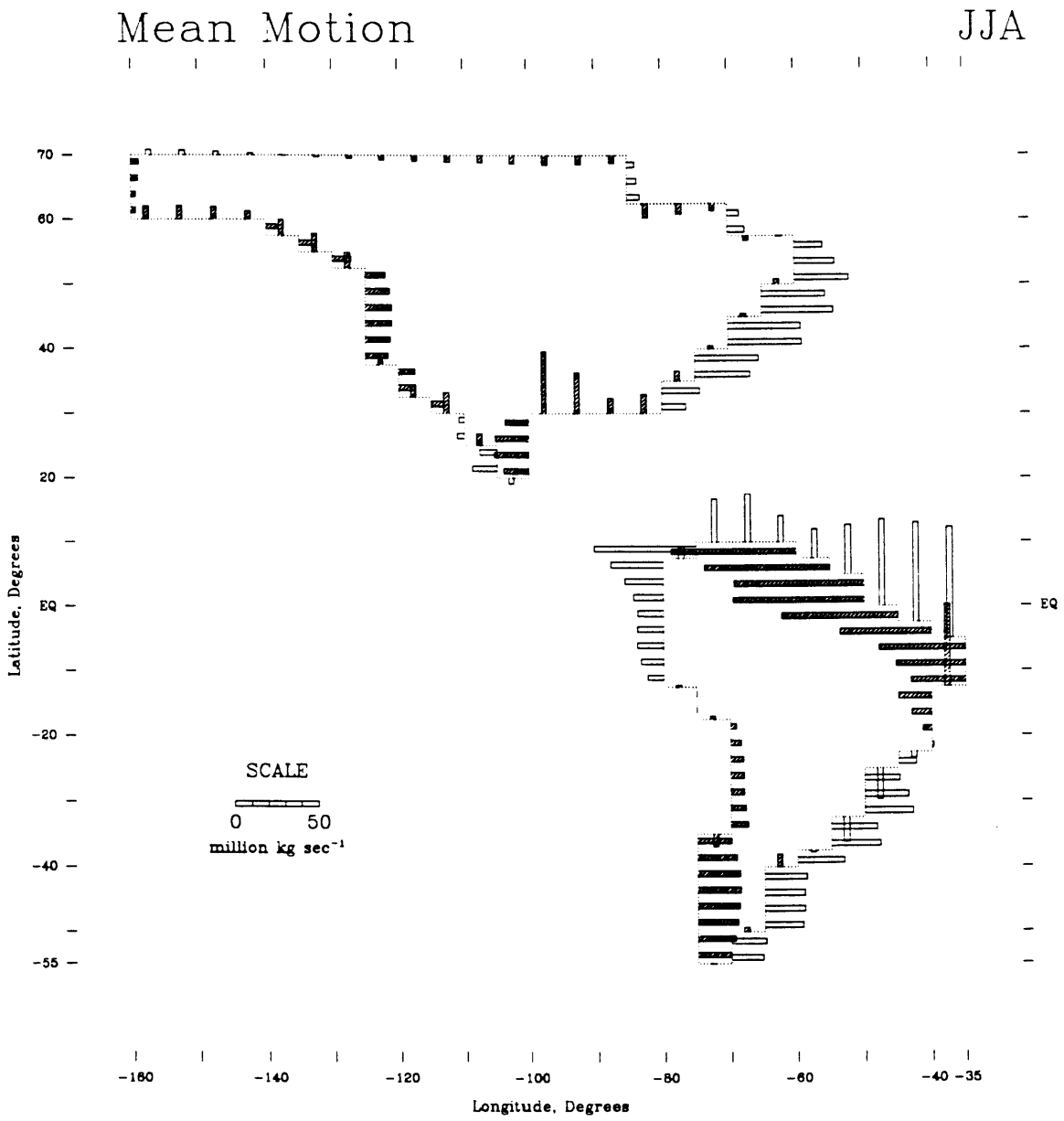

Figure 1.16: The moisture flux by monthly mean motion across segments of horizontal regional boundaries, for North and South America. Values shown are the average of monthly average values for June, July and August, 1963–1973.

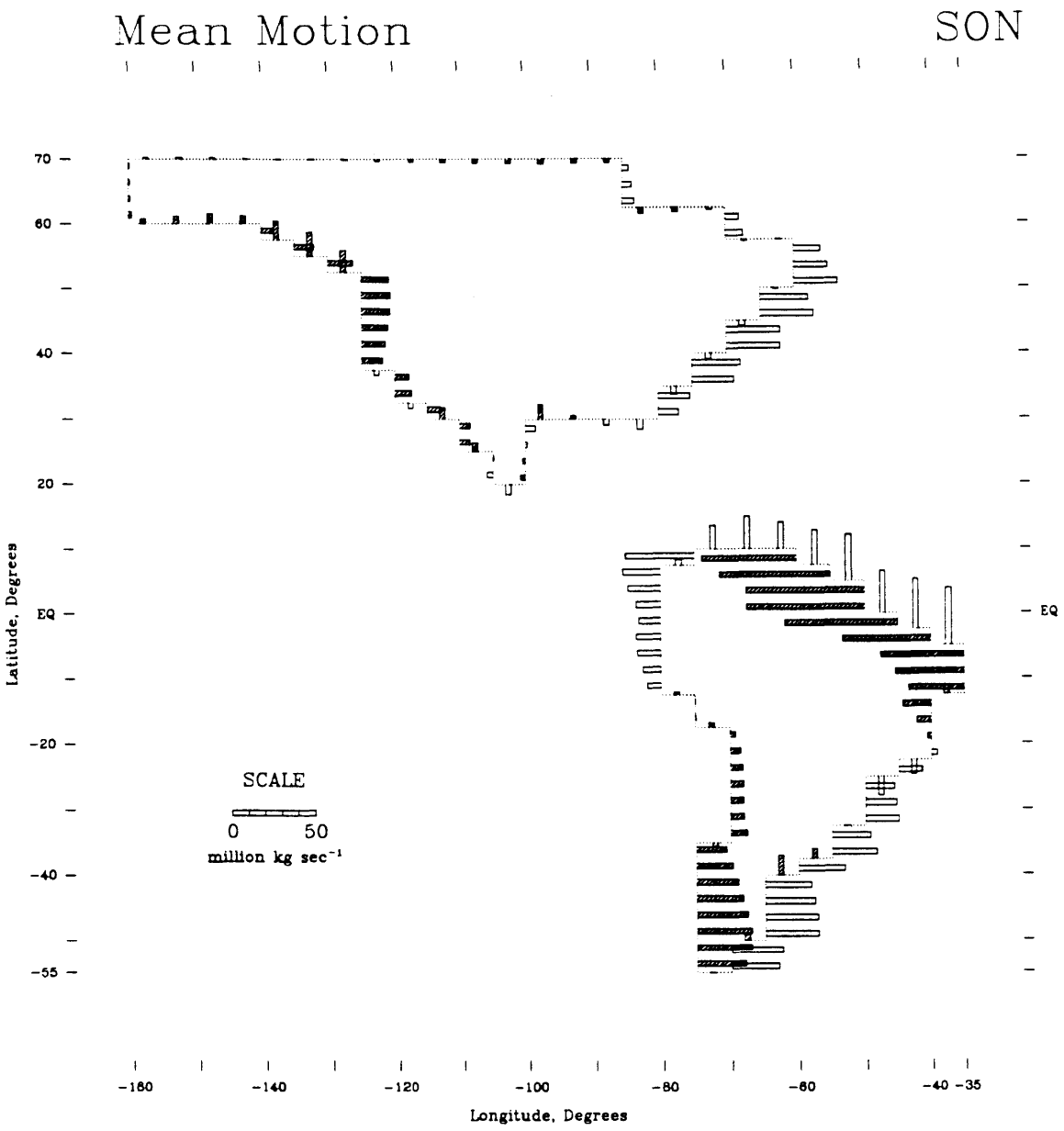

Figure 1.17: The moisture flux by monthly mean motion across segments of horizontal regional boundaries, for North and South America. Values shown are the average of monthly average values for September, October and November, 1963–1973.

easterly trade winds and the mid–latitude westerlies is clearly reflected in the zonal transport. The warm air moving off the equatorial Atlantic Ocean delivers moisture at an extremely high rate over the northeast coast of South America. The large magnitudes of the segment fluxes both onto and off Patagonia (the southern tip of South America) are attributable to the high wind velocities in the "roaring forties" latitudes; at these latitudes the winds circle the globe almost entirely over ocean, which provides much less resistance to air flow than does land, and at the same time allows development of high relative humidity. These bars are longer by half in the Southern Hemisphere summer (DJF) than in the winter (JJA), due to the higher saturation vapor pressure of the warmer air. On the other hand, the very low landward values of f along the west coast of South America between 35 S and 20 S are due to the barrier posed by the Andes range. Computationally, as can be seen from Figure 1.3, the vertical integration of $\vec{Q}$ for these grid nodes begins fairly high in the atmosphere, where specific humidity is low. Physically, the small bars reflect the loss of water from the air due to adiabatic cooling and resulting condensation as the air is forced up over the mountain range. Two major streams of atmospheric water vapor onto North America are evident: flow from the Pacific Ocean and from the Gulf of Mexico. The latter source is strongest in the Northern Hemisphere spring, MAM.

The meridional transient eddy flux of moisture onto these continents is poleward in all seasons (Figures 1.10–1.13). In North America, f_{TE} is most prominent off the Gulf of Mexico, where it is greatest in the Northern Hemisphere winter, accounting for more than half the total flux across the boundary between 100 W and 80 W. Because the rectilinear regional boundary does not exactly follow the eastern coastline of North America, it is

not clear whether the meridional bars on those boundary segments actually correspond to onshore transport of moisture. The apparent unimportance of the transient eddy mode for the South American continent is possibly attributable to data sparsity.

Figures 1.14 through 1.17 do not include any new information because f_M can be obtained by subtracting f_{TE} from f. However, they are included for comparison purposes. In particular, f_M from the Gulf of Mexico is quite large in MAM and JJA; recalling that f_{TE} is quite small across that boundary in JJA, it is interesting to note that the year–round supply of moisture from the Gulf of Mexico is accomplished by different modes in different seasons. The zonal mean vapor transport off the Gulf of Mexico reverses direction in the course of the year, from westerly in DJF to easterly in JJA, an important factor in the annual march of precipitation in the Southwest USA (Hastenrath, 1966). Across a number of boundary segments along the east coast of North America, f_M and f_{TE} are of opposite sign; this opposition holds mostly for meridional transport, although in DJF (Figs. 1.10 and 1.14), a small zonal f_{TE} is opposite f_M between 4 S and 60 N. In South America, meridional values of f_{TE} and f_M tend to be of opposite sign along the southeast coast.

Bar graphs of the boundary flux of $\vec{Q}$ are a useful technique for the presentation of moisture flux data. Although it would entail substantial interpolation between nodes, the ability to define more realistic continental boundaries would improve the method.

Chapter 2
Estimation of Continental Precipitation Recycling

2.1 Introduction

The total amount of water that precipitates on a region of land comes from two sources: 1) water vapor transported into the region by atmospheric advection (as described in Chapter One), and 2) water vapor formed by evaporation and transpiration from the land surface of the region. This second source is tantamount to the local recycling of precipitation water within the region.

The sources of precipitation water are indicated schematically in Figure 2.1, which shows a simplified model of the atmospheric moisture fluxes over a land region. The horizontal arrows indicate the advective flux of water vapor into and out of the atmospheric control volume; W is the amount of water vapor contained in the control volume; E is the net evapotranspiration from the underlying land surface; and P is the net precipitation onto the land surface. The two sources of precipitation are indicated by the two small branches that join to form the larger arrow labeled P; P_m is precipitation of local (evaporative) origin, and P_a is that of advective origin. The arrow labeled E splits into two branches, indicating that a certain fraction of the locally evaporated or transpired water is not returned to the land surface as precipitation, but joins the atmospheric vapor reservoir and is advected out of the control volume.

In discussing precipitation recycling, it is important to clarify the term "recycling." In this study, *recycled precipitation* is defined as *water that evaporates from the land surface within a specified control volume and falls*

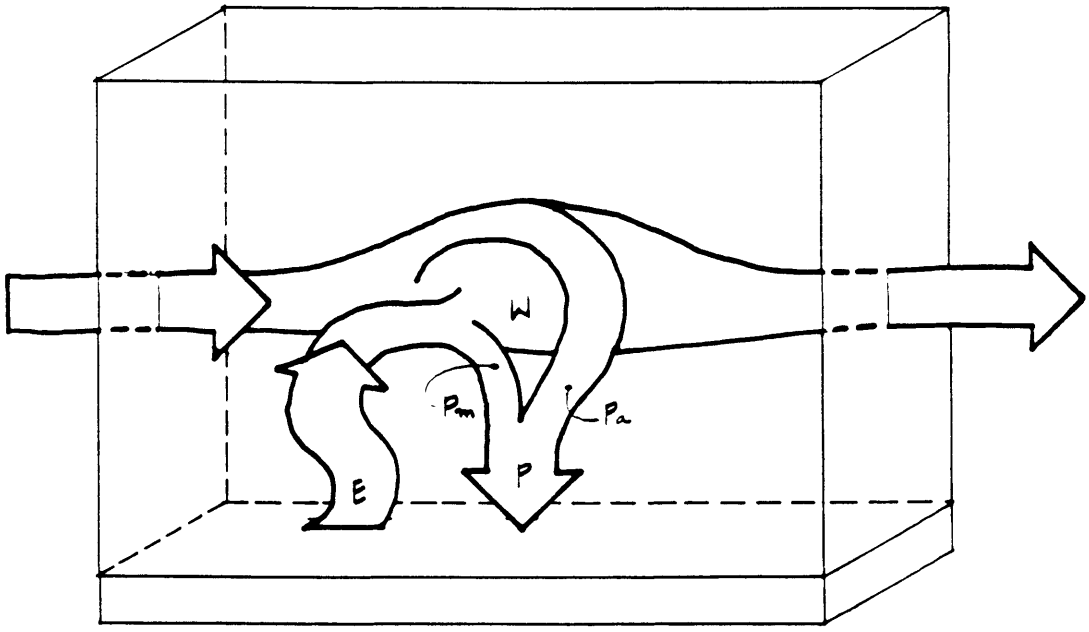

Figure 2.1: Simplified model of the atmospheric moisture fluxes over a land region. P_m and P_a are precipitation of local evaporative and advective origin, respectively.

again as precipitation within the same control volume. The remainder of the precipitation falling inside the control volume is considered to be of *advective* origin, without regard to whether it most recently evaporated from an ocean surface or from a land surface outside the control volume. With recycling defined in this manner, the distinction between recycled and advected precipitation is not necessarily the same as the distinction between precipitation water of terrestrial origin (i.e., most recently evaporated from the land surface) and oceanic origin (i.e., most recently evaporated from the ocean surface). Advected precipitation water is equivalent to oceanic precipitation water if and only if the inflow boundary of the control volume lies along the coastline. For an inland region, it is important to assure compatibility of definitions before comparing different estimates of the sources of the region's precipitation.

The extent to which a region's precipitation is supplied by locally–evaporated water is an indicator of the importance of land surface processes in the water balance of the region and may also be an indicator of general climatic sensitivity to land surface change. The recycling process is a potentially significant climate feedback mechanism and land surface–atmosphere interaction, which may contribute to the persistence and intensification of droughts (Rodriguez–Iturbe, Entekhabi and Bras, 1991a). The objective of the work described in this Chapter is to obtain quantitative estimates of the degree to which land–atmosphere moisture recycling is active over several large continental regions.

2.2 Literature Review

Until the late 1930's, according to Benton et al. (1950), it was generally believed that the water precipitated over the continents was directly derived

from moisture evaporated from the continents. Under this view, the flux of water in the atmosphere from the oceans to the continents was assumed to be only that required to replenish the loss of water from the continents by runoff. Apparently, there was no conception that vast quantities of incoming water vapor from the oceans could pass over continental regions without precipitating, or that water vapor which evaporated from the continent could be carried away by the wind as atmospheric runoff.

Benton et al. critiqued the theory that precipitation is largely land–derived and described developments leading to a more correct description of the role of the atmosphere in the hydrologic cycle. They emphasized two concepts: First, vertical motions in the atmosphere are necessary in order to produce significant precipitation, therefore increasing the water vapor in the air over a region does not necessarily increase precipitation. Second, the atmosphere is in continuous motion, carrying very large quantities of water vapor across the continents from the oceans; moisture added to the atmosphere by evaporation and transpiration may travel hundreds or thousands of miles before being reprecipitated.

In the same paper, Benton et al. estimated the relative contributions of the sources of precipitation over the Mississippi watershed. They distinguished between precipitation events from, and evaporation into, maritime and continental air masses, and estimated that not more than ten percent of the total precipitation of the Mississippi watershed is moisture having a land source within the watershed, while at least 90 percent is external in origin.

McDonald (1962) argued against what he called "the evaporation–precipitation fallacy," that is, the idea that local water shortages might be alleviated by creating open areas from which water could evaporate and enhance local

precipitation. In arguments parallel to those of Benton et al., he attributed the fallacy to misconceptions concerning the magnitude of and distance scales involved in atmospheric water vapor transport.

Budyko (1974, pp. 239–243) used a simple one–dimensional model (which is described in Section 2.3) to estimate, for the European U.S.S.R., the contributions of locally evaporated and advected moisture to regional precipitation. Budyko defined β as the ratio of total precipitation to precipitation due to moisture advected from outside the region. On an annual basis, only about 10 percent of the precipitation in the European U.S.S.R. is of local origin, according to Budyko's estimate; on a monthly basis, the estimated contribution of locally–evaporated water ranged from four percent in October to 18 percent in April and May. Budyko stated, "Even on the most extensive continents, where the relative role of local evaporation is the greatest, as calculations show, the main portion of precipitation is formed from water vapor of external origin, not local." Shiklomanov (1989) used aerological data to enhance Budyko's model, and obtained monthly estimates of the local fraction of precipitation in the European U.S.S.R. ranging from .1 percent in January and February to 20 percent in June.

The significance of the oceans as sources of precipitation water to the continents is no longer disputed. This understanding of the atmospheric branch of the hydrologic cycle has been strengthened by analysis and observation during the last half century. However, during the same period, studies have shown that land regions can also be significant sources of water vapor to the atmosphere.

Thornthwaite (1946) observed that the average July evapotranspiration in the eastern United States (between 5.5 and 6.0 inches) exceeded the July

evaporation from the water surface in the Gulf of Mexico and the Caribbean (about 4.0 inches). Benton and Estoque (1954) showed that the North American continent, as a whole, is a source of moisture to the atmosphere in summer (May–August) and a sink during the rest of the year. Starr and Peixoto (1958) observed strong maxima of vapor flux divergence over three separate arid regions, implying a large excess of evaporation over precipitation in these areas. Stidd (1967) stated,

> If we consider that in most areas the soil will be drier in the fall than in the spring and that the difference will represent a *net* loss of moisture to the atmosphere (in the absence of runoff), it is not hard to understand that land areas in general furnish a source of moisture to the atmosphere in summer and that the oceans provide a sink, so that, in effect, the hydrologic cycle is reversed.

If the land surface acts as a significant source of moisture to the atmosphere during certain seasons, then it is reasonable to expect that the balance of locally–evaporated versus advected precipitation might be shifted during those seasons (assuming the presence of the dynamical processes required to produce precipitation at all). Furthermore, it is reasonable to expect that alterations in the storage properties or to the recharge–discharge cycle of the land surface and subsurface might affect the precipitation regime.

Stidd (1967) studied local modifications in climate following large–scale irrigation development in the Columbia River Basin. His analysis showed an increase in July and August precipitation, extending to several thousand square kilometers around the project. Fowler and Helvey (1974) re–examined the topic by alternate procedures and concluded that a large increase in precipitation due to nearby irrigation was improbable, and that Stidd's claim of a significant increase in precipitation did not appear sound. Stidd replied (1975) with statistical analysis supporting his earlier claim. He argued that Fowler and Helvey examined the problem on too small a scale, citing the fact

that the irrigation project lies near the center of the drainage basin, and that the additional moisture added to the air by irrigation would be expected to precipitate not immediately adjacent to the irrigation project, but in the foothills downwind, as the moist surface air is carried over the surrounding mountains. This explanation is in agreement with the statements of Benton et al. (1950) and McDonald (1962) that increasing the water vapor content of the air will increase precipitation only if an uplift mechanism exists.

Natural or anthropogenic changes that enhance (or inhibit) convection could alter the contribution of local moisture to precipitation. Dettwiller and Chagnon (1976) found upward trends in the warm season rainfall at Paris, St. Louis and Chicago, and suggested that the urban heat island contributes to larger and more intense shower clouds. Schickedanz (1976, pp. 99–100) found evidence for irrigation–related increases in summer rainfall in several areas of the U.S. Great Plains; he hypothesized that

> . . . any increased rainfall does not come directly from the increased atmospheric moisture alone, but by thermodynamic and physical side effects produced by the presence of a cool, moist dome over the irrigated area.

Anthes (1983) speculated that if human activities can inadvertently affect precipitation, perhaps humans could make intentional changes in surface characteristics so as to modify precipitation in a useful way. He proposed planting bands of vegetation in semi–arid regions, hypothesizing that the bands could increase convective precipitation through three mechanisms: increased low–level moist static energy, the generation of mesoscale circulations, and increased atmospheric water vapor.

Lettau et al. (1979) used climatonomic methods (Lettau, 1969) to quantify precipitation recycling in the Amazon River Basin, in an effort to assess the possible climatic consequences of large–scale deforestation in

the region. Among their results were estimates of the ratio of total regional precipitation to the regional flushing of precipitable water of direct oceanic origin (γ). In the six 5° wide regions that they analyzed, γ increased with distance downwind of the coast, reaching a maximum value of 1.884. This value of γ indicates that 47% of the precipitation falling on the subregion at 75°W has been most recently evaporated from the continent, both upwind of and within that particular subregion. It should be noted that Lettau et al.'s comparison of γ with Budyko's β for this inland region is not valid; β compares total precipitation to that of advective origin, where the advective term includes moisture evaporated from the land lying between the coast and the inland region's boundary in addition to water of oceanic origin, whereas γ compares total precipitation to that of oceanic origin only.

Salati et al. (1979) studied the inland gradient of the oxygen–18 content of precipitation in the Amazon Basin. For yearly–averaged station data, the gradient $d(\delta^{18}O)/dx$ is much smaller than in other continental areas. The small inland decrease in isotopic content of precipitation is an indication that significant amounts of moisture are added to the air mass as it passes over the region, and that this re–evaporated moisture is important in precipitation falling on the region; this effect varies with the season and the location. Salati et al. did not give a numerical estimate of precipitation recycling, but they cited a study by Marques et al. (1972), which found that inflowing moisture accounted for only 52 percent of the precipitation between Belém and Manaus.

In atmospheric General Circulation Models (GCMs), water can be tagged according to its evaporation site and traced in order to determine the relative contributions of different evaporative sources to a region's precipitation.

Joussame et al. (1986) conducted such an experiment for the month of July, using the Laboratoire de Meteorologie Dynamique GCM; they produced global charts showing the influence of ocean and continental source regions in continental precipitation. Koster et al. (1986) used the NASA/Goddard Institute for Space Studies GCM for a similar experiment, for all four seasons. Koster et al. (1988) also studied the inverse problem, that is, the characteristic distances and directions traveled by water evaporating from a source region. Shukla and Mintz (1982) conducted a sensitivity experiment with the Goddard Laboratory for Atmospheric Sciences GCM, in which two different constraints were placed upon the land–surface evapotranspiration: in the first case, no evapotranspiration was allowed, and in the second case, evapotranspiration was set equal to the model–calculated potential evapotranspiration. They found that "land–surface evapotranspiration has a large influence on the precipitation, temperature, and motion fields of the atmosphere."

The importance of land regions in supplying moisture to the atmosphere has been well demonstrated. There are indications that land–evaporated moisture supplies a large fraction of the precipitation for some continental regions. Questions remain concerning the contribution of *local* evaporation to *local* precipitation. Several quantitative estimates have been made, and there is general agreement on the physical factors necessary for such a recycling process to occur.

Recent research by Rodriguez–Iturbe et al. (1990a, 1990b, 1991) and by Entekhabi et al. (1991) has shown that the close coupling between the land surface and the atmosphere in continental–type climates helps to explain the statistical structures exhibited by climatic variables. In their work, the coupling is explicitly represented by including the precipitation recycling

mechanism in the land surface water balance equation. The resulting functional dependence of precipitation on soil moisture, together with the stochastic nature of soil and climate parameters, results in a bimodal probability distribution of soil moisture states, corresponding to drought and pluvial conditions. Further, the dynamics of the soil moisture equation can exhibit fixed point, limit cycle and chaotic behavior.

The importance of precipitation recycling as an index of land surface–atmosphere coupling is a compelling motivation for further study of this process and for quantification of the degree to which it is active over a variety of continental regions.

2.3 Recycling Model

Budyko's Model

Budyko (1974) considered a land region having length scale ℓ, average precipitation P, and average evapotranspiration E. The average precipitation is composed of an advective portion (P_a) and a local evaporative portion (P_m), i.e.,

$$P = P_a + P_m \ . \tag{2.1}$$

The water vapor content of the air moving across the region is also composed of an advected and an evaporated portion. As shown in Figure 2.2, air enters the region at velocity u and with moisture content w. The vertical flux quantities--P_a, P_m and E--are treated as constants equal to their average values; therefore the locally–evaporated moisture content of the air increases

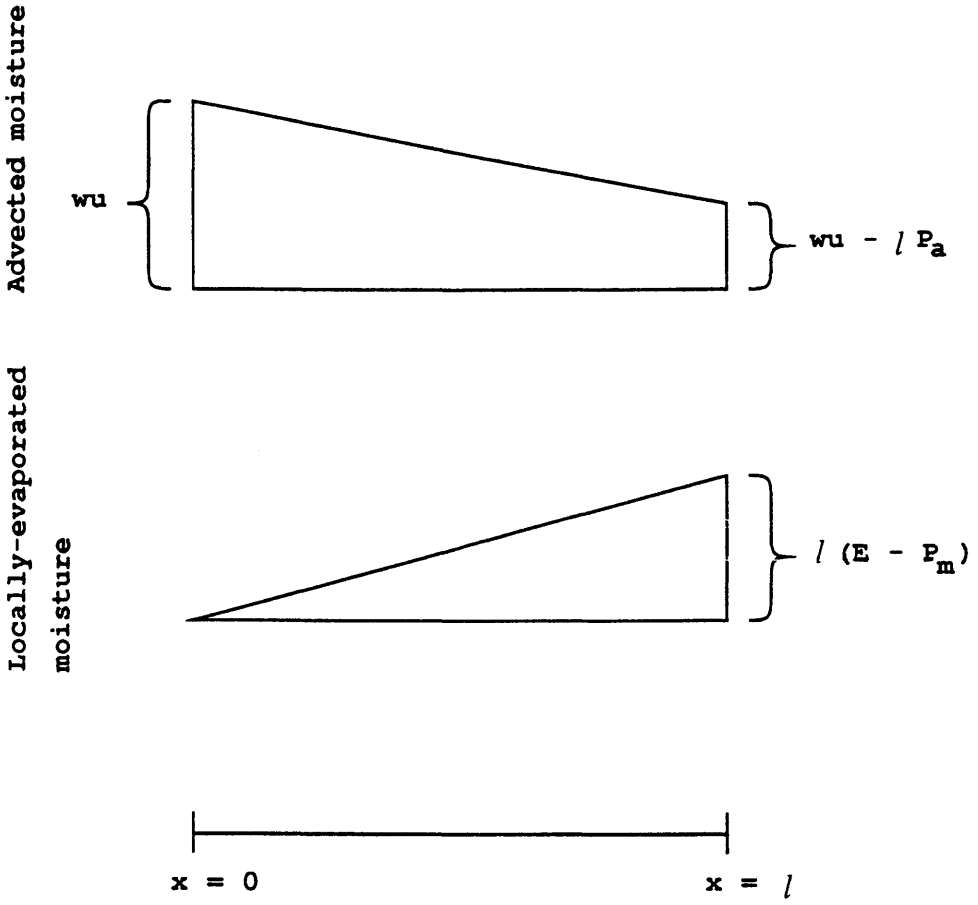

Figure 2.2: Fractions of advected and locally–evaporated moisture in the air as it moves across a region of length ℓ.

linearly, and the advected moisture content decreases linearly, as the air moves across the region. It follows that the average horizontal flux of advected moisture over the region is

$$Q_a = wu - \frac{\ell P_a}{2} \tag{2.2}$$

and the average horizontal flux of locally–evaporated moisture is

$$Q_m = \frac{\ell}{2}(E - P_m) \ . \tag{2.3}$$

The atmosphere is assumed to be fully mixed, so that the ratio of advected to locally–evaporated water falling as precipitation is equal to the ratio of advected to evaporated moisture present in the air. That is

$$\frac{P_a}{P_m} = \frac{Q_a}{Q_m} = \frac{wu - \frac{\ell P_a}{2}}{\frac{\ell}{2}(E - P_m)} \ . \tag{2.4}$$

Equations (2.4) and (2.1) are solved for the ratio of total to advected precipitation, which is Budyko's recycling coefficient (β):

$$\beta \equiv \frac{P}{P_a} = 1 + \frac{E\ell}{2wu} \ . \tag{2.5}$$

The second term on the right–hand side of (2.5) is the ratio of locally–evaporated to advected precipitation. In this model the relative contribution of locally–evaporated water is directly proportional to the evaporation rate and the length scale of the region, and inversely proportional to the rate at which external moisture enters the region. The inverse of β is the fraction of precipitation due to advective origin, i.e.,

$$\frac{P_a}{P} = \frac{1}{\beta} \tag{2.6}$$

and the fraction of precipitation due to local origin is

$$\frac{P_m}{P} = 1 - \frac{1}{\beta} . \tag{2.7}$$

Shiklomanov's (1989) estimates of the recycling coefficient made use of the improved availability of aerological data, rather than estimates of average moisture content and wind speed. The equation or equations that Shiklomanov used to compute the recycling coefficients are not presented in his paper; however, the tabulations indicate that the procedure used was based upon extending Budyko's arguments to a *two–dimensional* land region, with moisture influx and efflux through the sides of an atmospheric control volume. As shown in Figure 2.3, the boundary of the region consists of a segment or set of segments (γ_{in}) across which the atmospheric moisture flux is inward, and a segment or set of segments (γ_{out}) across which the flux is outward. Integrating $\overline{Q} \cdot \hat{n}_\gamma$ separately over the two parts of the boundary gives F^+, the influx, and F^-, the efflux, of atmospheric moisture through the sides of the control volume:

$$F^+ \equiv - \oint_{\gamma_{in}} \vec{Q} \cdot \hat{n}_\gamma \, d\gamma \tag{2.8a}$$

and

$$F^- \equiv \oint_{\gamma_{out}} \vec{Q} \cdot \hat{n}_\gamma \, d\gamma \tag{2.8b}$$

in which $\hat{n}_\gamma$ is the *outward* unit normal vector.

By definition, F^+ contains only advective moisture; F^- contains the advected moisture that remains after P_a is removed, as well as moisture of local origin:

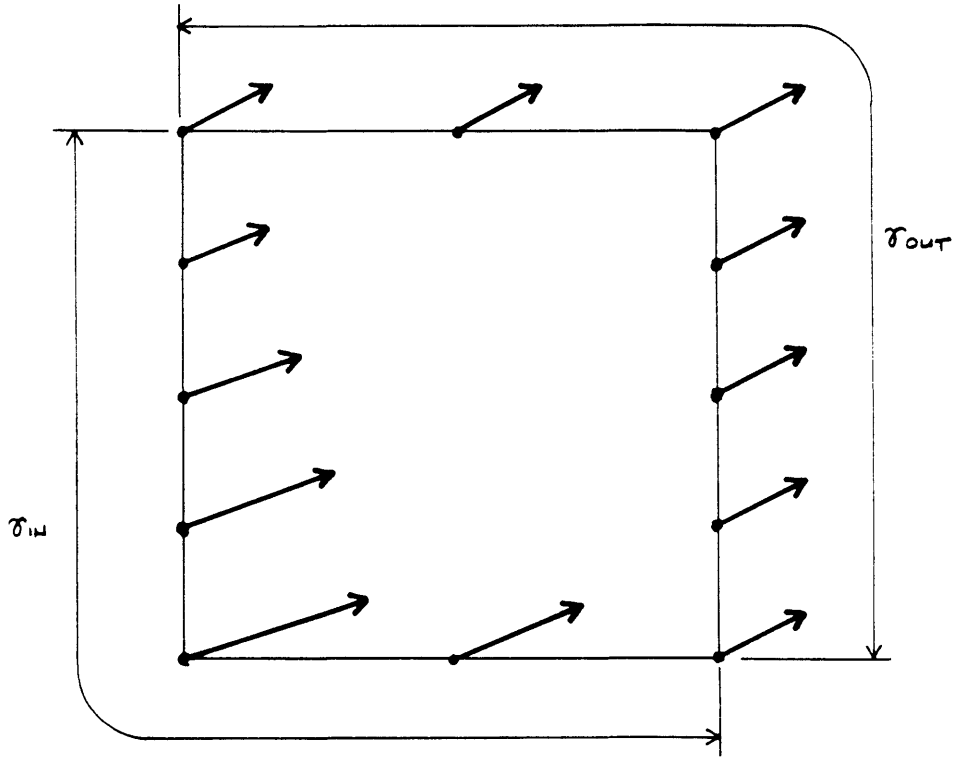

Figure 2.3: Plan view of a region, showing segments of the boundary (γ) across which the atmospheric moisture flux is inward (γ_{in}) and outward (γ_{out}).

$$F^{-} = (F^{+} - P_a A) + (E - P_m)A \tag{2.9}$$

in which A is the area of the region, and P_a, P_m and E are the rates of advective and local precipitation and evaporation per unit area. If the average horizontal flux of advected moisture over the region is taken as the arithmetic mean of the incoming and outgoing advective moisture, then

$$Q_a = \frac{F^{+} + (F^{+} - P_a A)}{2} = F^{+} - \frac{P_a A}{2} . \tag{2.10}$$

Likewise, the average horizontal flux of locally–evaporated moisture is the mean of the incoming and outgoing local portions,

$$Q_m = \frac{0 + (E - P_m)A}{2} = \frac{(E - P_m)A}{2} . \tag{2.11}$$

Invoking, as before, the assumption of a well–mixed atmosphere, the recycling ratio is

$$\frac{P}{P_a} = 1 + \frac{EA}{2F^{+}} . \tag{2.12}$$

Equation (2.12) is identical to (2.5), with F^{+} replacing wu, and A replacing ℓ.

Application of the Model in the Present Study

Depending upon the geometry of the region and the spatial variability of $\vec{Q}$, F^{+} as defined in (2.8a) may not be strictly analogous to wu in Budyko's one–dimensional model. Figure 2.4 shows an example of a situation in which the analogy is weak; the mean wind blows at an angle, α, to the axis of the region. The moisture influx across segment γ_1 is greater than that across segment γ_2; however, the air entering across γ_2 travels greater distances across

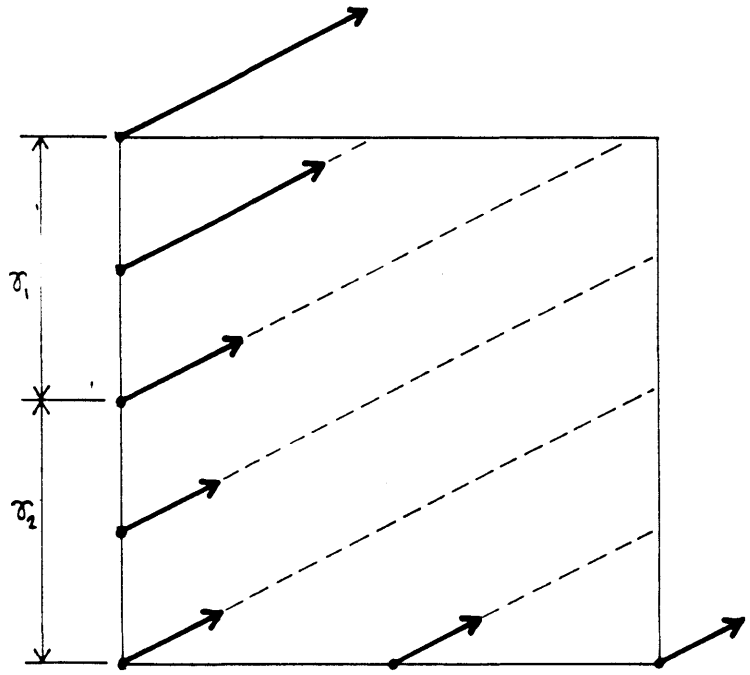

Figure 2.4: Plan view of a region in which F^+, the net moisture influx, is not strictly analogous to wu in Budyko's model.

the region. A more representative value of the moisture influx is an average value weighted according to the distance traveled across the region. Alternatively, one might delineate the region parallel to the direction of flow; however, the latter approach is undesirable for two reasons. First, the direction of flow may change with the seasons, whereas the study region should remain fixed. Second, the need for interpolation is minimized if regions are defined by connected nodes on the latitude–longitude grid of the data set. The following procedure is used in the present study to determine effective values of ℓ and wu in Budyko's original equation:

A simple rectangular region is defined by connected nodes on the grid of the data set. A spatial average of $\vec{Q}$, $\langle\vec{Q}\rangle$, is computed by areally averaging the components of $\vec{Q}$ over the region. A unit direction vector is defined,

$$\hat{u} \equiv \frac{\langle\vec{Q}\rangle}{\|\langle\vec{Q}\rangle\|} \tag{2.13}$$

which is, essentially, the moisture–weighted average direction of air flow across the region. This direction establishes one or two sides of the rectangle as the influx boundary, and one or two as the efflux boundary.

The effective length, ℓ_{eff}, is the average distance across the region in the direction of $\hat{u}$. The expression for ℓ_{eff} is derived in Appendix A; the result is as follows:

$$\ell_{eff} = \frac{\Delta x\ \Delta y}{\Delta y|\cos\theta| + \Delta x|\sin\theta|} = \frac{A}{\Delta y|\cos\theta| + \Delta x|\sin\theta|} \tag{2.14}$$

where θ is the angle formed by $\hat{u}$ and the positive x axis, Δy is the south–north length of the region, and Δx is the mean west–east length of the region,

$$\Delta x \equiv \frac{A}{\Delta y} . \tag{2.15}$$

The definition of Δx arises from the latitude–dependent relation of degrees longitude and west–east distance on the globe.

The moisture influx term, $(wu)_{eff}$, is computed as the length–weighted average of the moisture flux vector component parallel to $\hat{u}$ across the influx boundary, i.e.,

$$(wu)_{eff} = \frac{\oint_{\gamma_a}^{\gamma_b} (\vec{Q} \cdot \hat{u})\ \ell(\gamma) \sin \alpha \, d\gamma}{A} \tag{2.16}$$

where γ_a and γ_b are the endpoints of the influx boundary and α is the angle formed by $\hat{u}$ and $\vec{d\gamma}$ (the derivation of this expression is given in Appendix A).

The recycling model, incorporating the effective parameters, is

$$\beta = \frac{P}{P_a} = 1 + \frac{\ell_{eff} E}{2(wu)_{eff}} . \tag{2.17}$$

Equation (2.17) is formally identical to (2.5); however, the spatial variability of the aerological data is incorporated through use of the effective length and effective moisture influx terms. The recycling coefficient, β, as estimated by (2.17), is representative of the region only to the extent that $\hat{u}$ is representative.

2.4 Estimation Techniques and Study Regions

The ratio of local to total precipitation, P_M/P, was estimated using (2.7) and (2.17). The effective length and effective moisture influx terms were computed from the GFDL data as described in Appendix A.

Evapotranspiration was computed from (1.7), neglecting $\langle \frac{\partial W}{\partial t} \rangle$, i.e.,

$$\langle E \rangle \cong \langle P \rangle + \frac{1}{A} \oint \vec{Q} \cdot \hat{n}_\gamma \, d\gamma = \langle P \rangle + \langle \nabla \cdot \vec{Q} \rangle \qquad (2.18)$$

in which all quantities now refer to mean monthly values, and the overbar is dropped for simplicity. The rationale for estimating evapotranspiration as a residual is that the atmospheric water balance reflects *actual* evapotranspiration, whereas pan evaporation data estimate *potential* evapotranspiration, and model equations for actual evapotranspiration generally require estimates of soil and vegetation parameters that would be difficult to obtain for all regions, and on continental scales.

The divergence term, $\langle \nabla \cdot \vec{Q} \rangle$, was computed from the GFDL data as described in Section 1.4. Regional average precipitation, $\langle P \rangle$, was computed by the Thiessen polygon method from the NCAR station data as follows: First, $\langle P \rangle$ was computed for each month from May 1963 through April 1973, then the ten January values, ten February values, and so on, were averaged to give a set of monthly average precipitation figures representative of the 10–year period. Estimation by (2.17) is referred to as the *Modified 1–D* method hereafter.

The ratio P_m/P was also estimated using (2.12), in order to make a comparison of the two methods and to evaluate the claim that $(wu)_{eff}$ is more representative of the moisture influx than F^+. Estimation by (2.12) is referred to as the *2–D* method. The 2–D method is computationally simpler than the Modified 1–D method because the terms $F^+$and F^- can be incrementally summed as trapezoidal rule integration proceeds along the boundary, by adding each f_k to the appropriate sum according to its sign. The Modified 1–D

method is currently developed only for rectangular study regions, which limits its usefulness somewhat.

Besides the rectangularity requirement, there were no constraints on the selection of continental regions for analysis. As explained before, the method is general, in that the distinction is made between local and advected precipitation, rather than terrestrial and oceanic precipitation. The method can, therefore, be applied to regions in the interior of continents as well as coastal regions. Regions were selected on the basis of hydrological interest and the existence of former recycling estimates with which to compare the results.

The four regions selected for analysis are shown in Figure 2.5. The North American region lies east of the Continental Divide and within the Mississippi basin (except for the northeast corner, which lies in the Great Lakes drainage). Several estimates of local recycling or of the land–evaporated fraction of precipitation have been made for this region, which receives atmospheric moisture from the west and the south. The European region corresponds roughly to the European part of the U.S.S.R., a region for which monthly water budgets and recycling ratios have been reported by Budyko (1984) and Shiklomanov (1989). The South American region contains most of the Amazon river system and rainforest. This region is currently the focus of intense hydroclimatological interest, due to the threat of massive deforestation, with possible ramifications for the region's climate, and the climate system of the Earth as a whole. The African region lies south of the Sahara Desert and includes most of the drainage basin of the Niger River. This region is threatened by drought and desertification, and its annual cycle of atmospheric moisture supply exhibits unique characteristics.

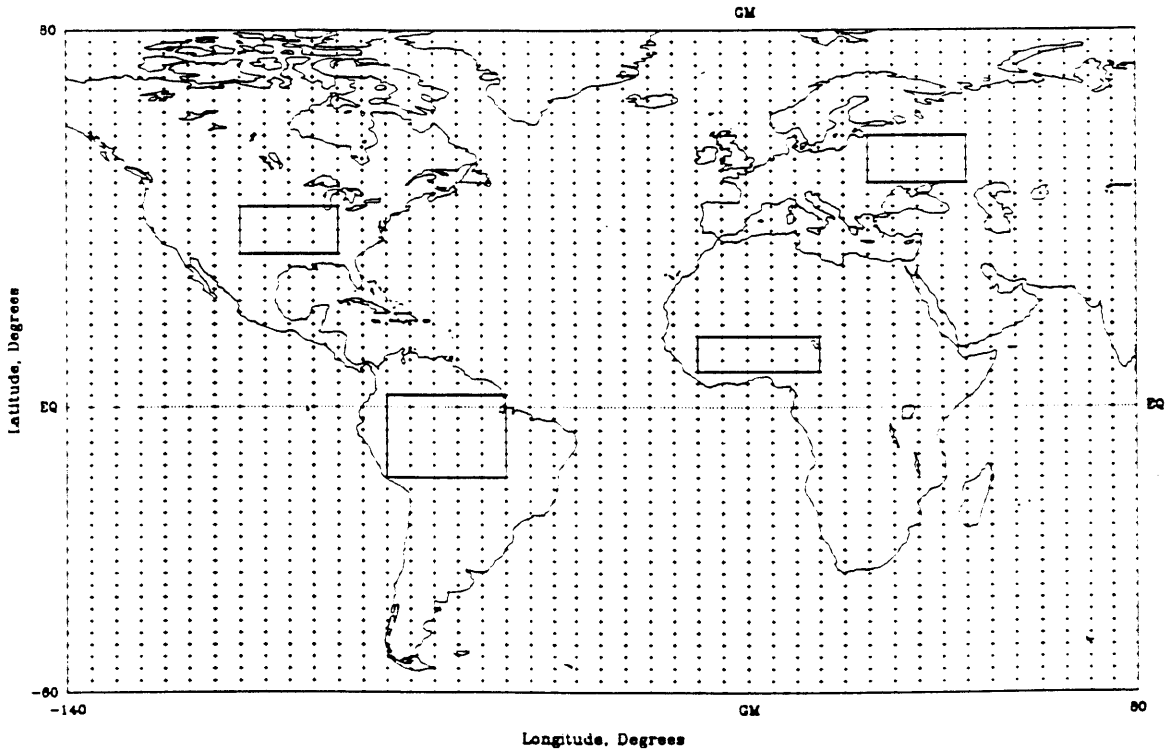

Figure 2.5: Regions selected for precipitation recycling analysis. The analysis technique dictated a rectangular shape; otherwise, the regions were chosen on the basis of hydrological and historical interest.

2.5 Results

Eurasian Region

The results for the Eurasian region are presented in graphic form in Figures 2.6 through 2.8, and in tabular form in Tables 2.1 and 2.2. By the Modified 1–D method, the greatest recycled fraction of precipitation (Figure 2.6) is 0.39 in June, and the lowest is 0.0 in February. By the 2–D method, the largest P_m/P is also in June, but somewhat lower than the Modified 1–D result. Figure 2.7 shows separate plots of the various terms used in calculating P_m/P. The annual march is as expected for atmospheric moisture convergence, precipitation, and evaporation. The fourth plot in Figure 2.7 compares the influx terms used in the two estimation methods. Equation (2.17) can be rewritten as

$$\beta = 1 + \frac{E}{2\,\frac{(wu)_{eff}}{\ell_{eff}}} \tag{2.19}$$

and (2.12) as

$$\beta = 1 + \frac{E}{2\,\frac{F^+}{A}} \,. \tag{2.20}$$

The terms in the denominator both represent normalized influx terms and have units of length. For the Eurasian region, $(wu)_{eff}/\ell_{eff}$ is consistently less than F^+/A except in July. The difference is greatest in May and June. Figure 2.8 is included to illustrate the reasons for such differences. Figure 2.8 is a set of bar graphs of the boundary flux of water vapor, as introduced in Section 1.4. The pattern in May recalls Figure 2.4, the constructed example of a situation on which F^+ is not perfectly analogous to Budyko's wu. The bars in Fig. 2.8 do not represent vector components, as do the lines in Fig. 2.4; nonetheless, the same arguments apply: $(wu)_{eff}/\ell_{eff}$ is less than F^+/A because the former

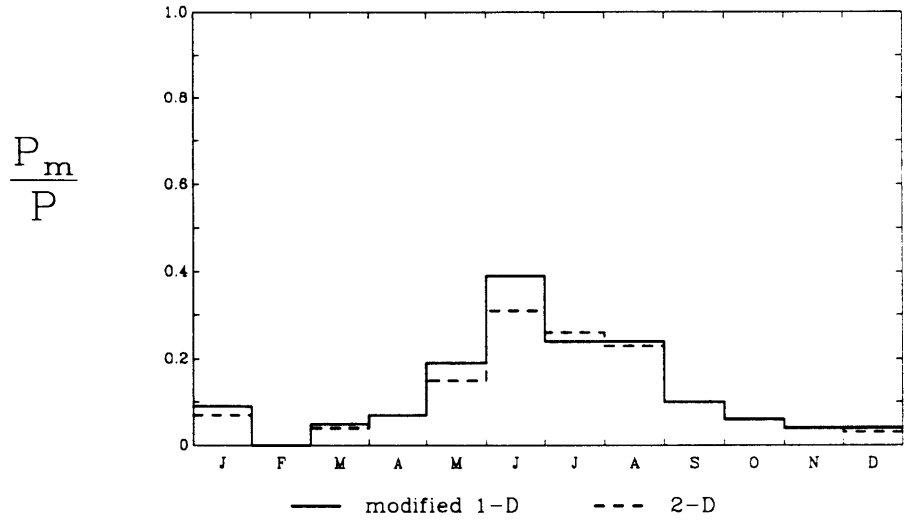

Figure 2.6: Eurasian Region. The ratio of locally–evaporated to total precipitation, as estimated by the Modified 1–D and the 2–D method.

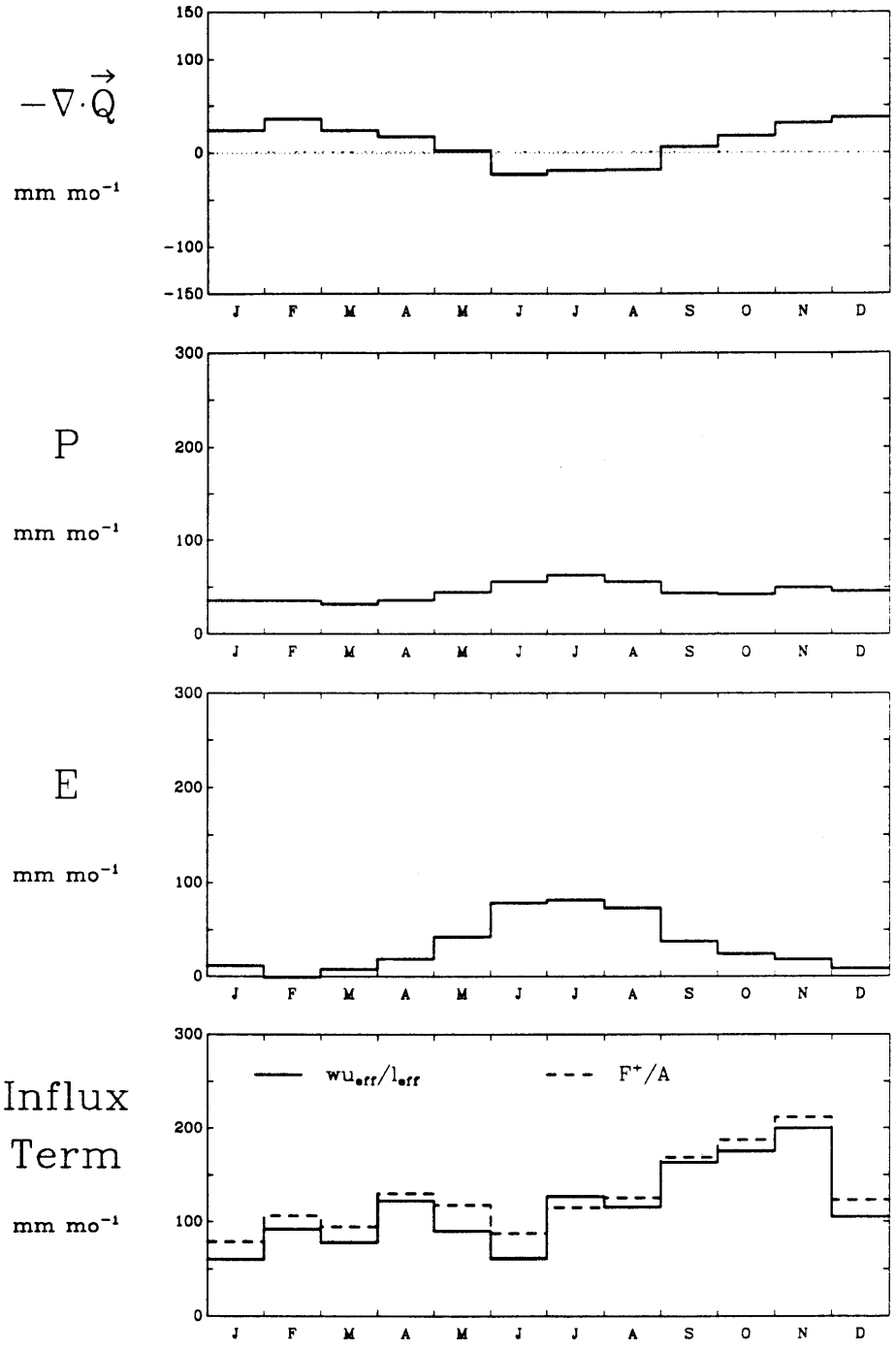

Figure 2.7: Eurasian Region. Terms used in estimating P_m/P by two methods. Atmospheric moisture convergence ($-\nabla\cdot\vec{Q}$), Precipitation (P) and Evaporation (E) are common to both methods; wu_{eff}/ℓ_{eff} is used in the Modified 1–D method, F^+/A in the 2–D method.

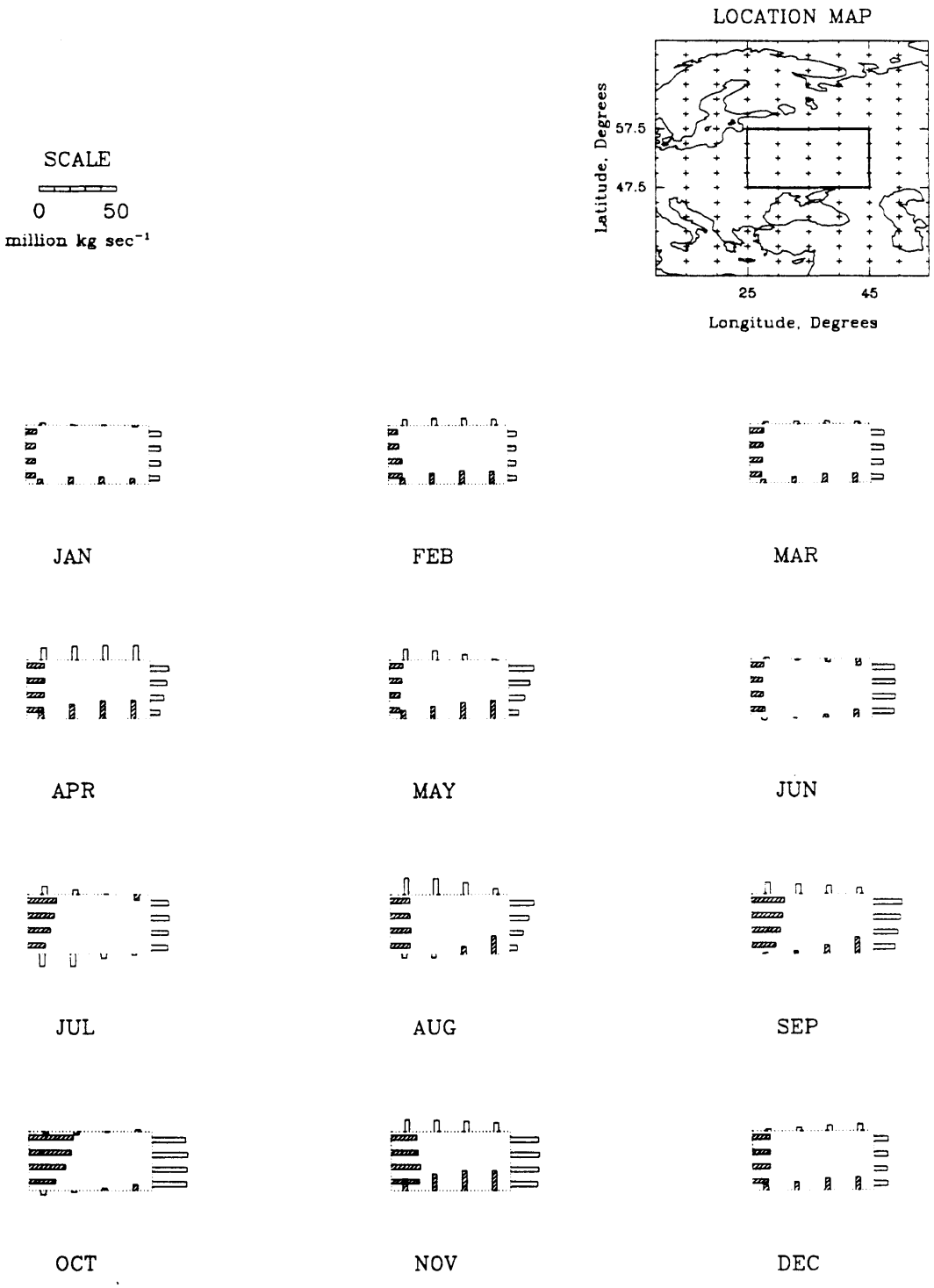

Figure 2.8: Eurasian Region. Bar graphs of the moisture flux across segments of the boundary. Each bar represents the integral of the normal component of $\vec{Q}$ along the segment at the base of the bar.

Table 2.1 Eurasian Region. Components in the estimation of P_m/P.

				Modified 1-D Method							2-D Method			
Month	-DivQ	P	E	Theta	L(eff)	wu(eff)	wu(eff) / L(eff)	P / P(a)	P(a) / P	P(m) / P	F+ / A	P / P(a)	P(a) / P	P(m) / P
	[mm/mo]	[mm/mo]	[mm/mo]	[deg]	[m]	[m mm/mo]	[mm/mo]				[mm/mo]			
jan	24.0	35.3	11.3	14.8	1.06E+06	6.38E+07	60.3	1.09	0.91	0.09	79.0	1.07	0.93	0.07
feb	36.5	35.7	-0.8	38.2	8.79E+05	8.12E+07	92.3	1.00	1.00	-0.00	106.4	1.00	1.00	-0.00
mar	24.4	32.2	7.8	18.7	1.01E+06	7.91E+07	78.2	1.05	0.95	0.05	94.8	1.04	0.96	0.04
apr	17.3	36.3	19.0	41.2	8.70E+05	1.06E+08	122.2	1.08	0.93	0.07	130.4	1.07	0.93	0.07
may	2.2	44.7	42.5	38.6	8.78E+05	7.91E+07	90.1	1.24	0.81	0.19	117.6	1.18	0.85	0.15
jun	-22.6	56.0	78.6	0.4	1.34E+06	8.19E+07	61.1	1.64	0.61	0.39	87.6	1.45	0.69	0.31
jul	-18.4	63.1	81.5	-7.6	1.17E+06	1.49E+08	126.9	1.32	0.76	0.24	115.2	1.35	0.74	0.26
aug	-17.7	55.7	73.4	30.3	9.15E+05	1.06E+08	115.6	1.32	0.76	0.24	125.6	1.29	0.77	0.23
sep	6.4	43.9	37.5	15.9	1.04E+06	1.71E+08	163.5	1.11	0.90	0.10	168.7	1.11	0.90	0.10
oct	18.3	42.7	24.4	-1.4	1.31E+06	2.31E+08	175.6	1.07	0.94	0.06	187.9	1.06	0.94	0.06
nov	31.9	50.0	18.1	24.1	9.59E+05	1.92E+08	200.2	1.05	0.96	0.04	211.9	1.04	0.96	0.04
dec	37.7	46.0	8.3	19.5	1.00E+06	1.05E+08	105.1	1.04	0.96	0.04	123.1	1.03	0.97	0.03

Table 2.2 Comparison of estimates of the recycled fraction of precipitation and intermediate terms for the Eurasian region.

	jan	feb	mar	apr	may	jun	jul	aug	sep	oct	nov	dec
P(m)/P [Percent]												
Budyko (1974), European USSR	7	9	8	18	18	16	14	10	8	4	5	6
Shiklomanov (1989), European USSR	0	0	0	10	13	18	20	14	9	8	2	1
This Study, Eurasian Region												
Modified 1-D Method	9	0	5	7	19	39	24	24	10	6	4	4
2-D Method	7	0	4	7	15	31	26	23	10	6	4	3
-DivQ [mm/mo]												
Shiklomanov (1989), European USSR	34	31	32	13	17	-14	-20	-4	13	23	51	35
This Study, Eurasian Region	24	37	24	17	2	-23	-18	-18	6	18	32	38
Precipitation [mm/mo]												
Budyko (1974) European USSR	27	23	24	28	38	55	63	59	51	49	38	32
Shiklomanov (1989), European USSR	36	32	32	35	57	69	81	76	65	64	61	40
This Study, Eurasian Region	35	36	32	36	45	56	63	56	44	43	50	46
Evapotranspiration [mm/mo]												
Budyko (1974) European USSR	5	5	10	36	50	54	50	39	22	11	7	5
Shiklomanov (1989), European USSR	0	0	1	26	45	87	107	77	46	36	7	2
This Study, Eurasian Region	11	-1	8	19	43	79	82	73	38	24	18	8
Influx Term [mm/mo]												
F+/A												
Shiklomanov (1989), European USSR (1)	100	82	89	97	141	157	172	186	178	162	146	111
This Study, Eurasian Region	79	106	95	130	118	88	115	126	167	188	212	123
wu/l												
Budyko (1974), European USSR (2)	35	36	53	74	113	142	152	158	126	103	70	43
wu(eff)/l(eff)												
This Study, Eurasian Region	60	92	78	122	90	61	127	116	164	176	200	105

(1) Assuming area = 5.76E+6 km^2 (2) Assuming l = 2300 km

weights the flux at the west end of the southern boundary more heavily than that at the east end, whereas the latter gives equal weight to all the influx. In June, the direction of moisture transport across the region is nearly due eastward; therefore $(wu)_{eff}/\ell_{eff}$ neglects the small influxes over the northern and southern boundaries, whereas F^+ includes them. The computations for both the Modified 1–D and 2–D methods are summarized in Table 2.1.

In Table 2.2, the intermediate calculations and the final P_m/P results are compared to the work of Budyko (1974) and Shiklomanov (1989). This study is in general agreement with their results in all but the summer months, lending further support to the claim that external moisture sources dominate in supplying precipitation to this region for much of the year. The differences in the summer months may simply be due to use of different study regions (the region considered in this study does not include the entire European U.S.S.R, which was the study region for the former work) and different data sets.

North American Region

The results for the North American region are presented in Figures 2.9 through 2.11 and in Table 2.3. The order of presentation is the same as for the Eurasian region. Referring to Figure 2.9, P_m/P as computed by the modified 1–D method lies between 0.2 and 0.4, with the notable exception of 0.63 in July and August. The minimum P_m/P by the Modified 1–D method occurs in April. By the 2–D method, P_m/P lies between 0.15 and 0.35, with minima in April and December; in July and August P_m/P by the 2–D method is half as large as by the Modified 1–D method. Referring to Figure 2.10, the annual march of $-\nabla\cdot\vec{Q}$ computed for this region is highly questionable. The

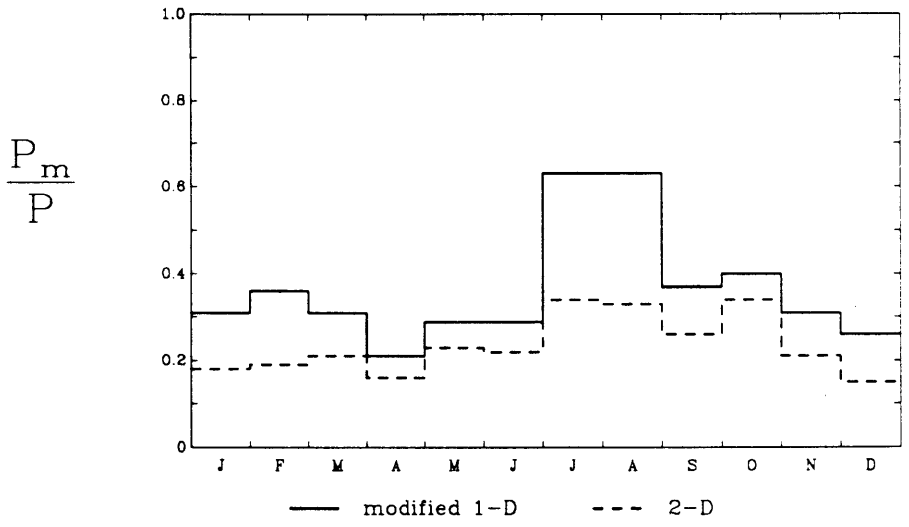

Figure 2.9: North American Region. The ratio of locally–evaporated to total precipitation, as estimated by the Modified 1–D and the 2–D method.

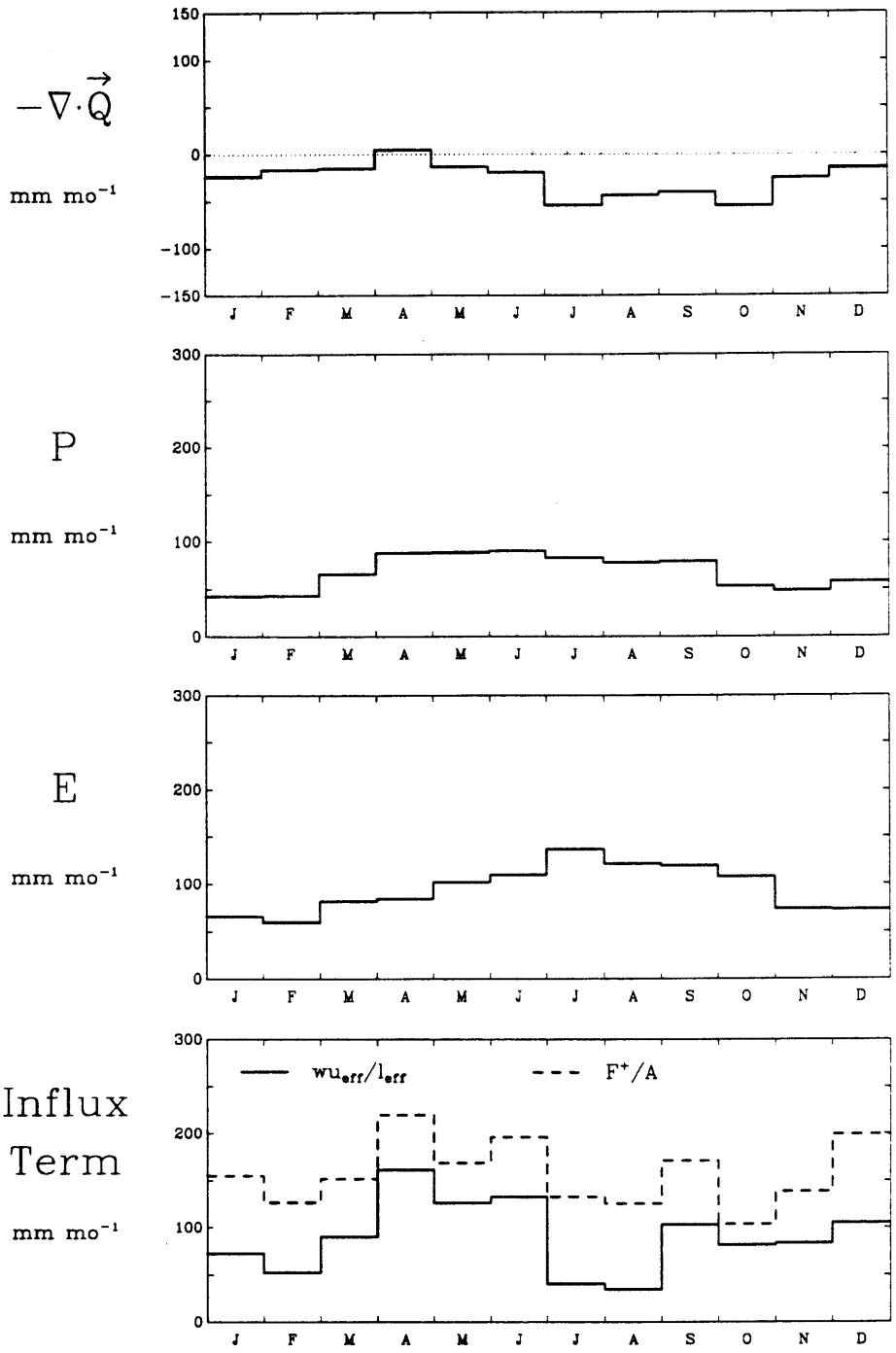

Figure 2.10: North American Region. Terms used in estimating P_m/P by two methods. Atmospheric moisture convergence ($-\nabla\cdot\vec{Q}$), Precipitation (P) and Evaporation (E) are common to both methods; wu_{eff}/ℓ_{eff} is used in the Modified 1–D method, F^+/A in the 2–D method.

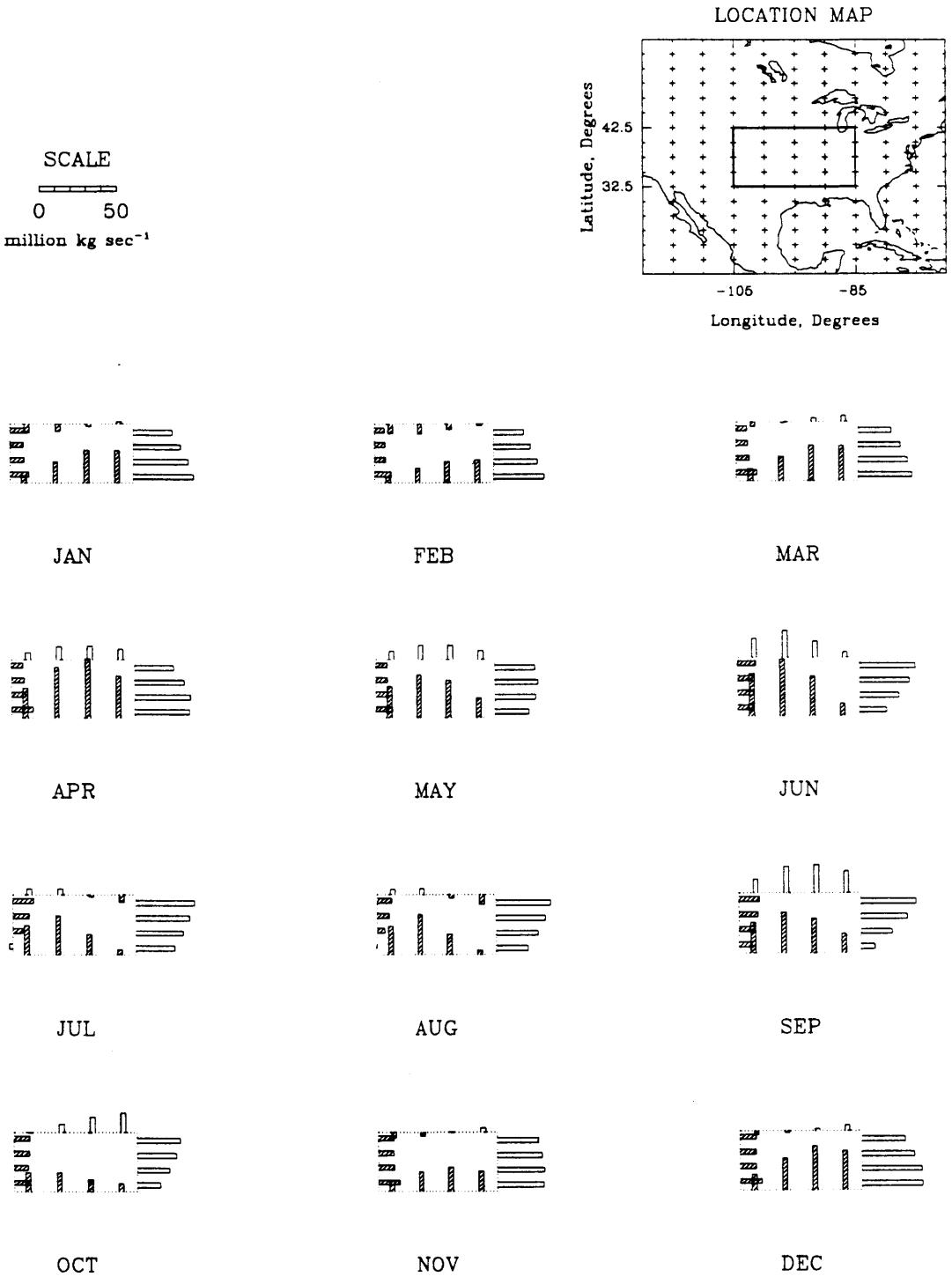

Figure 2.11: North American Region. Bar graphs of the moisture flux across segments of the boundary. Each bar represents the integral of the normal component of $\vec{Q}$ along the segment at the base of the bar.

Table 2.3 North American Region. Components in the estimation of P_m/P.

				Modified 1-D Method							2-D Method			
Month	-DivQ	P	E	Theta	L(eff)	wu(eff)	wu(eff) / L(eff)	P / P(a)	P(a) / P	P(m) / P	F+ / A	P / P(a)	P(a) / P	P(m) / P
	[mm/mo]	[mm/mo]	[mm/mo]	[deg]	[m]	[m mm/mo]	[mm/mo]				[mm/mo]			
jan	-23.4	42.5	65.9	7.4	1.47E+06	1.07E+08	72.4	1.46	0.69	0.31	155.0	1.21	0.82	0.18
feb	-16.4	43.4	59.8	3.4	1.61E+06	8.43E+07	52.3	1.57	0.64	0.36	126.5	1.24	0.81	0.19
mar	-15.1	66.4	81.5	14.0	1.30E+06	1.17E+08	90.0	1.45	0.69	0.31	151.7	1.27	0.79	0.21
apr	4.3	88.5	84.2	26.8	1.10E+06	1.77E+08	161.7	1.26	0.79	0.21	219.5	1.19	0.84	0.16
may	-13.3	88.8	102.1	26.3	1.10E+06	1.39E+08	126.1	1.40	0.71	0.29	168.7	1.30	0.77	0.23
jun	-19.2	90.7	109.9	29.8	1.06E+06	1.42E+08	133.0	1.41	0.71	0.29	196.4	1.28	0.78	0.22
jul	-54.1	83.4	137.5	12.8	1.33E+06	5.36E+07	40.3	2.70	0.37	0.63	133.2	1.52	0.66	0.34
aug	-43.2	78.2	121.4	15.7	1.27E+06	4.44E+07	35.1	2.73	0.37	0.63	125.6	1.48	0.67	0.33
sep	-40.1	79.5	119.6	29.6	1.07E+06	1.10E+08	103.4	1.58	0.63	0.37	171.2	1.35	0.74	0.26
oct	-54.4	53.5	107.9	15.9	1.26E+06	1.03E+08	81.6	1.66	0.60	0.40	104.0	1.52	0.66	0.34
nov	-25.2	48.9	74.1	7.6	1.47E+06	1.23E+08	83.8	1.44	0.69	0.31	138.6	1.27	0.79	0.21
dec	-15.0	58.0	73.0	12.6	1.33E+06	1.40E+08	105.2	1.35	0.74	0.26	199.4	1.18	0.85	0.15

top frame of Figure 2.10 shows atmospheric moisture convergence into this region only during April, and of very low magnitude. If $-\nabla\cdot\vec{Q}$ is systematically underestimated, then E is overestimated, which would inflate the P_m/P estimates.

For this region, F^+/A is significantly higher than $(wu)_{eff}/\ell_{eff}$ for most of the year, which results from the fact that a large part of the moisture influx occurs across the southern boundary (Figure 2.11), while at the same time the average direction of transport, θ in Table 2.3, is toward the east or northeast. As a result, the magnitude of $(wu)_{eff}$ is only slightly affected by the largest boundary influxes. In particular, for the months of July and August, the boundaries that are defined by θ as "influx" boundaries actually contain segments where the flux is outward; furthermore, these outward fluxes (in the southwest corner), although small, are the most heavily weighted terms in the computation of $(wu)_{eff}$.

For two GCM grid squares roughly corresponding to the region considered here, Koster et al.'s (1986) GCM tracer test showed that the percentage contributions of the North American source region to local precipitation were 36.4 and 41.6 percent in winter, and 80.1 and 61.9 in summer, for the western and eastern grid squares, respectively. The comparison is not exact, because Koster et al.'s North American source region is the entire continent, whereas this study considers only the evaporation and transpiration from within the study region. However, it is interesting to note the qualitative agreement between the estimates.

Both estimation methods give P_m/P considerably greater than Benton et al.'s (1950) estimate that 10 percent or less of precipitation on the Mississippi watershed has its evaporative source within the region. Their estimate was

based on distinguishing between continental and maritime air masses, with the assumption that evapotranspiration is greater into the former, and precipitation greater from the latter. The methods in the present study lump all air into the same averaging process, essentially ignoring any correlation between evapotranspiration or precipitation and air mass source.

South American Region

The results of the South American region are presented in Figures 2.12 through 2.14 and in Table 2.4. The order of presentation is the same as for the preceding regions. Referring to Figure 2.12, P_m/P by the Modified 1–D method is less than 0.3 for all twelve months, with maxima of 0.27 in October and November, a minimum of 0.13 in June, and values near 0.15 from July through September. The results by the 2–D method are very similar, with slightly higher values in the Southern Hemisphere summer, reaching 0.32 in December. Referring to Figure 2.13, divergence calculations show the region to be a sink of atmospheric moisture throughout the year, but particularly in the first four months of the year, corresponding to the southernmost excursion of the Intertropical Convergence Zone (ITCZ) during the Southern hemisphere (SH) summer. The season of least recycling is also the season of least precipitation and least evapotranspiration, the SH winter. Even then, the magnitudes of E and P are quite high, as can be seen by comparing Figure 2.13 to Figure 2.7 and Figure 2.11 (the latter with caution, noting the probable overestimation of E for the North American region.)

The boundary flux pattern (Figure 2.14) illustrates a conceptual problem in the Modified 1–D method. Consider the month of July. During July, the average direction of moisture flux was determined to be 168° (i.e., from the southeast), defining the southern and the eastern boundaries as influx

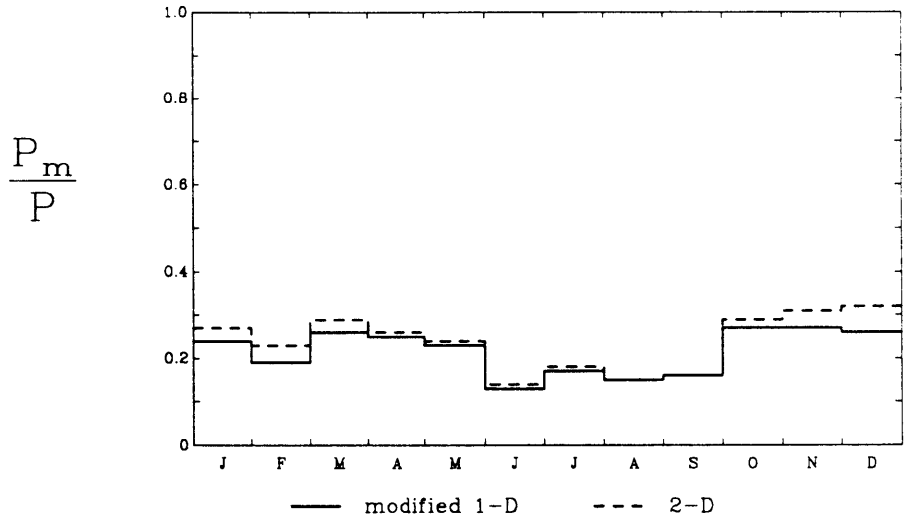

Figure 2.12: South American Region. The ratio of locally–evaporated to total precipitation, as estimated by the Modified 1–D and the 2–D method.

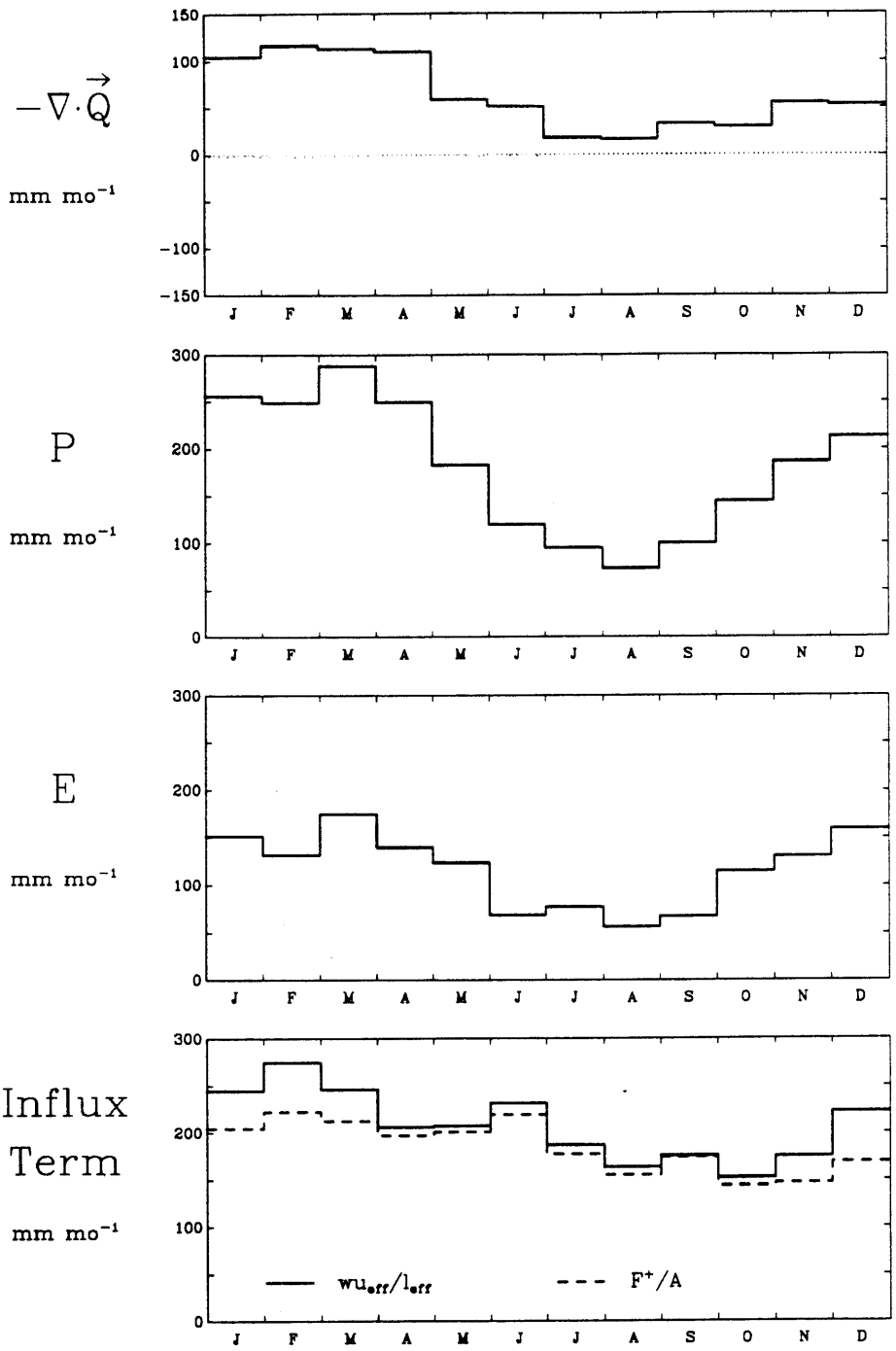

Figure 2.13: South American Region. Terms used in estimating P_m/P by two methods. Atmospheric moisture convergence $(-\nabla\cdot\vec{Q})$, Precipitation (P) and Evaporation (E) are common to both methods; wu_{eff}/ℓ_{eff} is used in the Modified 1–D method, F^+/A in the 2–D method.

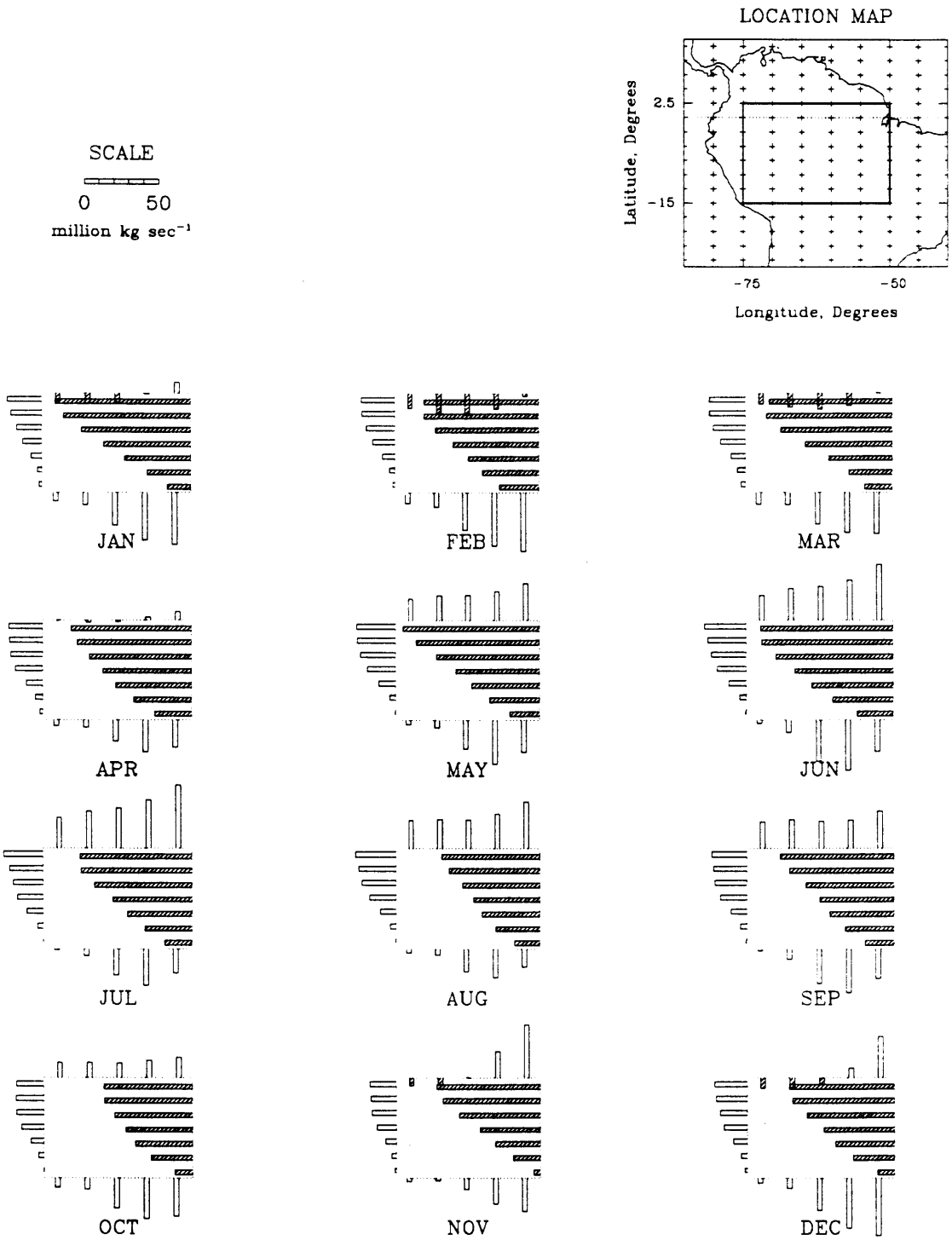

Figure 2.14: South American Region. Bar graphs of the moisture flux across segments of the boundary. Each bar represents the integral of the normal component of $\vec{Q}$ along the segment at the base of the bar.

Table 2.4 South American Region. Components in the estimation of P_m/P.

				Modified 1-D Method							2-D Method			
Month	-DivQ	P	E	Theta	L(eff)	wu(eff)	wu(eff) / L(eff)	P / P(a)	P(a) / P	P(m) / P	F+ / A	P / P(a)	P(a) / P	P(m) / P
	[mm/mo]	[mm/mo]	[mm/mo]	[deg]	[m]	[m mm/mo]	[mm/mo]				[mm/mo]			
jan	104.3	255.8	151.5	-172.2	2.33E+06	5.70E+08	244.9	1.31	0.76	0.24	204.6	1.37	0.73	0.27
feb	116.7	248.7	132.0	-166.5	2.11E+06	5.80E+08	274.7	1.24	0.81	0.19	222.8	1.30	0.77	0.23
mar	113.1	287.9	174.8	-171.7	2.31E+06	5.67E+08	246.1	1.36	0.74	0.26	212.5	1.41	0.71	0.29
apr	109.7	249.8	140.1	-178.2	2.64E+06	5.44E+08	206.2	1.34	0.75	0.25	197.0	1.36	0.74	0.26
may	58.7	182.5	123.8	174.7	2.44E+06	5.07E+08	207.5	1.30	0.77	0.23	200.9	1.31	0.76	0.24
jun	51.4	120.0	68.6	173.7	2.40E+06	5.54E+08	231.4	1.15	0.87	0.13	218.9	1.16	0.86	0.14
jul	18.4	95.1	76.7	168.0	2.16E+06	4.04E+08	187.0	1.21	0.83	0.17	177.2	1.22	0.82	0.18
aug	16.9	73.3	56.4	172.2	2.33E+06	3.81E+08	163.7	1.17	0.85	0.15	155.3	1.18	0.85	0.15
sep	33.1	100.3	67.2	177.9	2.62E+06	4.60E+08	175.5	1.19	0.84	0.16	173.9	1.19	0.84	0.16
oct	29.6	144.8	115.2	-178.6	2.66E+06	4.04E+08	152.0	1.38	0.73	0.27	143.8	1.40	0.71	0.29
nov	55.6	186.5	130.9	-173.9	2.40E+06	4.20E+08	174.8	1.37	0.73	0.27	146.5	1.45	0.69	0.31
dec	53.5	212.9	159.4	-168.5	2.18E+06	4.86E+08	222.8	1.36	0.74	0.26	168.7	1.47	0.68	0.32

boundaries. However, during July there is a bifurcation of the mean mass flow over the region, with the result that the southern boundary is actually an efflux boundary, and $\vec{Q}$ across the boundary contributes *negatively* to $(wu)_{eff}$ (Eq. 2.16). Nonetheless, the months when the bifurcation is strongest are also the months when F^+ and $(wu)_{eff}$ are most similar, indicating the need for further analysis and comparison of the estimation methods.

Thirty percent recycling for the region as a whole is compatible with Lettau et al.'s (1979) estimate that 47% of the precipitation falling at 75° W is of land–evaporated origin. If the contribution of local moisture varies linearly (Figure 2.2), then the fraction of locally evaporated water at $x = \ell$ will be greater than the average value. This study indicates that, on average, more than 70 percent of the region's precipitation is provided by inflowing moisture. This estimate is considerably higher than that of Marques et al. (1972), that inflowing moisture accounts for 52% of the precipitation between Belém and Manaus. Belém, at the mouths of the Amazon, lies to the east of the present study region, and Manaus (longitude 60° W), east of the center of the study region. By the same argument as above, the Modified 1–D model predicts that the advective fraction of precipitation for x less than $\ell/2$ will be greater than the average value; that is, P_a/P for the longitudes between Belém and Manaus is between 70 and 100 percent, or in terms of the local contribution, P_m/P is between 0 and 30 percent. Subdividing the study region would provide a more adequate basis for comparison.

African Region

The results for the African region are presented in Figures 2.15 through 2.17 and in Table 2.5. The order of presentation is the same as for the preceding regions. Referring to Figure 2.15, two peaks appear in the annual

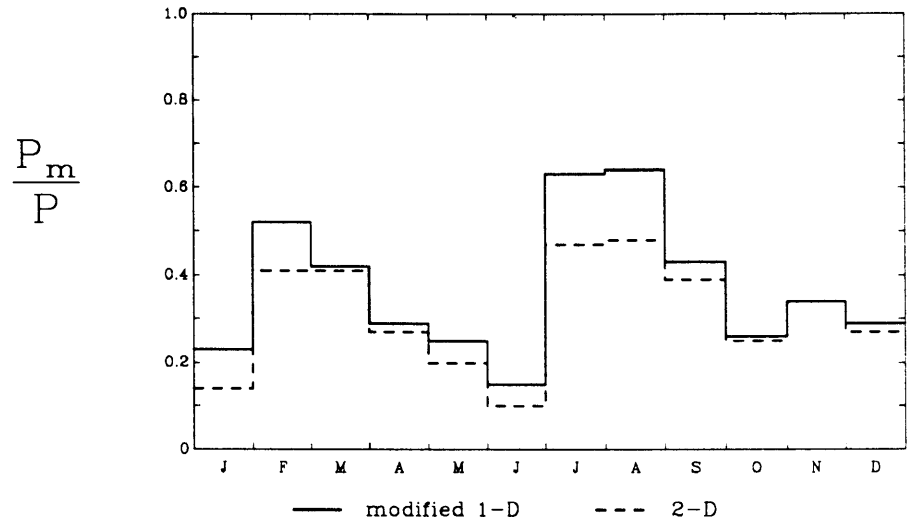

Figure 2.15: African Region. The ratio of locally–evaporated to total precipitation, as estimated by the Modified 1–D and the 2–D method.

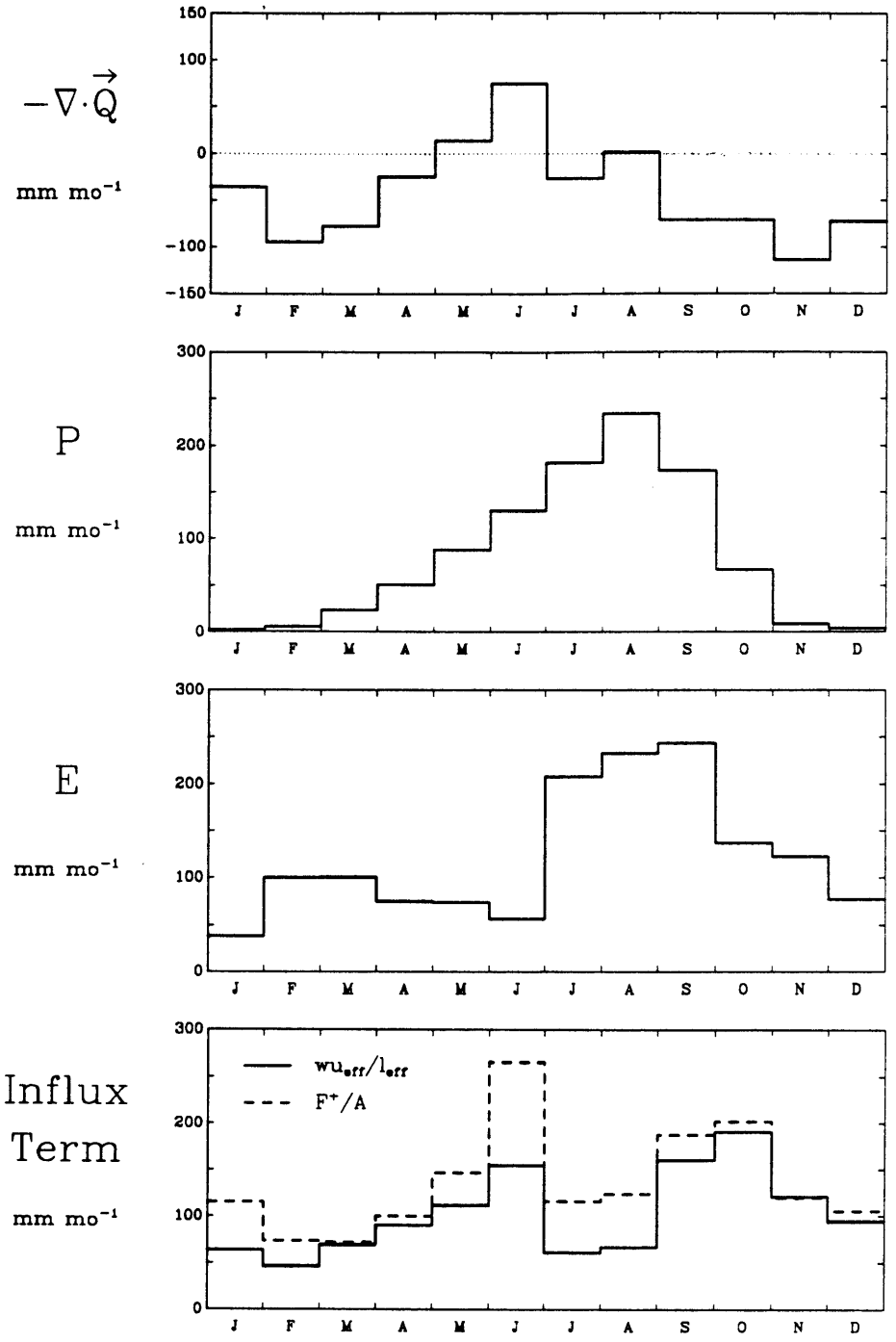

Figure 2.16: African Region. Terms used in estimating P_m/P by two methods. Atmospheric moisture convergence ($-\nabla\cdot\vec{Q}$), Precipitation (P) and Evaporation (E) are common to both methods; wu_{eff}/ℓ_{eff} is used in the Modified 1–D method, F^+/A in the 2–D method.

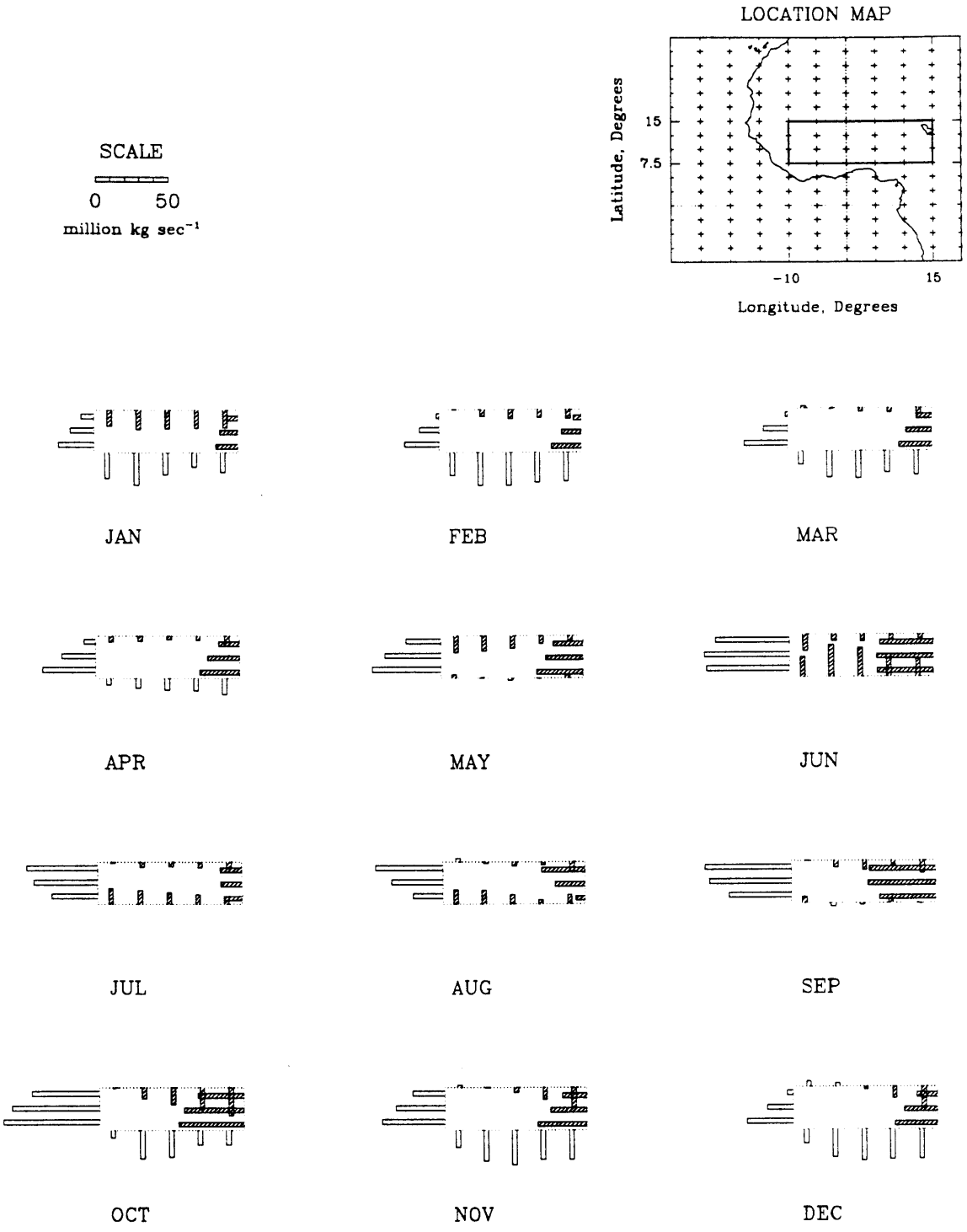

Figure 2.17: African Region. Bar graphs of the moisture flux across segments of the boundary. Each bar represents the integral of the normal component of $\vec{Q}$ along the segment at the base of the bar.

Table 2.5 African Region. Components in the estimation of P_m/P.

				Modified 1-D Method							2-D Method			
Month	-DivQ	P	E	Theta	L(eff)	wu(eff)	wu(eff) / L(eff)	P / P(a)	P(a) / P	P(m) / P	F+ / A	P / P(a)	P(a) / P	P(m) / P
	[mm/mo]	[mm/mo]	[mm/mo]	[deg]	[m]	[m mm/mo]	[mm/mo]				[mm/mo]			
jan	-35.6	2.2	37.8	-155.3	1.20E+06	7.56E+07	63.1	1.30	0.77	0.23	115.5	1.16	0.86	0.14
feb	-94.2	5.6	99.8	-156.9	1.24E+06	5.70E+07	46.1	2.08	0.48	0.52	73.3	1.68	0.59	0.41
mar	-77.2	23.2	100.4	-165.6	1.53E+06	1.06E+08	69.2	1.73	0.58	0.42	72.0	1.70	0.59	0.41
apr	-24.0	50.9	74.9	-170.1	1.76E+06	1.59E+08	90.5	1.41	0.71	0.29	100.3	1.37	0.73	0.27
may	13.8	87.8	74.0	-174.2	2.06E+06	2.30E+08	111.6	1.33	0.75	0.25	146.2	1.25	0.80	0.20
jun	74.2	130.1	55.9	177.7	2.41E+06	3.73E+08	154.7	1.18	0.85	0.15	265.1	1.11	0.90	0.10
jul	-26.6	181.4	208.0	175.7	2.19E+06	1.33E+08	60.8	2.71	0.37	0.63	116.1	1.90	0.53	0.47
aug	1.4	233.7	232.3	176.0	2.22E+06	1.48E+08	66.6	2.74	0.36	0.64	123.7	1.94	0.52	0.48
sep	-70.8	172.9	243.7	-179.3	2.62E+06	4.20E+08	160.4	1.76	0.57	0.43	187.9	1.65	0.61	0.39
oct	-70.8	66.6	137.4	-171.8	1.87E+06	3.57E+08	190.9	1.36	0.74	0.26	201.9	1.34	0.75	0.25
nov	-114.0	8.8	122.8	-169.1	1.70E+06	2.06E+08	120.9	1.51	0.66	0.34	119.8	1.51	0.66	0.34
dec	-72.4	4.6	77.0	-166.0	1.55E+06	1.47E+08	94.7	1.41	0.71	0.29	105.2	1.37	0.73	0.27

march of P_m/P: 0.52 in February and 0.64 in August by the Modified 1–D method; and 0.41 in February–March and 0.48 in August by the 2–D method. The February–March peak corresponds to fairly high E and low P in those months, while the July–August peak corresponds to very high E and P (Figure 2.16). Analogous to the South American region, large differences in the two influx terms occur in months of strong convergence; the month of June is the best example (Figure 2.17). The convergent boundary flux during June corresponds to the northernmost excursion of the ITCZ during the northern hemisphere summer. During June, according to calculations, the average direction of moisture flux is 178°, nearly due westward; as a result $(wu)_{eff}$ virtually ignores the influx over the southern boundary, whereas F^+ includes that influx, as well as the influx across the northern boundary.

Besides the June convergence noted above, Figure 2.17 illustrates several interesting characteristics of the atmospheric water balance for this study region. In February and March, the striking difference between the inward–directed bars on the northern boundary and the outward directed bars on the southern boundary probably reflects the evaporating power of the dry air that moves off the Sahara desert and gains moisture as it traverses the study region.

The estimated monthly rates of moisture convergence (Figure 2.16) indicate that, except during May and June, the territory defined as the African region is a net source of moisture to the atmosphere. The defined region includes the expansive lower Niger marshlands, where a large volume of the water drained from the Guinea highlands and the tropical upper Niger evaporates into the semi–arid surroundings. There is considerable excess of

evaporation over precipitation in this region during the months when the highland river discharge spreads over the expansive marshland and evaporates into the atmosphere. During May and June when the River experiences its lowest monthly flow rates (and even dries completely in some years) the marshlands disappear and the regional evaporation is accordingly reduced. During this season, the precipitation water is mostly derived from advected moisture, as evident in Figure 2.15. Furthermore, there will be a net regional convergence of moisture ($-\langle\nabla\cdot\vec{Q}\rangle > 0$) during these months when the sources of water vapor lie outside of the defined territory (Entekhabi, personal communication, 1991).

The significant contribution to precipitation of locally evaporated moisture in July and August can readily be inferred from Fig. 2.16. Precipitation is at its maximum during these months, yet the influx of atmospheric water vapor (by either method of estimation) is much less than in June and September; the larger part of precipitation must be supplied by local evapotranspiration.

2.6 Discussion

Both of the precipitation recycling estimation methods used in this study are modifications of Budyko's linear model of the water vapor content of the air moving over a land region. The critical assumption of the model is that locally–evaporated and advected water vapor molecules condense and fall as precipitation proportionally to their respective fraction of the total number of vapor molecules contained in the entire atmospheric column. Stidd (1967) argued against the fully–mixed assumption: "Since precipitation is normally associated with rising currents of air, it is logical to suppose that most of the

excess moisture associated with a storm has come recently from a layer of air close to the ground." The larger fraction of locally–evaporated moisture in the lower layers then would imply a larger fraction of local moisture in convective precipitation. On the other hand, if *non–precipitating* convection mixes the troposphere vertically (Paluch, 1979; Taylor and Baker, 1991), the assumption of a well–mixed atmospheric moisture reservoir is strengthened for regions and seasons in which convection is active.

A more serious concern, for the present study, is the problem of air mass divergence in the GFDL analyzed data. In this study, the North American region (where radiosonde data available for assimilation were rather densely distributed, when compared with the rest of the globe) appears to be a net source of moisture to the atmosphere on an annual basis. The Mississippi River and many of its tributaries provide an inward flux across the horizontal boundaries of the region; furthermore, the region is underlain by several major groundwater aquifers which are known to be in a depletion trend due to pumping for agriculture. The former flux is reflected as a positive R_{in}, and the latter as a negative $\frac{\partial S}{\partial t}$ in (1.10). However, it is doubtful that these additional sources of water are reflected in the atmospheric water balance, and such speculation is moot while air mass divergence errors distort the accuracy of $\langle \nabla \cdot \vec{Q} \rangle$. In Savijärvi's (1988) modified GFDL data (Figure 1.2), the year–round divergent area fraction of North America appears to be substantially reduced from the original GFDL data (Figure 1.1).

A priority for further work along these lines is to correct the air mass divergences. Alestalo's method would provide corrected values of $\nabla \cdot \vec{Q}$ at grid nodes. For the present study's Modified 1–D recycling estimation method, a minor adjustment would be required in order to estimate $\langle \nabla \cdot \vec{Q} \rangle$ by an area integral rather than a boundary flux integral. However, the 2–D method

would require corrected values of the components of $\vec{Q}$, in order to distinguish γ_{in} from γ_{out}, and to compute F^+. Savijävi's correction technique provides corrected components of the mean wind, and is more physically based than Alestalo's technique.

Another assumption in the recycling estimation methods is the use of areally–averaged precipitation over arbitrarily–defined regions. Precipitation is an extremely variable process. Although time averaging smooths the series at a point in space, substantial spatial variation may exist, depending upon the topography (and other surface properties) and atmospheric circulation characteristics of a region. As an extreme example, the model is invalid if all of a region's precipitation falls near the upwind boundary, before any locally–evaporated moisture has been added to the air. In such a situation, P_m/P would be overestimated, because the model assumes that the same amount of total precipitation falls from the air while the fraction of locally–contributed moisture in the air increases linearly.

A claim was made in Section 2.3 that the distance–weighted average moisture influx, $(wu)_{eff}$, is more representative of the rate of water vapor advection into the region than is the total moisture influx F^+. The results show that the two terms, when appropriately normalized, are generally compatible, with certain exceptions. In three regions (all but South America), F^+/A is consistently greater than $(wu)_{eff}/\ell_{eff}$. In South America, the two are nearly equal, with the greatest differences occurring in the months when the average moisture flux over the region, $\langle\vec{Q}\rangle$, is most southward (as indicated by θ in Table 2.4). The supposed superiority of $(wu)_{eff}$ is not clearly confirmed. The process of resolving $\vec{Q}$ parallel to $\hat{u}$ at the boundaries essentially neglects any curvature in the streamlines of $\vec{Q}$ over the region, and eliminates a

possibly significant portion of the influx, as illustrated in Figure 2.18. Another complication arises, as mentioned before, when the sides of the rectangular boundary that are designated as inflow segments by the direction of $\hat{u}$ are not truly inflow segments along their entire length (as for the African region in December, Figure 2.17 and Table 2.5). The use of $(wu)_{eff}$ introduces unforeseen problems, which call into question the general applicability of the Modified 1–D method. The simpler 2–D method may be more appropriate to the geometry of $\vec{Q}$, but more analysis is needed. In the meantime, it is probably safer to believe the lower estimate of P_m/P in those cases in which a large difference exists between the two estimates, as for the North American region in July and August, and the African region in January, February, July and August.

The local precipitation ratio, as estimated herein, is diagnostic. The values are indicators of the importance of land–atmosphere interaction to regional climate, for climatic conditions during the years 1963–1973. As such, the estimates are not predictive; for example, it does not follow that reducing evapotranspiration to zero in the Eurasian region during June (even if that were possible) would reduce June precipitation by 35 percent. Many complex, interrelated factors, both internal and external to the region, control the region's precipitation.

It is clear that a great deal of variety exists in the importance of the precipitation recycling process to different regions and at different seasons. Therefore, Budyko's (1974) conclusion that the relative role of local recycling is limited, and Lettau et al.'s (1979) conclusion that it is quite important, are not contradictory. The reason is that the process depends, not only on the region's length scale and evapotranspiration rate, but also on the presence of the physical mechanisms that cause precipitation to occur at all.

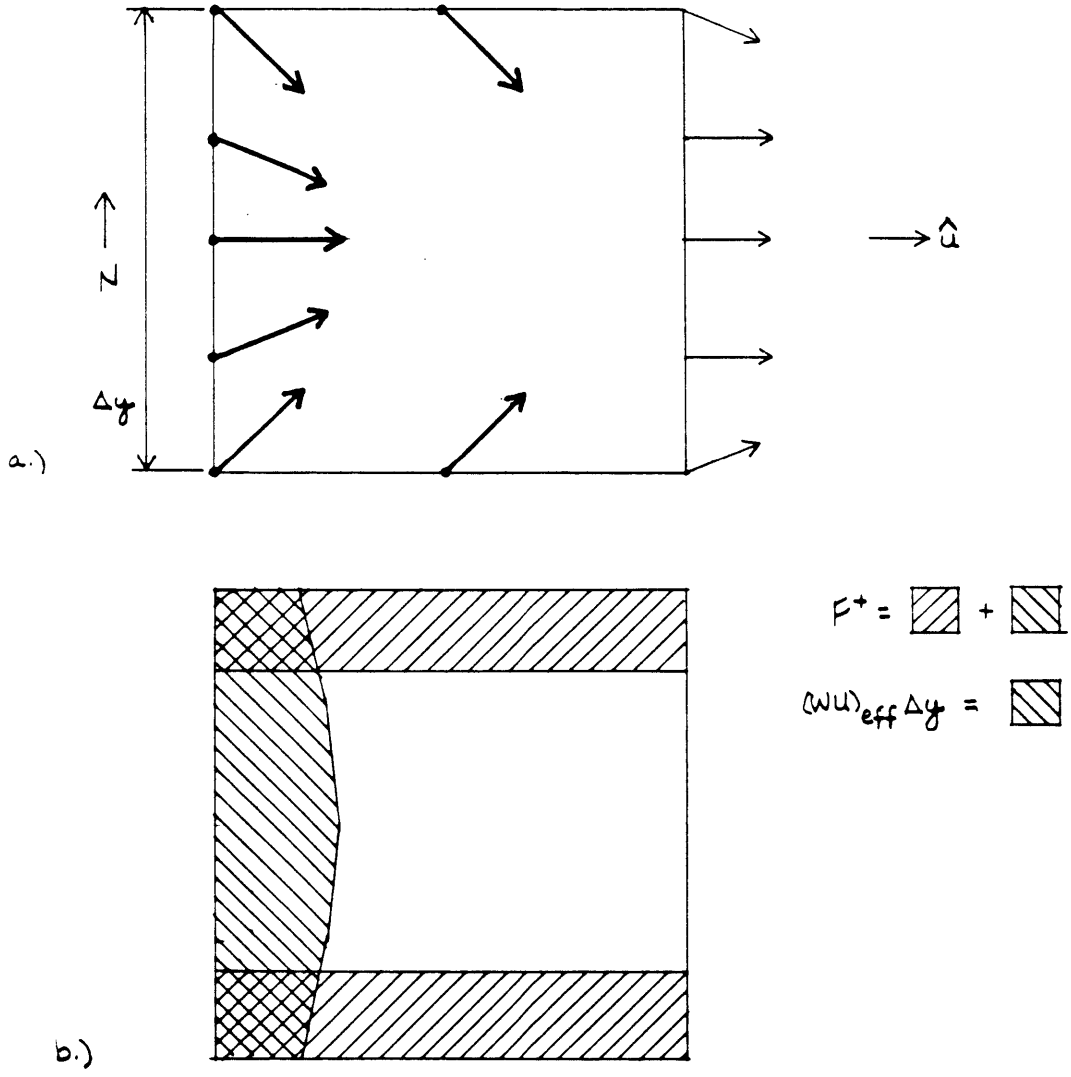

Figure 2.18: a) Plan view of a region with convergent moisture flux, and with constant $\|\vec{Q}\|$ along the inflow boundaries. By symmetry, the average direction of moisture flux ($\hat{u}$) is due eastward.

b) The difference between the total boundary integral of influx (F^+) and the integral of boundary influx resolved parallel to $\hat{u}$ $[(wu)_{eff}\ \Delta y]$.

If a sufficiently high orographic barrier is present at the downwind boundary of a region, most of the moisture present in the air, regardless of its evaporative source, precipitates on the windward side. By the definition of recycling used in this study, the moisture content due to evapotranspiration within the region—which lies simultaneously upwind and downhill—falls back into the region as recycled precipitation. This mechanism illustrates the sensitivity of the recycling notion to the choice of control volume, and sheds some light on why increased irrigation could increase rainfall in the Columbia River Basin (Stidd, 1967) whereas building a large lake on the southern border of Arizona would not increase rainfall in that state (McDonald, 1962).

The causal connection between evapotranspiration and convective precipitation merits further investigation. Adding moisture to the air at low levels tends to reduce the stability of the atmosphere by building up a reservoir of latent heat in the lower layers (Stidd, 1967). By this contribution, increased evapotranspiration could enhance convective precipitation. If so, advective precipitation (P_a) would likely be increased as well as P_m, whereas with the orographic mechanism, increased evapotranspiration would only increase P_m.

In this study, the partition of precipitation between local and advective sources has been emphasized rather than the oceanic/terrestrial distinction. For studies of the interactions between the land surface and regional climate, the internal vs. external supply of water vapor is of interest, whether that external supply comes from an ocean or a land surface. As noted before, the definitions merge if the control volume is taken as an entire continent. A pragmatic reason for the advective vs. local distinction in the present study is that the analysis technique currently dictates the use of rectangular regions, incompatible with the shapes of the Earth's continents.

The regions examined in this study were somewhat arbitrarily selected. They vary widely in size and hydroclimatological characteristics. More systematic selection and study of regions is certainly called for, in tandem with improvements to the analysis technique to allow the delineation of boundaries along natural drainage divides and coastlines.

Future work should make use of corrections to the GFDL data, and of additional data sets. Four–dimensional data assimilation techniques, now routinely used in weather forecasting, provide gridded fields of the variables required for recycling estimates. The improved temporal resolution provided by these analyses (four times daily, at present) would better capture diurnal variations (noted by Rasmusson, 1967) and help correct bias in the $\vec{Q}$ computations now based on once–daily/twice–daily observations. In addition, the estimation of $\langle P \rangle$ should be improved, and methods devised to use other water balance quantities such as runoff to provide closure and a check on the evapotranspiration term.

Chapter 3

Parameterization of a Simple Climate Model

3.1 Introduction

Atmospheric General Circulation Models (GCMs) are the hydrologist's or climatologist's experimental apparatus for large–scale investigations of the atmospheric branch of the hydrologic cycle and land surface–atmosphere interactions (Henderson–Sellers and McGuffie, 1987). However, certain components of GCMs require improvement before the models can be fully useful operationally, for regional studies, or for reliable predictions (Eagleson, 1982; Entekhabi and Eagleson, 1989). One such component is the representation of land surface hydrology.

General circulation models are based on numerical solutions to the basic equations of mass, momentum and energy in the atmosphere. The equations are solved at nodes of a three–dimensional mesh, with horizontal grid spacing on the order of 10^4 to 10^5 km^2. Any physical process that occurs on scales smaller than the grid resolution must be parameterized. *Parameterization* refers to the process of developing equations that capture the integrated effects of the smaller scale processes on the scale resolved by the model. Usually the equations require numerical values, or *parameters*, that characterize the process at a particular location or time.

Several problems arise when new parameterizations are developed for GCMs. First, repeated simulations are required in order to test the effects of the parameterization; the cost of such extensive computation may be prohibitive. Second, feedbacks in the GCM climate make it difficult to isolate

specific climatic processes and the effects of the candidate parameterization.

A one–dimensional screening model has been developed to test possible modifications of the GCM land surface hydrology parameterization before the changes are implemented in the full GCM (Koster et al., 1988; Entekhabi and Eagleson, 1989; Koster and Eagleson, 1990). The screening model is a simple representation of the interaction among a land surface, an ocean surface, and their overlying atmosphere. Because the screening model does not simulate three–dimensional dynamics, a simple linear transfer scheme is used to parameterize the lateral convergence of heat and moisture from the atmospheric column overlying the ocean to the column overlying the land surface.

The objectives of the work described in this Chapter are 1) to determine whether the simple linear parameterization of heat and moisture convergence produces a realistic environment for the testing and screening of candidate land surface hydrology parameterizations; and 2) to determine a range of appropriate numerical values for the transport parameter required in the screening model. The present study focuses on the moisture convergence. The vertical distributions of heat and moisture in the atmosphere are similar, and advection is the dominant mechanism of lateral transport for both. Therefore, the results for moisture should be applicable to heat as well.

3.2 The Model

The one–dimensional screening model is described by Koster and Eagleson (1990). A brief summary is given here.

The hydrologic cycle of the model consists of the interaction between two dimensionless regions, one land and one ocean. Basically, the land and ocean regions are reservoirs with the appropriate characteristics for storage and vertical fluxes of heat and water. To each region there corresponds an

atmospheric control volume, defining a box with unit horizontal area whose base is the land or ocean surface.

In the long term, the net transport of water vapor from the ocean box into the land box must balance the net liquid runoff from the land box to the ocean box. A fixed value of the atmospheric convergence will thus dictate the climatic response of the surface. Parameterization using a fixed convergence would therefore severely distort the land surface's response due to changes in hydrologic parameterization (soil and vegetation type, etc.) and would be counter to the purpose of the model, which is to determine the sensitivity of the model climate to such changes.

Therefore, the lateral convergence rates of heat and moisture must be represented in such a way that they may adjust to the changing atmospheric profiles that are brought about by changes in model specifications or parameterizations. A first–order appproximation for the exchange rate is to assume it proportional to the difference in concentration of the quantity--specific heat or specific humidity--in neighboring boxes. Thus, moisture moves from the oceanic to the continental box at a rate specified as follows:

$$\frac{dq_{c,i}}{dt} = \frac{q_{o,i} - q_{c,i}}{\chi} \tag{3.1}$$

in which q is the specific humidity at pressure level i; the subscript c or o refers to continent or ocean, respectively; and χ is the proportionality constant, having units of time. A system such as (3.1), in which the outflow is proportional to the storage is known in engineering as a linear reservoir.

In the screening model, the land and ocean air columns form a loop, in that the inflow to one is the outflow from the other. The moisture exchange between boxes is followed by evaluation of the equations controlling the various vertical fluxes and readjustments of the atmospheric profile in each box.

3.3 Estimation Technique

The objectives of the study require a comparison between the moisture convergence behavior of the model and of real Earth regions. The procedure used to make this comparison is now described.

The transport parameter χ is prescribed for the model and controls the rate of moisture exchange between the oceanic and continental boxes. Different values of χ produce different values of moisture convergence onto the continent. A series of ordered pairs (χ, $-\nabla\cdot\vec{Q}$) can be obtained by assigning values of χ and integrating the model for a sufficient number of time steps to obtain a climatic value of $-\nabla\cdot\vec{Q}$ (where $-\nabla\cdot\vec{Q}$ is the net moisture convergence integrated through the depth of the atmospheric column, as defined in Chapter One).

In order to evaluate the parameter χ for continents and oceans on the Earth, Equation (3.1) must be modified slightly. In general, geographic regions on the Earth differ from the model in several respects. First, there is no Earth region where flow cycles between a single continent and a single ocean source region; that is, the real–world ocean–to–continent moisture exchange is not a closed loop, as it is in the model. Second, the surface areas of the geographic ocean and continental regions may or may not be equal. Third, the model does not include surface topography whereas in the

geographic continental region elevation changes produce differences in surface pressure and consequently the mass of the column of air overlying points on the surface is not constant over the land region.

The model equation for moisture convergence is modified to account for the differences in geometry by taking the net moisture influx to the continental region as proportional to the difference in water vapor loads averaged over the regions. The constant of proportionality is $\hat{\chi}$ (where the symbol $\hat{}$ will denote data estimates of χ). For the data, then,

$$\frac{d\langle q_c \rangle}{dt} = \frac{\langle q_o \rangle - \langle q_c \rangle}{\hat{\chi}} \tag{3.2}$$

where the angled brackets indicate an areal average. The average moisture content of the air overlying the continental region is

$$\langle q_c \rangle = \frac{M_c}{A_c} \tag{3.3}$$

in which M_c is the total mass of water present in the atmospheric control volume, i.e.,

$$M_c = \iint_{\text{continent}} \int_0^{p_s} q \, \frac{dp}{g} \, dA \tag{3.4}$$

and A_c is the total mass of air overlying the continent, i.e.,

$$A_c = \iint_{\text{continent}} \int_0^{p_s} \frac{dp}{g} \, dA \; . \tag{3.5}$$

Similarly, for the ocean region, the total mass of atmospheric water vapor is

$$M_o = \iint_{ocean} \int_0^{p_s} \frac{dp}{g}\, dA \ . \tag{3.6}$$

and the total mass of air overlying the ocean is

$$A_o = \iint_{ocean} \int_0^{p_s} \frac{d_p}{g}\, dA \ . \tag{3.7}$$

Assuming that the total mass of air remains constant (this is tantamount to neglecting changes in surface pressure), Equation (3.2) may be rewritten as

$$\frac{d}{dt}\frac{M_c}{A_c} = \frac{1}{A_c}\frac{dM_c}{dt} = \frac{\frac{M_o}{A_o} - \frac{M_c}{A_c}}{\hat{\chi}} \tag{3.8}$$

or

$$\frac{dM_c}{dt} = \frac{\frac{A_c}{A_o} M_o - M_c}{\hat{\chi}} \ . \tag{3.9}$$

The left–hand side of (3.9) is the net lateral atmospheric inflow from the ocean control volume into the land control volume, which corresponds to $-\nabla\cdot\vec{Q}$. Thus $\hat{\chi}$ may be estimated from the data as follows:

$$\hat{\chi} = \frac{\frac{A_c}{A_o} M_o - M_c}{(-\nabla\cdot\vec{Q})} \ . \tag{3.10}$$

The quantities defined in (3.4), (3.5) (3.6) and (3.7) were evaluated from the GFDL gridded data using trapezoidal rule integration, and allowing for the spherical surface geometry in the area integrals by the method described in Appendix A. Equation (3.10) was used to obtain a value of $\hat{\chi}$ for each month

of the year. The result is a series of twelve ordered pairs $(-\nabla\cdot\vec{Q},\ \hat{\chi})$ for the observational data. The model $(-\nabla\cdot\vec{Q},\ \chi)$ and the data $(-\nabla\cdot\vec{Q},\ \hat{\chi})$ can then be compared. It was assumed that intra–annual changes in the dynamics of the ocean–continent interaction would be reflected as different values of $\hat{\chi}$ for the different months.

3.4 Study Region

The one–dimensional screening model is an abstraction, by definition. It is not meant to represent any particular location on the Earth. Rather, it is a simple one–loop hydrologic cycle, operating between two reservoirs, where the conditions of the reservoirs and the rate of exchange between them are allowed to vary.

Few continental regions behave like the land air column in the model. First, the model continent is a constant sink of atmospheric water whereas, as discussed in the preceding chapters, actual land regions may act as moisture sources to the atmosphere at certain times of the year. Second, because of the three–dimensional, time–varying circulation of the Earth's atmosphere, it is difficult to define a unique ocean source region corresponding to a given continental region. Third, the model has no topography, whereas in real regions, topography affects many aspects of climate.

The region selected for estimation of $\hat{\chi}$ was equatorial South America. This land region exhibits atmospheric moisture convergence throughout the year. Furthermore, as shown by the streamlines of moisture flux (Figure 3.1), there is a reasonably well–defined ocean source region. Two land regions and corresponding ocean regions were delineated; they are shown in Figures 3.2 and 3.3. The analysis described in Section 3.3 was applied to each continent–ocean pair of study regions separately.

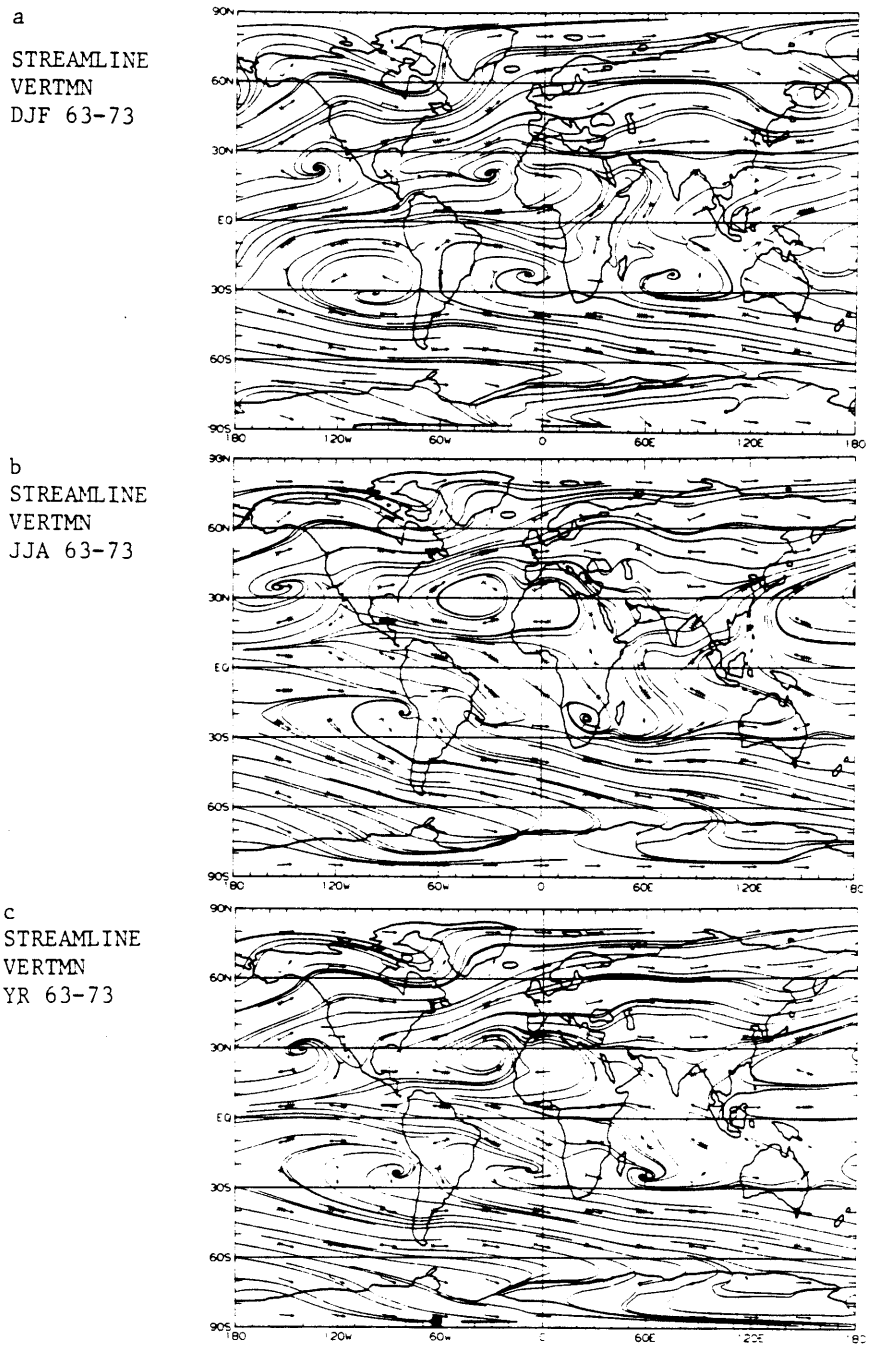

Figure 3.1 Streamlines of the total aerial runoff, $\vec{Q}$; each barb represents 2 g kg^{-1} m s^{-1}: a, DJF; b, JJA; c, year. [Source: Peixóto and Oort, 1983]

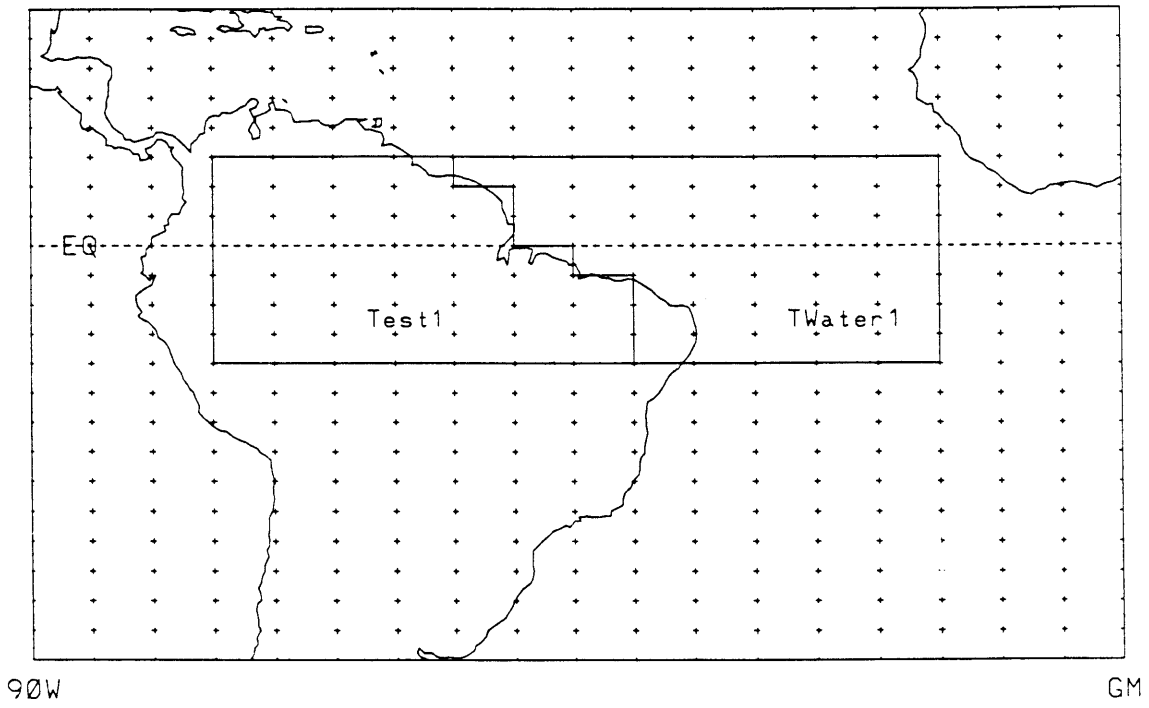

Figure 3.2: The continent and ocean regions used to estimate the transport parameter, $\hat{\chi}$, from observations: Experiment 1.

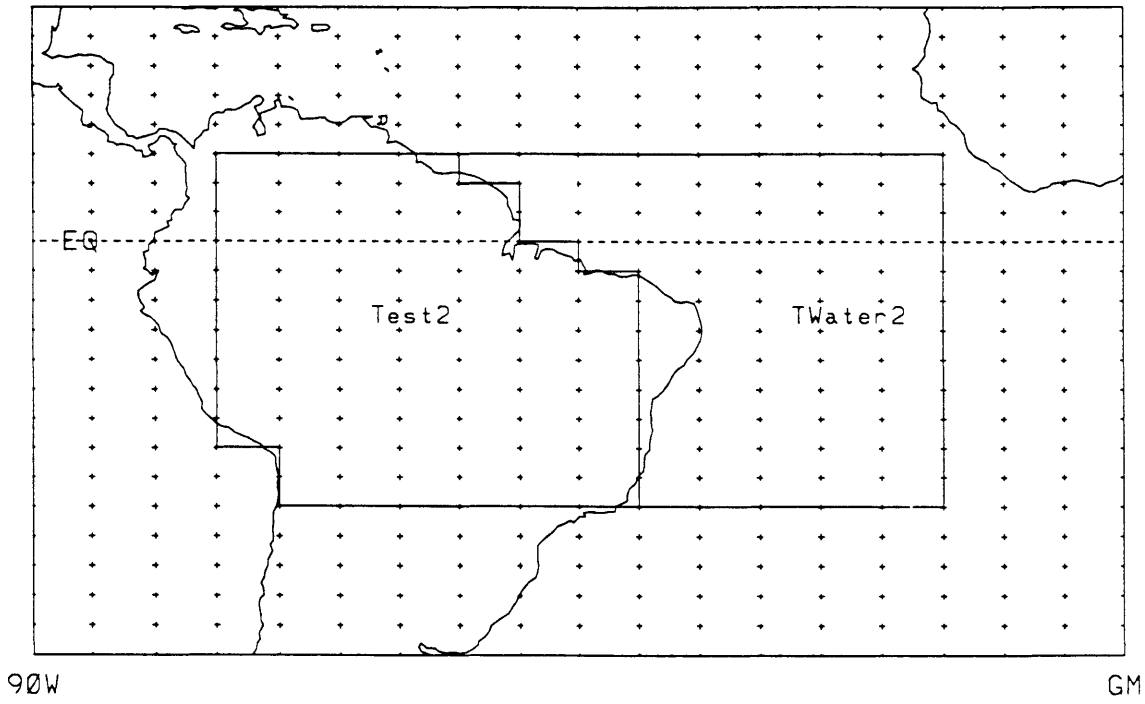

Figure 3.3: The continent and ocean regions used to estimate the transport parameter, $\hat{\chi}$, from observations: Experiment 2.

3.5 Results

Series of pairs $(-\nabla\cdot\vec{Q},\ \chi)$ for six different runs of the one–dimensional screening model were generated (Entekhabi, personal communication, 1991). The six runs, "Run a" through "Run f", differed in the settings of several fixed parameters of the screening model. The various runs were conducted solely to give a range of model environments from which to collect the $(-\nabla\cdot\vec{Q},\ \chi)$ pairs, and did not constitute an attempt to match the model climate statistics to the geographic test regions.

The model settings used in the six runs are listed in Table 3.1; the reader is referred to Entekhabi and Eagleson (1989) for descriptions of the parameters and their roles in the model. The model was run for perpetual July 1 at 10° North latitude, which assured that the solar radiation received at the top of the column remained constant, except for the diurnal cycle; therefore any changes to the radiation regime that affected the model hydrologic cycle were brought about by the model climate and the composition of the atmospheric profile.

The model was integrated for 250 days, for each of 25 prescribed values of χ, for each of the six runs. The values of χ ranged from 0.1 to 20 days. The runs produced six $(-\nabla\cdot\vec{Q},\ \chi)$ sequences; they are plotted in Figure 3.4 and tabulated in Table 3.2.

The $(-\nabla\cdot\vec{Q},\ \hat{\chi})$ pairs obtained by evaluating (3.10) for the two geographic continent–ocean pairs (Test1–Twater1 and Test2–Twater2) are plotted in Figure 3.5. The values of $(-\nabla\cdot\vec{Q},\ \hat{\chi})$ from the geographic study regions are tabulated, together with some intermediate calculations, in Tables 3.3 and 3.4.

Table 3.1 One–dimensional screening model parameters used in Runs a through f. [Source: Entekhabi, personal communication, 1991]

COMMON PARAMETERS

Latitude:	10 North
Simulation Period:	250 days (75 days spin-up) Perpetual July 1st.
Initial Soil-Water:	Saturated
Cloud Temperature Standard Deviation σ_c:	3 degrees Celsius
Land Surface Wind:	2 m/s
Soil Depth and Textture:	1.5 meters (5 layers with ticknesses=0.10,0.15,0.35,0.40,0.50 meters). Composition: 31% Sand , 9% Silt , 60% Clay [From Zobler and Cory (1984) data-set for the Amazon]
Vegetation:	Full cover with -15 bars wilting point
Surface Albedos:	25% Ocean, 35% Land

SIMULATION PARAMETERS

Run Name	Soil Moisture Coeff.Var.[ ]	PPT Fractional Wetting [ ]	Fixed Ocean Temp. [C]	Ocean Surface Wind [m/s]
runa	1.0	0.6	28	4
runb	0.5	0.6	28	4
runc	1.0	0.6	30	4
rund	1.0	0.3	29	4
rune	1.0	0.3	28	8
runf	0.5	0.3	28	8

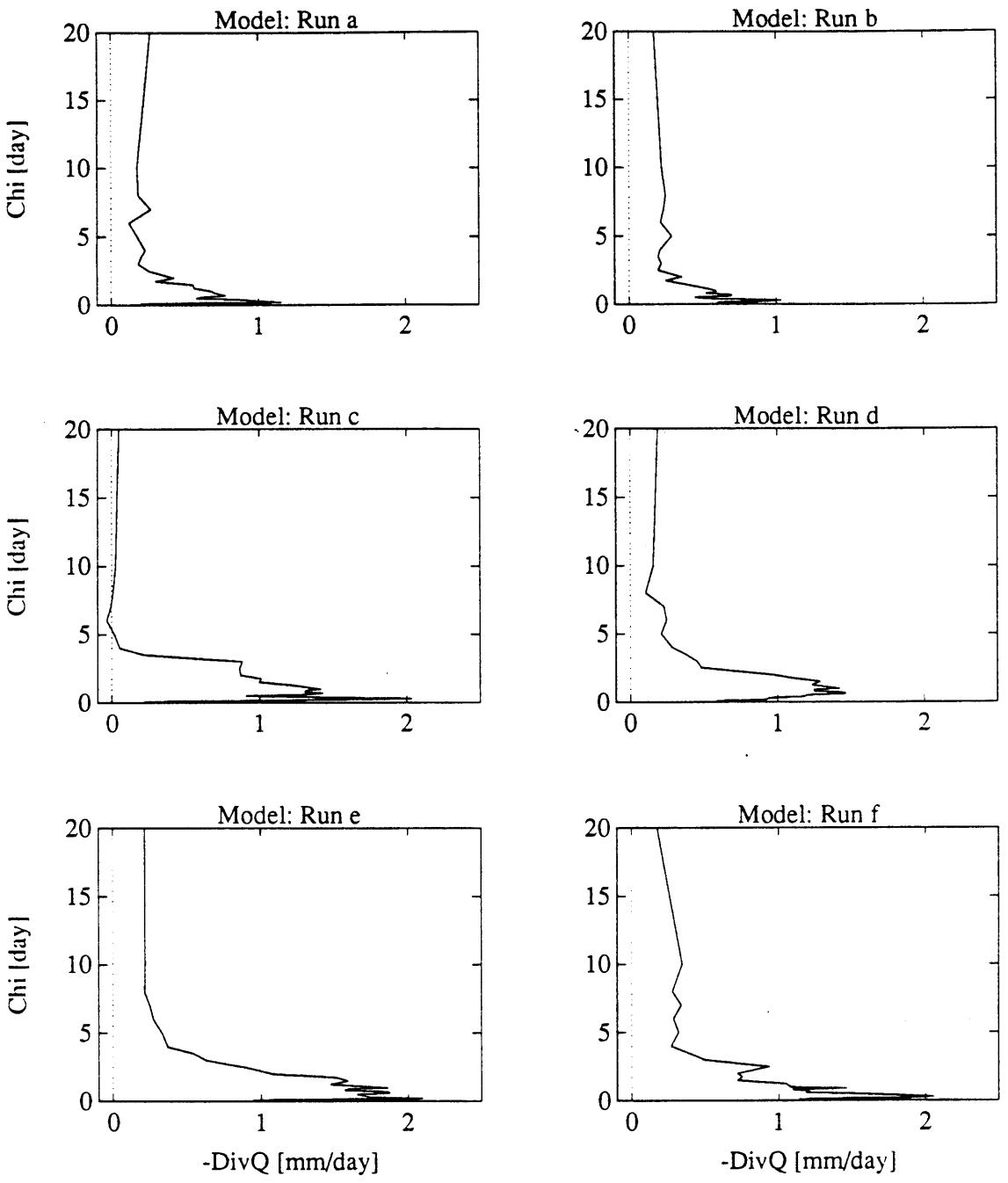

Figure 3.4: χ and $-\nabla\cdot\vec{Q}$ for six different runs of the screening model. For each run, all other model parameters were held fixed while χ was varied; the model was integrated over 250 days for each $(-\nabla.\vec{Q}, \chi)$ pair.

Table 3.2 Moisture convergence values for screening model runs a through f.
[Source: Entekhabi, personal communication, 1991.]

	-Div_Q					
CHI	Run_A	Run_B	Run_C	Run_D	Run_E	Run_F
0.100	0.207	0.596	0.227	0.581	0.948	1.137
0.150	0.534	0.649	0.872	0.813	1.477	1.416
0.200	1.155	0.901	1.330	0.928	2.101	1.921
0.300	0.989	1.032	2.033	0.942	1.746	2.054
0.400	0.869	0.533	1.359	1.180	1.701	1.794
0.500	0.580	0.447	0.912	1.197	1.655	1.549
0.600	0.630	0.690	1.325	1.461	1.875	1.185
0.700	0.780	0.696	1.435	1.454	1.865	1.206
0.800	0.737	0.517	1.306	1.247	1.573	1.098
0.900	0.700	0.591	1.315	1.245	1.604	1.461
1.000	0.685	0.582	1.418	1.421	1.863	1.083
1.250	0.563	0.480	1.245	1.233	1.476	1.048
1.500	0.556	0.367	1.000	1.287	1.594	0.719
1.750	0.302	0.251	1.010	1.097	1.512	0.750
2.000	0.425	0.359	0.873	0.962	1.084	0.718
2.500	0.257	0.198	0.865	0.482	0.894	0.935
3.000	0.185	0.220	0.883	0.449	0.629	0.493
3.500	0.203	0.198	0.218	0.373	0.543	0.385
4.000	0.232	0.212	0.054	0.285	0.370	0.269
5.000	0.179	0.291	0.016	0.211	0.331	0.320
6.000	0.123	0.216	-0.036	0.247	0.273	0.285
7.000	0.269	0.237	-0.007	0.229	0.250	0.338
8.000	0.185	0.249	0.008	0.104	0.214	0.278
10.000	0.177	0.223	0.025	0.157	0.218	0.344
20.000	0.267	0.172	0.049	0.189	0.216	0.176

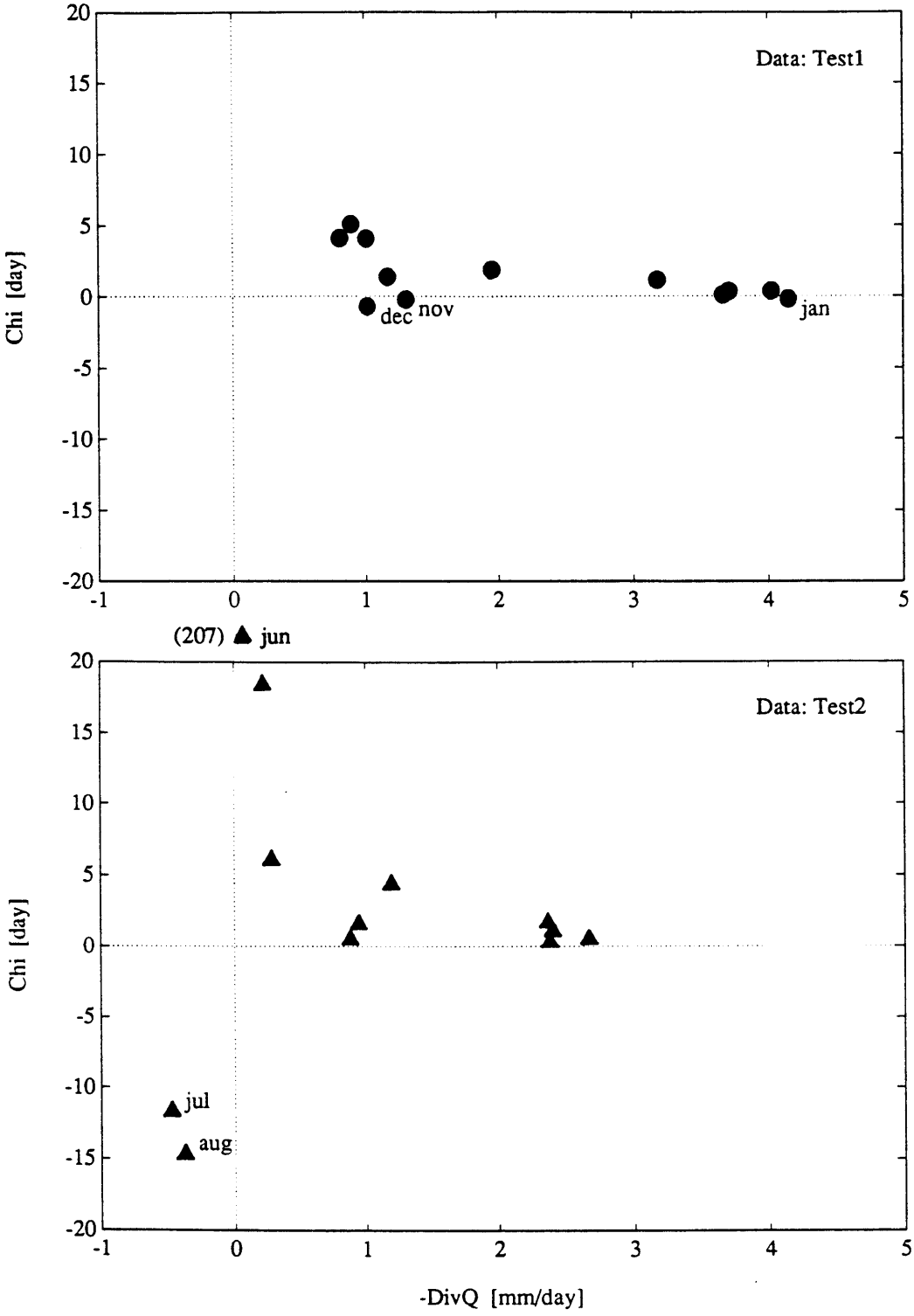

Figure 3.5: Estimates of $\hat{\chi}$ and $-\nabla \cdot \vec{Q}$ from the observational data for each of twelve months. The observations that do not satisfy model assumptions are labeled by month.

Table 3.3 Estimation of $\hat{\chi}$ from observational data, Experiment 1.

Regions:	CONTINENT	OCEAN
	Test1	Twater1
Ac,Ao [kg]	6.121E+16	6.735E+16
Area (m^2)	6.308E+12	6.619E+12

Month	Mc	Mo	-DivQ		Ac -- Mo Ao	Ac -- Mo - Mc Ao	<qc>	<qo>	Chi	
	[kg]	[kg]	[kg/sec]	[mm/day]	[kg]	[kg]	[g/kg]	[g/kg]	[sec]	[day]
JAN	2.37E+14	2.55E+14	3.04E+08	4.16	2.32E+14	-4.84E+12	3.9	3.8	-1.59E+04	-0.18
FEB	2.35E+14	2.64E+14	2.69E+08	3.68	2.40E+14	4.36E+12	3.8	3.9	1.62E+04	0.19
MAR	2.46E+14	2.80E+14	2.71E+08	3.71	2.54E+14	7.71E+12	4.0	4.2	2.85E+04	0.33
APR	2.47E+14	2.85E+14	2.94E+08	4.03	2.59E+14	1.19E+13	4.0	4.2	4.06E+04	0.47
MAY	2.29E+14	2.79E+14	2.33E+08	3.19	2.54E+14	2.48E+13	3.7	4.1	1.07E+05	1.23
JUN	2.19E+14	2.67E+14	1.43E+08	1.96	2.43E+14	2.40E+13	3.6	4.0	1.68E+05	1.95
JUL	2.09E+14	2.59E+14	7.48E+07	1.02	2.35E+14	2.65E+13	3.4	3.8	3.54E+05	4.10
AUG	1.95E+14	2.46E+14	6.54E+07	0.90	2.24E+14	2.86E+13	3.2	3.7	4.38E+05	5.07
SEP	1.97E+14	2.41E+14	5.99E+07	0.82	2.19E+14	2.14E+13	3.2	3.6	3.58E+05	4.14
OCT	2.09E+14	2.42E+14	8.58E+07	1.18	2.20E+14	1.06E+13	3.4	3.6	1.24E+05	1.44
NOV	2.31E+14	2.53E+14	9.65E+07	1.32	2.30E+14	-1.16E+12	3.8	3.8	-1.20E+04	-0.14
DEC	2.23E+14	2.41E+14	7.49E+07	1.03	2.19E+14	-4.43E+12	3.6	3.6	-5.92E+04	-0.69

Table 3.4 Estimation of $\hat{\chi}$ from observational data, Experiment 2.

Regions:	CONTINENT	OCEAN
	Test2	Twater2
Ac,Ao (kg)	1.058E+17	1.050E+17
Area (m^2)	1.120E+13	1.032E+13

Month	Mc	Mo	-DivQ		Ac -- Mo Ao	Ac -- Mo - Mc Ao	<qc>	<qo>	Chi	
	[kg]	[kg]	[kg/sec]	[mm/day]	[kg]	[kg]	[g/kg]	[g/kg]	[sec]	[day]
JAN	3.82E+14	3.88E+14	3.10E+08	2.39	3.91E+14	9.26E+12	3.6	3.7	2.99E+04	0.35
FEB	3.87E+14	4.01E+14	3.48E+08	2.68	4.04E+14	1.64E+13	3.7	3.8	4.70E+04	0.54
MAR	3.95E+14	4.22E+14	3.13E+08	2.41	4.25E+14	3.01E+13	3.7	4.0	9.62E+04	1.11
APR	3.81E+14	4.20E+14	3.09E+08	2.38	4.23E+14	4.21E+13	3.6	4.0	1.36E+05	1.58
MAY	3.42E+14	3.98E+14	1.56E+08	1.20	4.01E+14	5.92E+13	3.2	3.8	3.80E+05	4.39
JUN	3.22E+14	3.76E+14	3.13E+06	0.02	3.78E+14	5.61E+13	3.0	3.6	1.79E+07	207.30
JUL	3.02E+14	3.60E+14	-6.04E+07	-0.47	3.63E+14	6.14E+13	2.9	3.4	-1.02E+06	-11.77
AUG	2.86E+14	3.44E+14	-4.75E+07	-0.37	3.46E+14	6.03E+13	2.7	3.3	-1.27E+06	-14.70
SEP	2.98E+14	3.40E+14	2.80E+07	0.22	3.42E+14	4.45E+13	2.8	3.2	1.59E+06	18.39
OCT	3.30E+14	3.47E+14	3.82E+07	0.29	3.50E+14	1.99E+13	3.1	3.3	5.22E+05	6.04
NOV	3.58E+14	3.71E+14	1.23E+08	0.95	3.74E+14	1.57E+13	3.4	3.5	1.28E+05	1.48
DEC	3.59E+14	3.61E+14	1.15E+08	0.89	3.64E+14	4.75E+12	3.4	3.4	4.13E+04	0.48

For the geographic regions, there were several months that did not match the construct of the simple one–dimensional model. During November, December, and January in Experiment 1, the computations showed negative values of $\left[\frac{A_c}{A_o} M_o - M_c\right]$, with moisture convergence onto the continent, giving negative values of $\hat{\chi}$. During July and August in Experiment 2, the computations showed a net divergence of moisture from the continent, despite a positive moisture gradient between ocean and continent. This caused $\hat{\chi}$ to be negative for those months. In the screening model, χ is always positive. Therefore, for purposes of comparison, only the positive $\hat{\chi}$'s from the data were used. The outliers are included and labeled in Figure 3.5 for the sake of completeness

To improve legibility, the observational $(-\nabla\cdot\vec{Q},\ \hat{\chi})$ pairs, excluding the outliers, are plotted and labeled by month on semilog plots in Figure 3.6. A seasonal cycle in $\hat{\chi}$ is observed, with lower values occurring in January, February, March, and April and highest values in June, July, August, and September. The values of $\hat{\chi}$ range over four orders of magnitude, from .2 to 250 days, although most lie between 10^{-1} and 10^{1} days. The lower values of $-\nabla\cdot\vec{Q}$ correspond roughly to maximum $\hat{\chi}$, while the highest $-\nabla\cdot\vec{Q}$ is associated with $\hat{\chi}$ around 0.5 day, for both regions.

Finally, the series of $(-\nabla\cdot\vec{Q},\ \chi)$ for all six model runs and the observational $(-\nabla\cdot\vec{Q},\ \hat{\chi})$ for both geographic study regions are compared in Figures 3.7 through 3.12. Each figure shows one model run as a solid line, plotted with the observational data from Experiment 1 (indicated by filled circles) in the top frame and Experiment 2 (indicated by filled triangles) in the bottom frame.

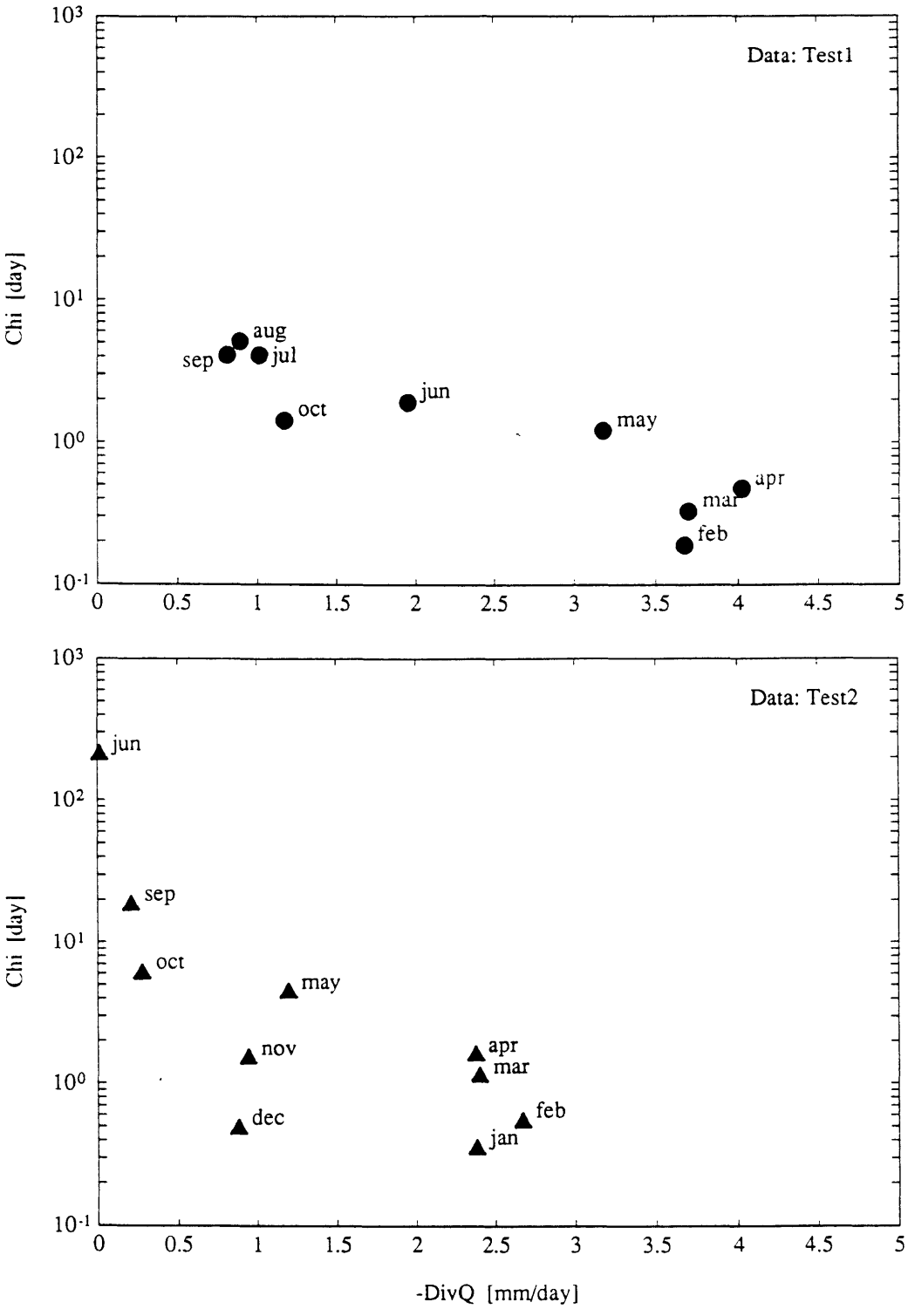

Figure 3.6: Estimates of $\hat{\chi}$ and $-\nabla \cdot \vec{Q}$ from the observational data, for selected months. The observations that did not satisfy model assumptions have been excluded.

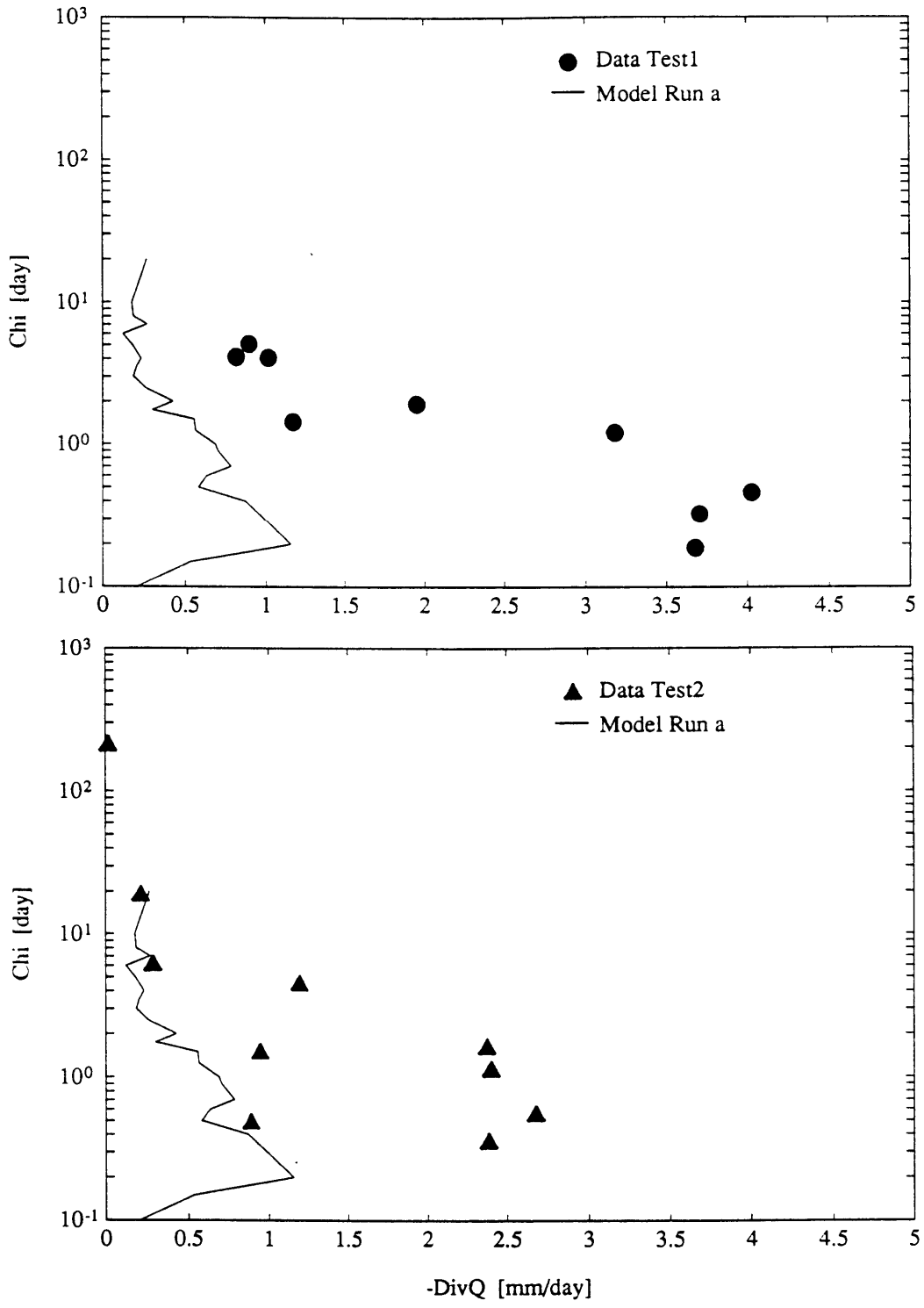

Figure 3.7: Observational estimates of $(-\nabla\cdot\vec{Q},\ \hat{\chi})$ compared with model output $(-\nabla\cdot\vec{Q},\ \chi)$ produced by varying χ with all other parameters fixed, Run a.

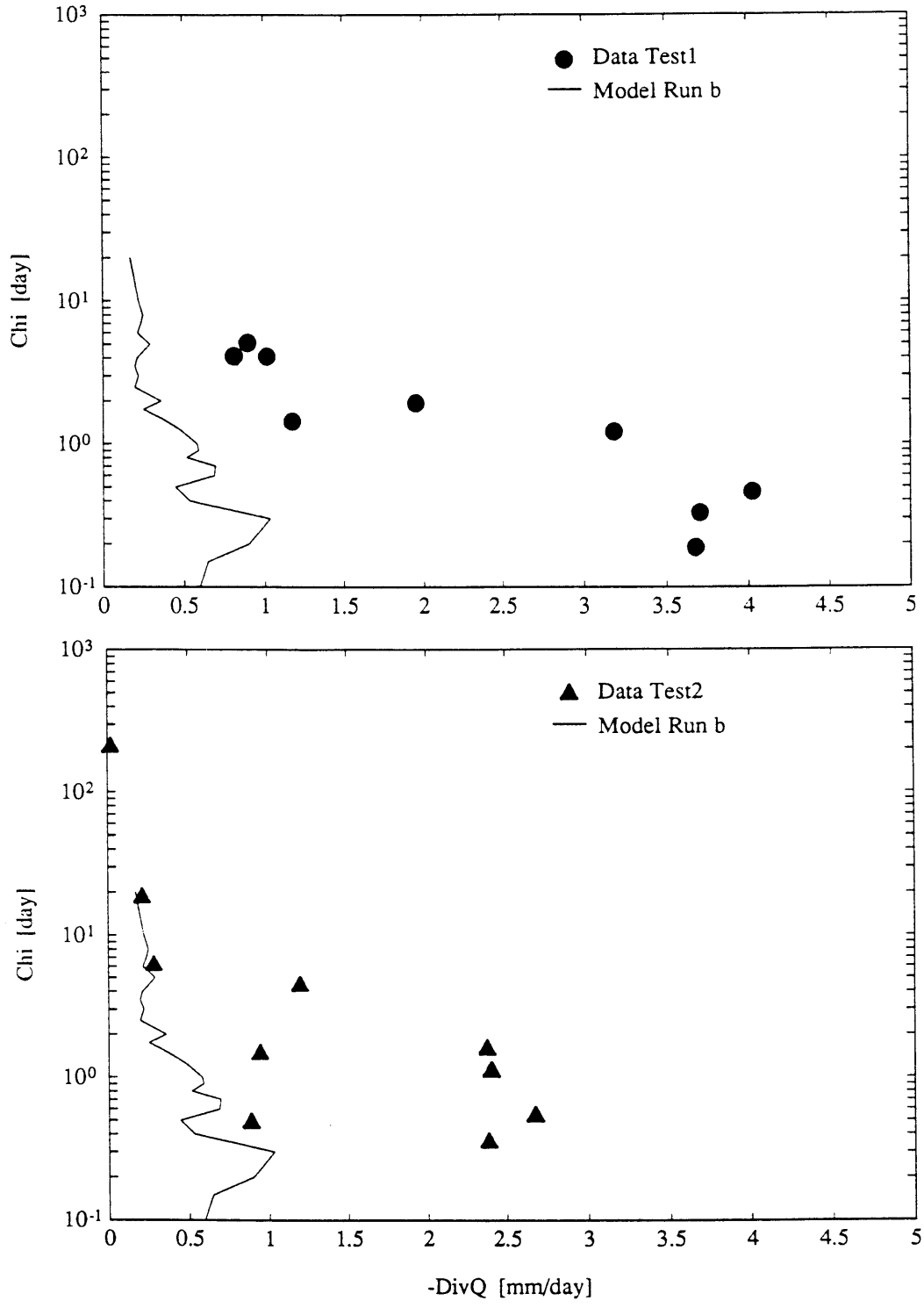

Figure 3.8: Observational estimates of $(-\nabla\cdot\vec{Q},\ \hat{\chi})$ compared with model output $(-\nabla\cdot\vec{Q},\ \chi)$ produced by varying χ with all other parameters fixed, Run b.

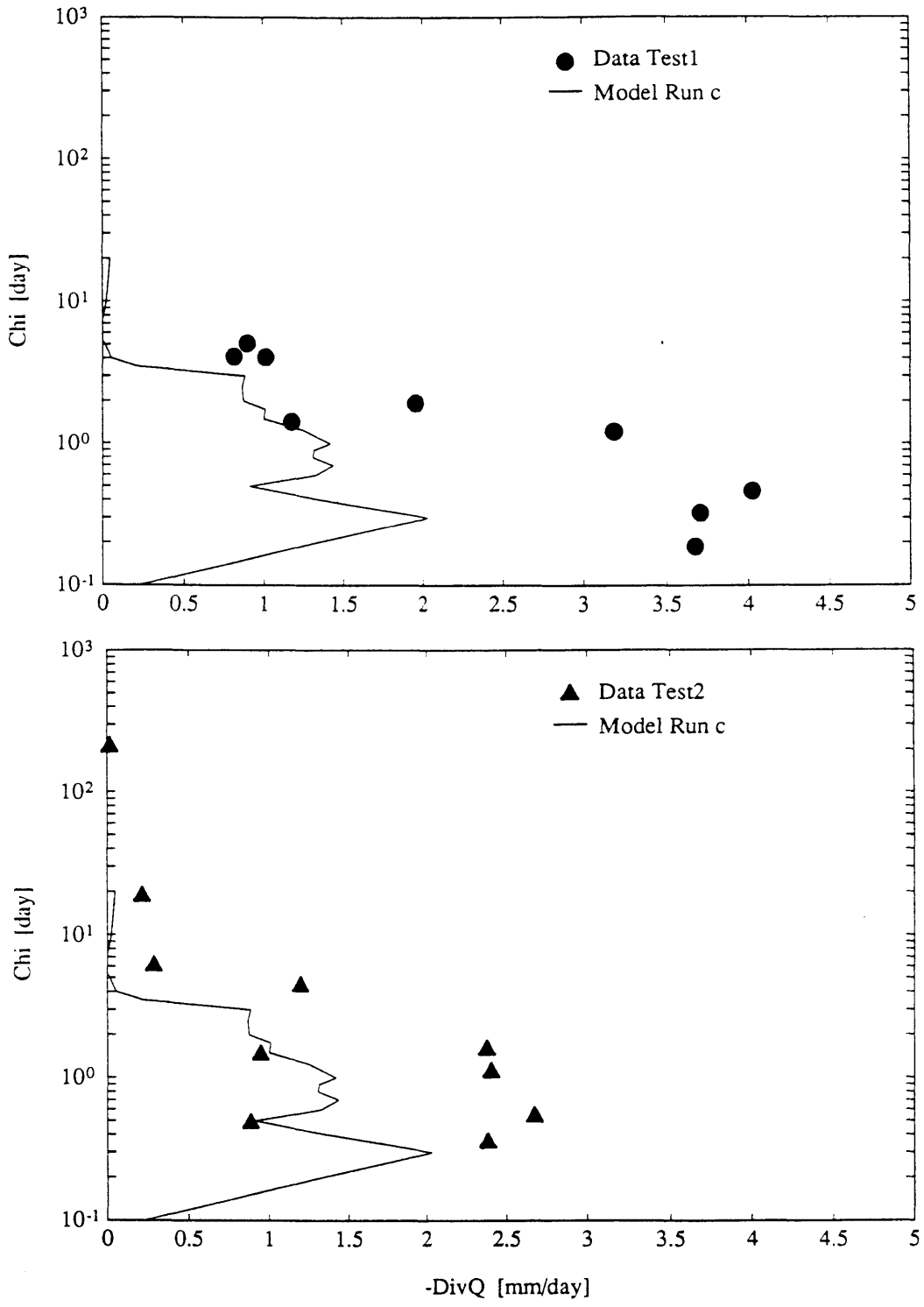

Figure 3.9: Observational estimates of $(-\nabla\cdot\vec{Q},\ \hat{\chi})$ compared with model output $(-\nabla\cdot\vec{Q},\ \chi)$ produced by varying χ with all other parameters fixed, Run c.

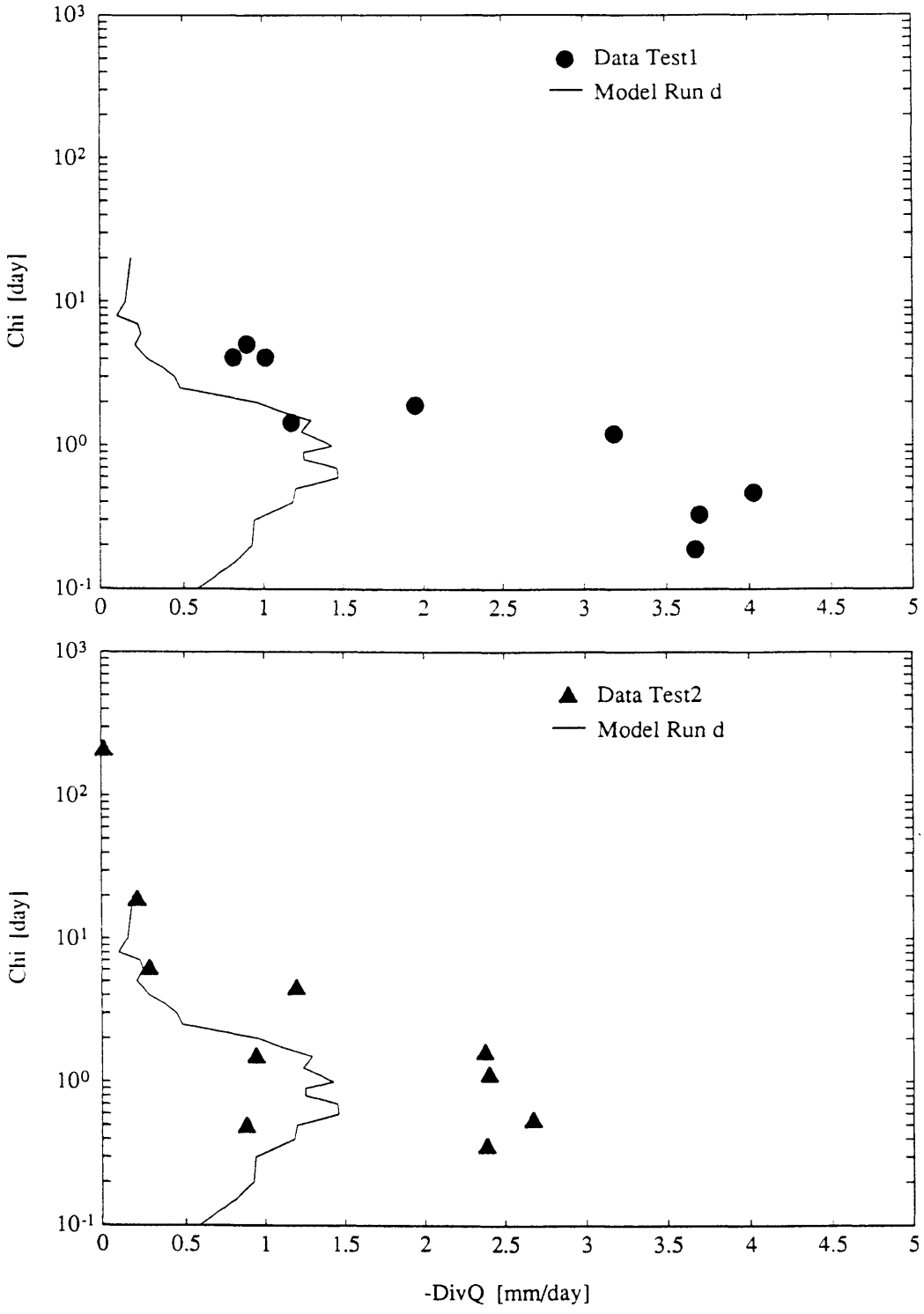

Figure 3.10: Observational estimates of $(-\nabla\cdot\vec{Q},\ \hat{\chi})$ compared with model output $(-\nabla\cdot\vec{Q},\ \chi)$ produced by varying χ with all other parameters fixed, Run d.

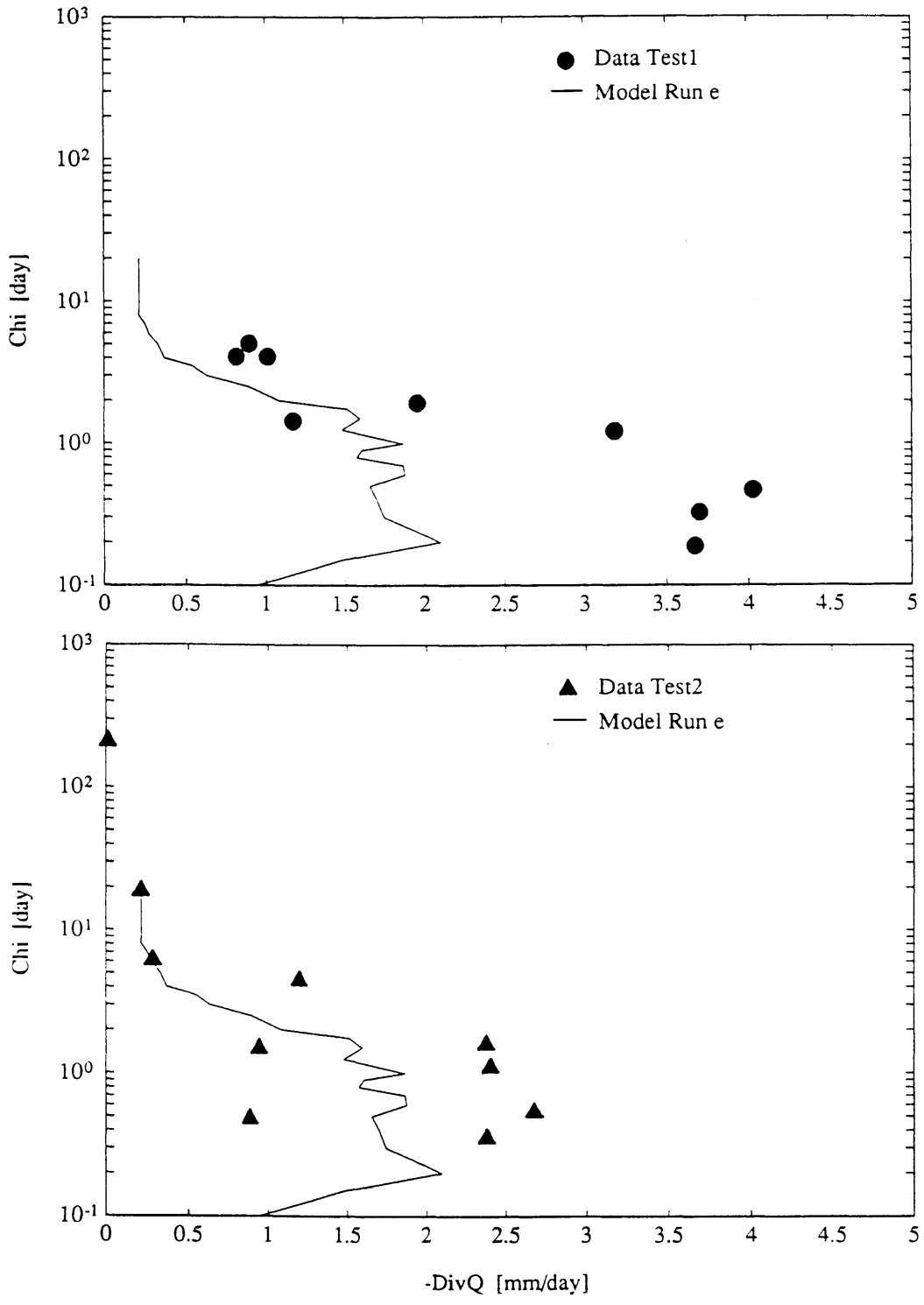

Figure 3.11: Observational estimates of $(-\nabla\cdot\vec{Q},\ \hat{\chi})$ compared with model output $(-\nabla\cdot\vec{Q},\ \chi)$ produced by varying χ with all other parameters fixed, Run e.

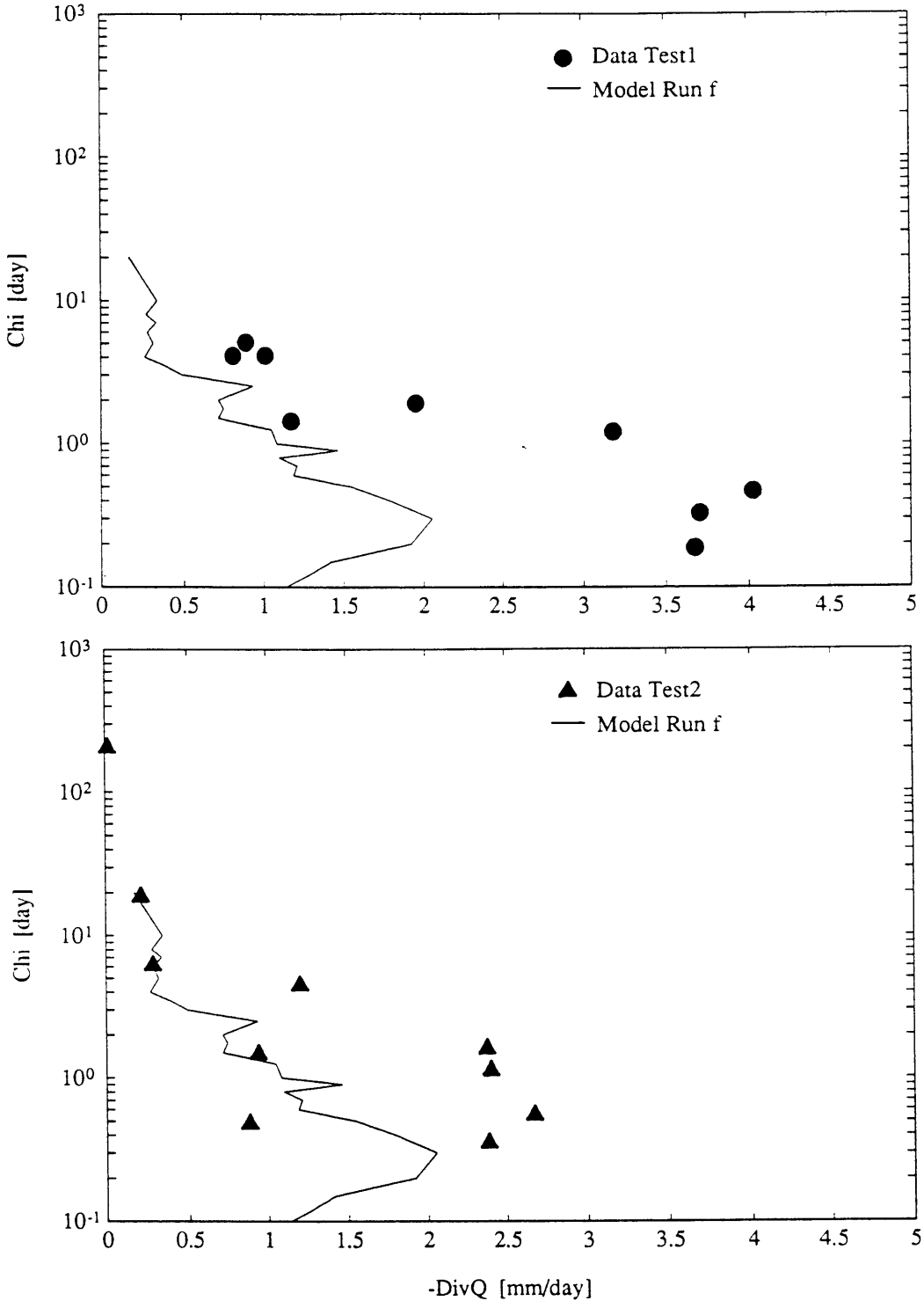

Figure 3.12: Observational estimates of $(-\nabla\cdot\vec{Q},\ \hat{\chi})$ compared with model output $(-\nabla\cdot\vec{Q},\ \chi)$ produced by varying χ with all other parameters fixed, Run f.

The model runs all exhibit a similar pattern, with the highest values of χ corresponding to the lowest values of $-\nabla\cdot\vec{Q}$, and a maximum value of $-\nabla\cdot\vec{Q}$ associated with a critical value of χ; the critical value lies between 0.2 and 1.0 day for all six runs. In addition, the model runs show a plateau of nearly constant low values of $-\nabla\cdot\vec{Q}$ for χ greater than a value lying between 2.0 and 5.0. The Test2 data show a similar peak and plateau structure, whereas the Test1 data show a peak, but no plateau.

In the model, with a large prescribed value of χ, the oceanic and the continental air columns are virutally isolated from one another. In this case, there is little mixing of air between the two halves of the model and the magnitude of $\nabla\cdot\vec{Q}$ will thus remain low. At lower values of prescribed χ in the model, the mixing is more efficient and the magnitude of $\nabla\cdot\vec{Q}$ will be larger, due to greater moisture exchange between the ocean and the land air columns. At even lower values of prescribed χ in the model, the mixing of the two air columns is essentially complete. In this case, the constraint on the magnitude of $\nabla\cdot\vec{Q}$ is the moist convection scheme, which vertically distributes the heat and mosture input at the surface interface of the air column. At very low values of prescribed χ, the $\nabla\cdot\vec{Q}$ rates (as a consequence of limits on precipitation) will be somewhat reduced and tend toward another plateau.

The model and data curves in Figures 3.7 through 3.12 do not match exactly. They were not expected to match, because the plots are not a comparison of theoretical prediction to experimental results. The model runs were not an attempt to model the Amazon basin. This is a comparison between a simple numerical model of the hydrologic cycle in the abstract, and a continental region that exhibits one of the most self–contained hydrologic cycles observed on the Earth.

Concerning the objectives outlined in Section 3.1, two results emerge: 1) the response of moisture convergence to changing χ in the model follows a pattern that is qualitatively the same as the relationship between $-\nabla\cdot\vec{Q}$ and $\hat{\chi}$ for the South American region. In the sense of qualitative agreement the convergence parameterization is concluded to be a reasonable representation of the complex dynamics of moisture convergence. 2) Values of $\hat{\chi}$ for a real Earth region lie in the range 10^{-1} to 10^{3} days, with values above approximately 10 days corresponding to very low rates of moisture convergence and values of about .5 day corresponding to maximal moisture convergence. These results give an appropriate scale for the selection of χ for the screening model.

3.6 Discussion

The two sets of anomalous observational data that were excluded from Figures 3.6 through 3.12 are now discussed. In the case of Experiment 1, $\hat{\chi}$ was negative for the months of December, January, and February. As shown in Table 3.3 and Figure 3.13, atmospheric moisture converged onto the continental region during these months, despite the fact that the scaled water content of the oceanic control volume $\left[\frac{A_c}{A_o} M_o\right]$ was less than the water content of the continent control volume (M_c). In absolute terms, the water contents of the two reservoirs were most nearly equal during these months. However, the oceanic air mass is greater, due to the combined effect of the ocean region's greater surface area and the topography of the land region. The areal mean specific humidity of the selected ocean region was less than that of the land region throughout the year; this result may be attributable to

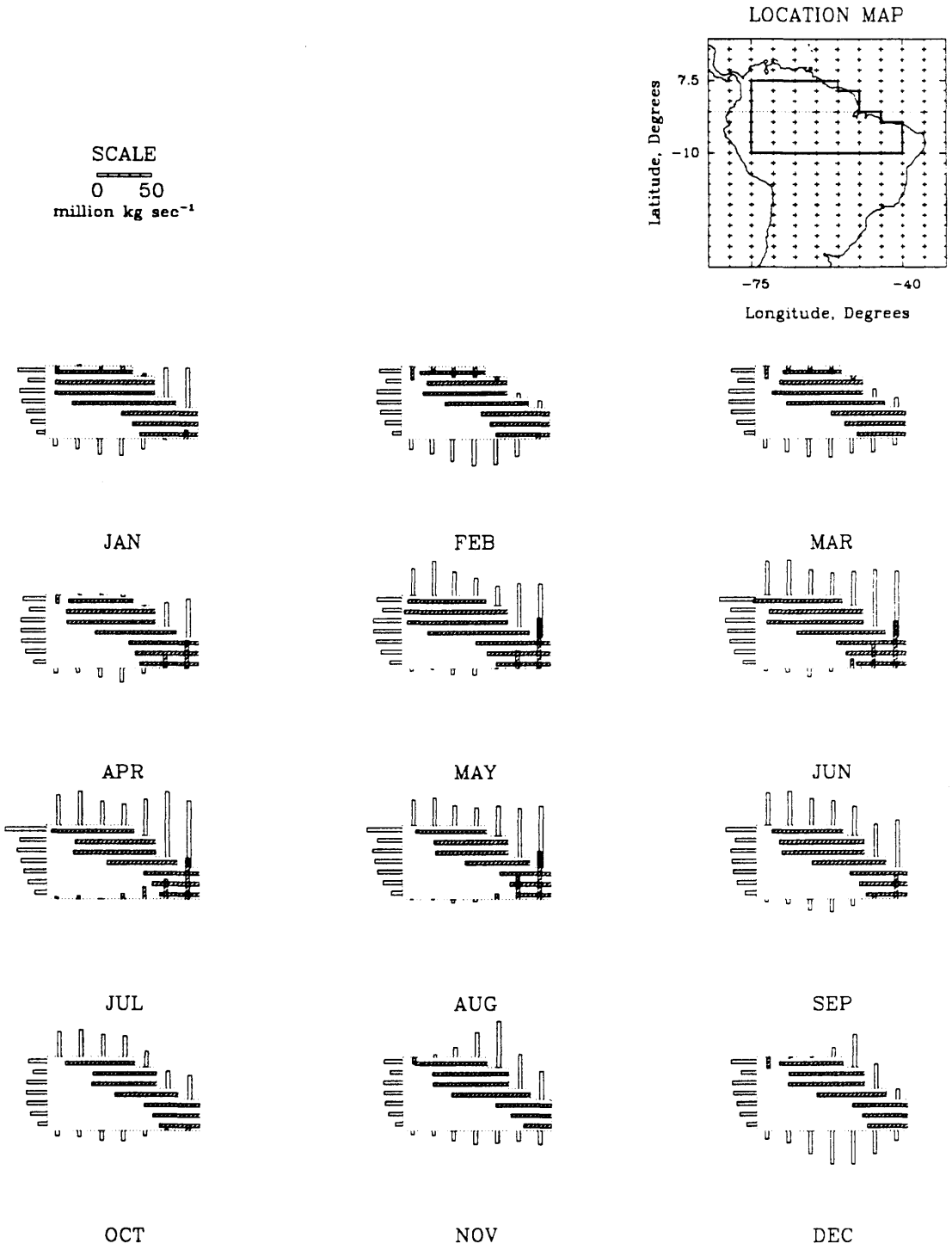

Figure 3.13: Region Test1. Bar graphs of the moisture flux across segments of the boundary. Each bar represents the integral of the normal component of $\vec{Q}$ along the segment at the base of the bar.

numerical error and to data sparsity for the Southern Hemisphere in general, and the oceans in particular.

For Experiment 2, the months of July and August exhibited net *divergence* of moisture from the continental region, rather than convergence, despite the fact that $\frac{A_c}{A_o} M_o$ was greater than M_c for these months. In Figure 3.1, the JJA map shows a strong northward component to the moisture transport off the ocean study region Twater2. This northward component is reflected in Figure 3.14 by the large outward bars on the northeast boundary of the continental region. Southward from the Equator, the boundary flux of moisture from the ocean source region decreases linearly, and reverses direction at the southeast corner. Because of the direction of net moisture transport in this season, the direct input of moisture from the assumed ocean source region to the continental region as a whole is not great. The same flow pattern applies to Experiment 1 in these months; however, Region Test1 (Figure 3.13) is truncated above the latitude where the linear decrease in landward moisture flux begins.

It is clear from Figures 3.13 and 3.14 that the continental regions Test1 and Test2 do not interact uniquely with the Atlantic Ocean source regions Twater1 and Twater2. Atmospheric runoff occurs over the western boundary into the Pacific Ocean, over the southern boundary onto an adjoining continental region, and over the northern boundary into the Caribbean Sea. The region is not a simple one inlet–one outlet hydrologic cycle, as was assumed when it was chosen to give real–world values of the model parameter χ. A more appropriate choice might be to include the Caribbean Sea and Eastern Pacific as part of the ocean study region in both experiments; although these ocean regions generally do not contribute moisture *to* the

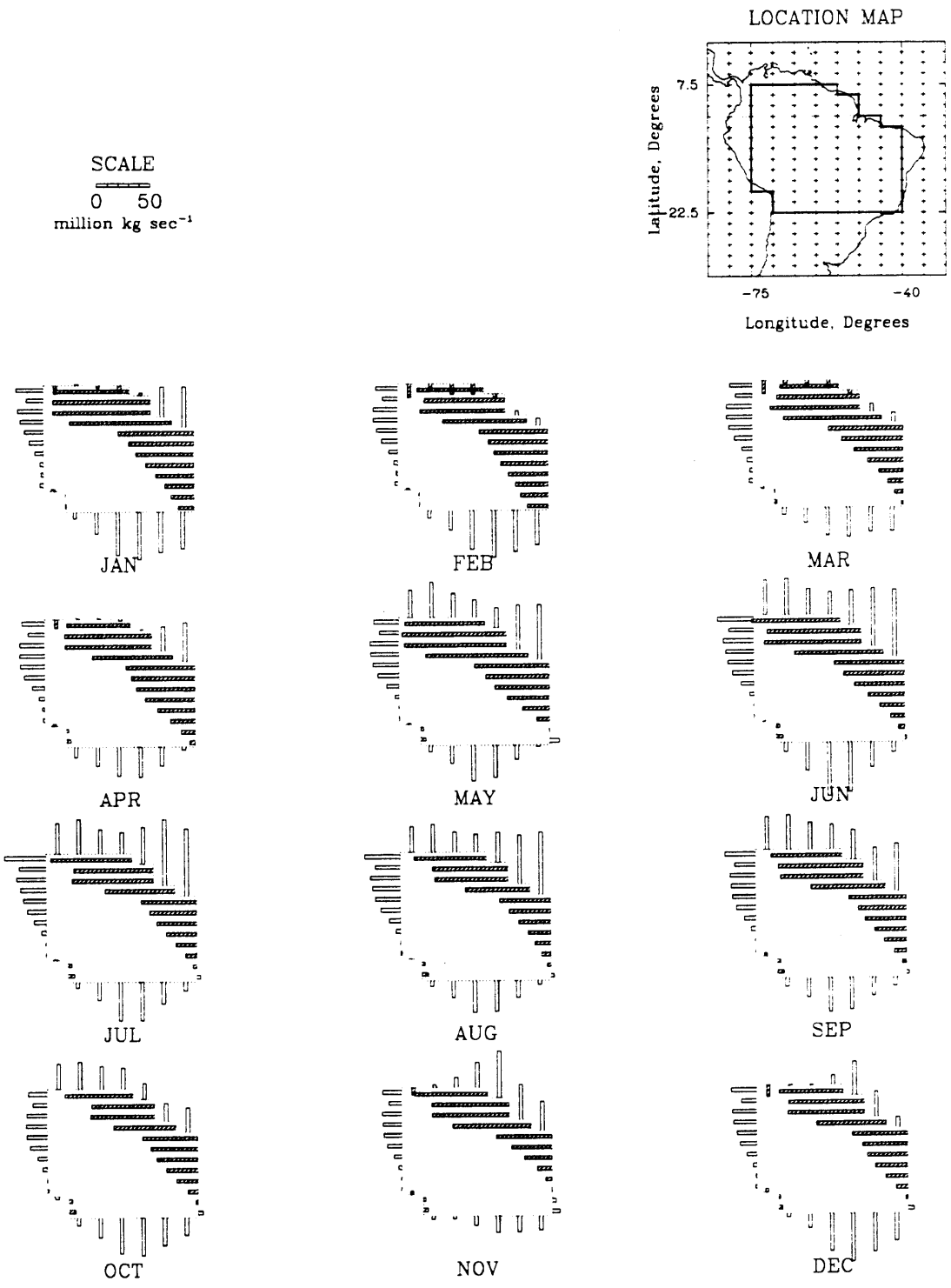

Figure 3.14: Region Test2. Bar graphs of the moisture flux across segments of the boundary. Each bar represents the integral of the normal component of $\vec{Q}$ along the segment at the base of the bar.

continent, they receive efflux *from* the continent. In the model, the same ocean box serves both functions. It is impossible to find such a situation on the Earth; however, including a ring of ocean around a continent might come closer than isolating a particular piece of ocean.

It has been demonstrated that the linear reservoir parameterization of ocean to continent moisture transport in the screening model produces a qualitatively realistic relationship between the transport and the climatic moisture convergence, when compared with one of the most straightforward continental hydrologic cycles on the Earth.

REFERENCES

Alestalo, M., 1983. The atmospheric water vapor budget over Europe. In *Variations in the Global Water Budget*, ed. A. Street–Perrot et al., pp. 67–79. Dordrecht: D. Reidel Publ. Co.

Anthes, R. A., 1984. Enhancement of convective precipitation by mesoscale variations in vegetative covering in semiarid regions. *Journal of Climate and Applied Meteorology*, 23: 541–554.

Benton, G. S., R. T. Blackburn and V. O. Snead, 1950. The role of the atmosphere in the hydrologic cycle. *Transactions*, American Geophysical Union, 31: 61–73.

Benton, G. S. and M. A. Estoque, 1954. Water vapor transfer over the North American continent. *Journal of Meteorology*, 11: 462–477.

Budyko, M. I., 1974. *Climate and Life*, Academic Press, 508 pp.

Chen, T.–C., 1985. Global water vapor flux and maintenance during FGGE. *Monthly Weather Review*, 113: 1801–1819.

Dettwiller, J. and S. A. Changnon, Jr., 1976. Possible urban effects on maximum daily rainfall at Paris, St. Louis and Chicago. *Journal of Applied Meteorology*, 15: 517–519.

Eagleson, P. S., ed., 1982. *Land Surface Processes in Atmospheric General Circulation Models.* Cambridge University Press, 560 pp.

Entekhabi, D. and P. S. Eagleson, 1989. Landsurface hydrology parameterization for atmospheric general circulation models: inclusion of subgrid scale spatial variability and screening with a simple climate model. *MIT Department of Civil Engineering, Ralph M. Parsons Laboratory Report No. 325*, 195 pp.

Entekhabi, D., I. Rodriguez–Iturbe and R. L. Bras, 1991. Interannual variability in a stochastic model of large–scale water balance with land surface–atmosphere interaction, submitted to *Journal of Climate.*

Fowler, W. B. and J. D. Helvey, 1974. Effect of large–scale irrigation on climate in the Columbia Basin. *Science* 184: 121–127.

Harris, R. G., A. Thomasell, Jr. and J. G. Welsh, 1966. Studies of techniques for the analysis and prediction of temperature in the ocean, Part III: Automated analysis and prediction. Interim Report, prepared by Travelers Research Center, Inc. for U. S. Naval Oceanographic Office, Contract #N62306–1675, 97 pp. (as cited in Oort, 1983).

Hastenrath, S. L., 1966. The flux of atmospheric water vapor over the Caribbean Sea and the Gulf of Mexico. *Journal of Applied Meteorology*, 5: 778–788.

Henderson–Sellers, A. and K. McGuffie, 1987. *A Climate Modelling Primer.* Chichester: John Wiley & Sons, 217 pp.

Joussame, S., R. Sadourny and C. Vignal, 1986. Origin of precipitating water in a numerical simulation of the July climate. *Ocean–Air Interactions*, 1: 43–56.

Koster, R. D., J. Jouzel, R. Suozzo, G. Russell, W. Broecker, D. Read and P. S. Eagleson, 1986. Global sources of local precipitation as determined by the NASA/GISS GCM, *Geophysical Research Letters*, 13: 121–124.

Koster, R. D., P. S. Eagleson and W. S. Broecker, 1988. Tracer water transport and subgrid precipitation variation within atmospheric general circulation models. *MIT Department of Civil Engineering, Ralph M. Parsons Laboratory Report No. 317*, 364 pp.

Koster, R. D. and P. S. Eagleson, 1990. A one–dimensional interactive soil–atmosphere model for testing formulations of surface hydrology. *Journal of Climate*, 3: 593–606.

Lettau, H., 1969. Evapotranspiration Climatonomy: 1. A new approach to numerical prediction of monthly evapotranspiration, runoff, and soil moisture storage. *Monthly Weather Review*, 97: 691–699.

Lettau, H., K. Lettau, and L. C. B. Molion, 1979. Amazonia's hydrologic cycle and the role of atmospheric recycling in assessing deforestation effects. *Monthly Weather Review*, 107: 227–238.

Lufkin, D., 1959. Atmospheric water divergence and the water balance at the Earth's surface. *General Circulation Project Sci. Rept. No. 4.*, 44 pp., Cambridge, MA: MIT Press.

Marques, J., J. M. Santos, N. A. Villa Nova, and E. Salati, 1977. Precipitable water and water vapor flux between Belem and Manaus. *Acta Amazonica* 7: 355–362 (as cited in Salati et al., 1979).

McDonald, J., 1962. The evaporation–precipitation fallacy. *Weather*, 17: 168–177.

Oort, A. H., 1983. Global atmospheric circulation statistics, 1958–1973. *NOAA Prof. Paper No. 14*, 180 pp. (+ 47 microfiches). Washington, D.C.: U. S. Government Printing Office.

Paluch, I. R., 1979. The entrainment mechanism in Colorado cumuli. *Journal of the Atmospheric Sciences*, 36: 2462–2478.

Peixóto, J. P., 1973. Atmosphere vapor flux computations for hydrological purposes. *Report No. 20, Reports on WMO/IHD Projects*, World Meteorological Organization (WMO), Geneva, Switzerland, 83 pp.

Peixóto, J. P. and A. H. Oort, 1983. The atmospheric branch of the hydrological cycle and climate. In *Variations in the Global Water Budget*, ed. A. Street–Perrot et al., pp. 5–65. Dordrecht: D. Reidel Publ. Co.

Rasmusson, E. M., 1967. Atmospheric water vapor transport and the water balance of North America. Part 1. Characteristics of the water vapor flux Field. *Monthly Weather Review*, 95: 403–426.

Rasmusson, E. M., 1968. Atmospheric water vapor transport and the water balance of North America. Part 2. Large scale water balance investigations. *Monthly Weather Review*, 96: 720–734.

Rasmusson, E. M., 1971. A study of the hydrology of eastern North America using atmospheric vapor flux data. *Monthly Weather Review*, 99: 119–135.

Rasmusson, E. M., 1977. Hydrological application of atmospheric vapor–flux analyses. *Operational Hydrology Report No. 11*, WMO, Geneva, Switzerland, 50 pp.

Rodriguez–Iturbe, I., D. Entekhabi and R. L. Bras, 1990. Non–linear dynamics of soil moisture at climate scales: stochastic analysis. *Massachusetts Institute of Technology Center for Global Change Science Report No. 5.*

Rodriguez–Iturbe, I., D. Entekhabi and R. L. Bras, 1990. Non–linear dynamics of soil moisture at climate scales: chaotic analysis. *Massachusetts Institute of Technology Center for Global Change Science Report No. 6.*

Rodriguez–Iturbe, I., D. Entekhabi and R. L. Bras, 1991. Non–linear dynamics of soil moisture at climate scales: 1. stochastic analysis. *Water Resources Research*, in press.

Rosen, R. D., D. A. Salstein and J. P. Peixóto, 1979. Variability in the annual fields of large–scale atmospheric water vapor transport. *Monthly Weather Review*, 107: 26–27 (as cited in Oort, 1983).

Salati, E., A. Dall'Olio, E. Matsui, and J. Gat, 1979. Recycling of water in the Amazon Basin: an isotopic study. *Water Resources Research*, 15: 1250–1258.

Savijärvi, H. I., 1988. Global energy and moisture budgets from rawinsonde data. *Monthly Weather Review*, 116: 417–430.

Schickedanz, P. T., 1976. The effect of irrigation on precipitation in the Great Plains. *National Science Foundation Report No. NSF GI–43871*, 105 pp.

Shiklomanov, I. A., 1989. Climate and water resources. *Hydrological Sciences Journal*, 34: 495–529.

Shukla, J. and Y. Mintz, 1982. Influence of land–surface evapotranspiration on the earth's climate. *Science*, 215: 1498–1501.

Starr, V. P. and J. P. Peixóto, 1958. On the global balance of water vapor and the hydrology of deserts. *Tellus*, 10: 189–194.

Stidd, C. K., 1967. Local moisture and precipitation. *Preprint No. 45A* (rev. July, 1968), Desert Research Institute, University of Nevada, Reno, 34 pp.

Stidd, C. K., 1975. Irrigation increases rainfall? *Science* 188: 279–281.

Sutcliffe, R. C., 1956. Water balance and the general circulation of the atmosphere. *Quarterly Journal of the Royal Meteorological Society*, 82: 385–395.

Taylor, G. R. and M. B. Baker, 1991. Entrainment and detrainment in cumulus clouds. *Journal of the Atmospheric Sciences*, 48: 112–121.

Thornthwaite, C. W., 1946. The moisture–factor in climate. *Transactions, American Geophysical Union*, 27: 41–48.

APPENDIX A

Computational Methods

A.1 Area integrals on the spherical surface

We wish to approximate the integral

$$\int\int h(x,y)\ dA \tag{A.1}$$

given values of h at nodes on a latitude longitude grid having n×m nodes (Figure A.1). We approximate (A.1) by a discrete sum,

$$\int\int h(x,y)\ dA \cong \sum_{i=1}^{n} \sum_{j=1}^{m} h_{ij}\ \Delta A_{ij}\ w_{ij} \tag{A.2}$$

in which h_{ij} is the value of the function h at node (i,j), ΔA_{ij} is the area of the rectangle with node (i,j) at its center, and w_{ij} is a weighting term, equal to 1.0, 0.5, or 0.25, depending upon what fraction of the rectangle is included in the region. As shown in Figure A.1,

$$w_{11} = w_{n1} = w_{1m} = w_{nm} = 0.25 \quad \text{(corner nodes)}$$

$$\left.\begin{aligned} w_{i1} = w_{im} &= 0.5, \quad i = 1 \text{ to } n \\ w_{1j} = w_{nj} &= 0.5, \quad j = 1 \text{ to } m \end{aligned}\right\} \quad \text{(edge nodes)} \tag{A.3}$$

$$w_{ij} = 1.0 \qquad \text{(all other nodes)}\ .$$

The area of a rectangle on the spherical surface, ΔA_{ij}, is approximated as

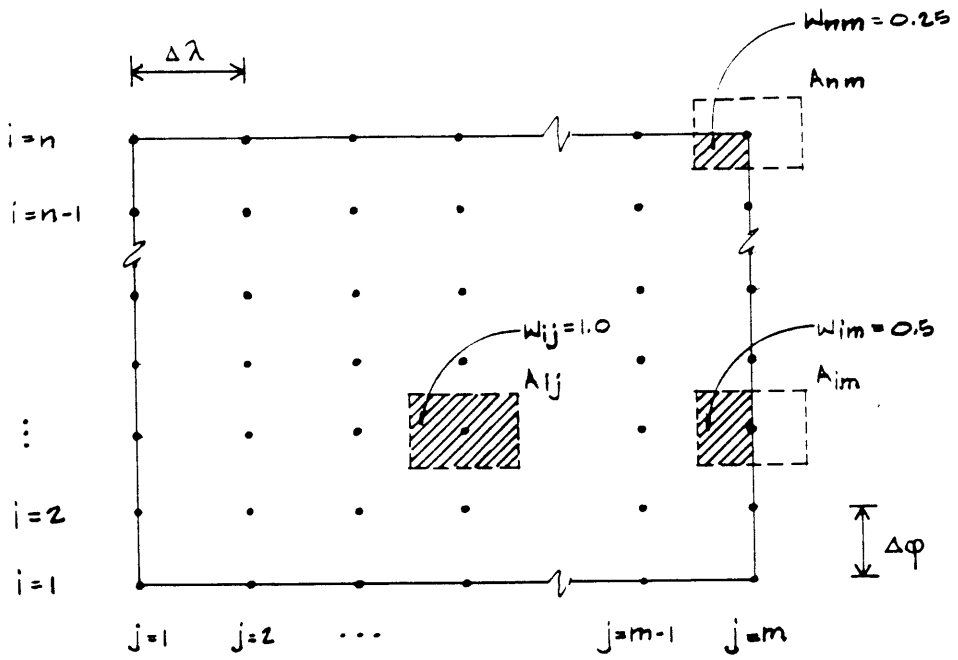

Figure A.1 Definition sketch for Section A.1.

$$\Delta A_{ij} \cong (\Delta\phi)(\Delta\lambda) \cos \phi_i R^2 \tag{A.4}$$

in which $\Delta\phi$ and $\Delta\lambda$ are, respectively, the latitude and longitude spacing of the grid, in radians; ϕ_i is the latitude at node (i,j), and R is the radius of the Earth, 6.37×10^6 m.

A.2 Effective length

The average moisture flux vector over a region, $\langle\vec{Q}\rangle$ has scalar components $\langle Q_\phi \rangle$ and $\langle Q_\lambda \rangle$, defined as

$$\langle Q_\phi \rangle = \frac{\int\int Q_\phi \, dA}{\int\int dA} \tag{A.5}$$

$$\langle Q_\lambda \rangle = \frac{\int\int Q_\lambda \, dA}{\int\int dA}$$

where the area integrals are evaluated as described in Section A.1. A unit direction vector is defined

$$\hat{u} = \frac{\langle\vec{Q}\rangle}{\|\langle Q\rangle\|} . \tag{A.6}$$

The angle between the positive x axis and $\vec{Q}$ is θ, i.e.

$$\theta = \tan^{-1} \frac{\langle Q_\phi \rangle}{\langle Q_\lambda \rangle} . \tag{A.7}$$

For purposes of this approximation, the entire region is treated as a plane rectangle with length Δx, where

$$\Delta x = \frac{A}{\Delta y} \tag{A.8}$$

in which A is the area and Δy the north–south dimension of the region.

We wish to find the average length of the region in the direction of $\hat{u}$. As shown in Figure A.2, the region can be represented as n strips of width δw. Each strip, i, has a length ℓ_i, and the average length is

$$\ell_{eff} = \frac{\sum_{i=n}^{n} \ell_i \Delta w}{\sum_{i=1} \delta w} \tag{A.9}$$

The unit direction vector defines at most two sides of the region as influx boundaries. Without loss of generality, assume that $0 < \theta < \frac{\pi}{2}$, as in Figure A.2. Along the north–south influx boundary, $\delta w = \delta y \cos \theta$ and along the west–east influx boundary, $\delta w = \delta x \sin\theta$. In the limit, taking δw (consequently δx and δy) infinitesimal,

$$\sum_{i=1}^{n} \delta w \longrightarrow \oint_{\substack{\text{influx} \\ \text{boundary}}} dw = \int_0^{\Delta y} dy \cos \theta + \int_0^{\Delta x} dx \sin \theta \, . \tag{A.10}$$

Noting that $\sum_{i=1}^{n} \ell_i \delta w = A$, (A.9) becomes

$$\ell_{eff} = \frac{A}{\Delta y \cos\theta + \Delta x \sin \theta}. \tag{A.11}$$

More generally, to allow for $\hat{u}$ in other quadrants,

$$\ell_{eff} = \frac{A}{\Delta y |\cos \theta| + \Delta x |\sin \theta|} \tag{A.12}$$

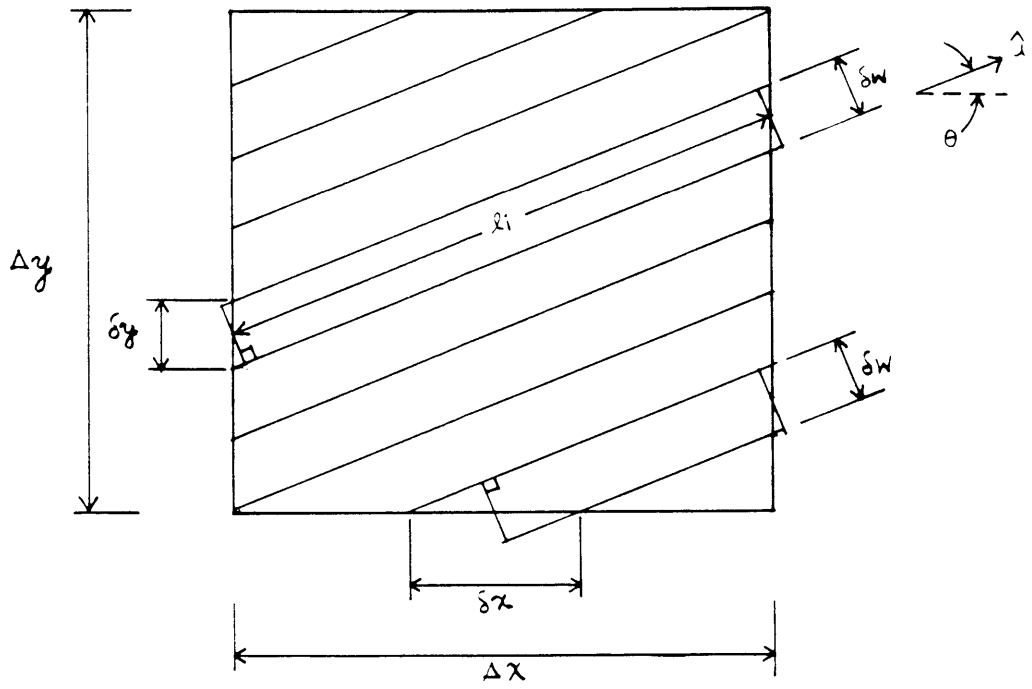

Figure A.2 Definition sketch for Section A.2.

A.3 Effective moisture influx

To determine $(wu)_{eff}$, we resolve $\vec{Q}$ along the influx boundary into a component parallel to $\hat{u}$ and a component perpendicular to $\hat{u}$. The parallel component is $\vec{Q}\cdot\hat{u}$. Following the same argument as above, the length weighted average $\vec{Q}\cdot\hat{u}$ is

$$(wu)_{eff} = \frac{\sum_{i=1}^{n} (\vec{Q}\cdot\hat{u})_i \, \ell_i \delta w}{\sum_{i=1}^{n} \ell_i \, \delta w} \quad . \tag{A.13}$$

In the limit, integrating along the influx boundary,

$$(wu)_{eff} = \frac{\int_{\gamma_a}^{\gamma_b} (\vec{Q}.\hat{u}) \; \ell(\gamma) \sin \alpha \; d\gamma}{A} \tag{A.14}$$

in which γ is the distance along the influx boundary, γ_a and γ_b are the endpoints of the influx boundary, $\vec{d\gamma}$ is the unit vector defining the direction in which the path is traced, and α is the angle between $\vec{d\gamma}$ and $\hat{u}$. As shown in Figure A.3, $\alpha = \theta$ along the west–east boundary, and $\alpha = \theta + \frac{\pi}{2}$ along the north–south boundary, when $0 < \theta < \frac{\pi}{2}$.

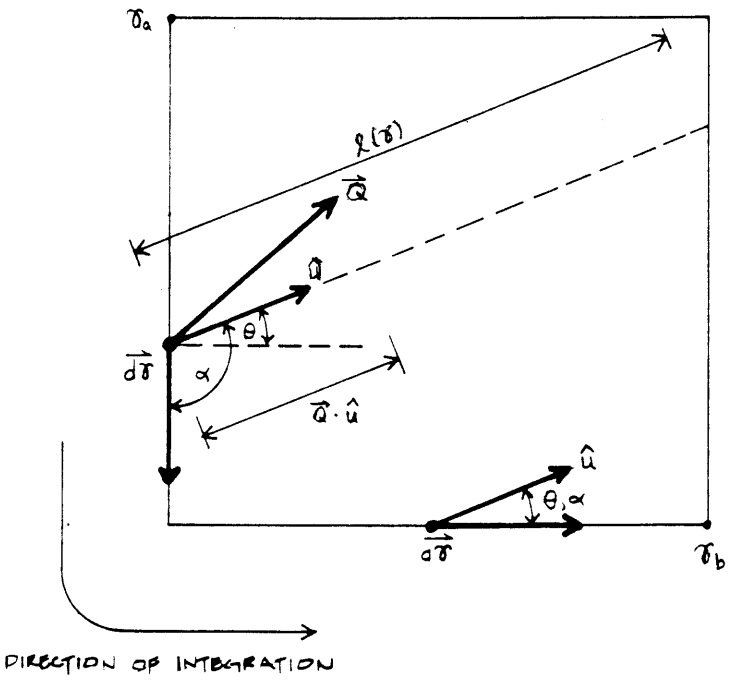

Figure A.3 Definition sketch for Section A.3.

APPENDIX B

Computer Programs

Programs include:

1. AREA. Computes the area of a region, given latitude, longitude, and weight factor for each node.

2. BFLUXW. Computes the net atmospheric vapor flux over a specified boundary on the plane

3. QEFF. Computes areally–averaged moisture flux vector components.

4. WU. Computes $(wu)_{eff}$, Equation (2.16).

Common to all the computer routines is a database of the components of $\vec{Q}$ in 73 × 73 (ILAT,JLON) arrays, where ILAT is the latitude index (1 at 90° S to 73 at 90° N) and JLON is the longitude index (1 at 180° E to 73 at 180° W). The components were computed by trapezoidal rule integration of Equation 1.15.

area.f Wed May 22 13:25:32 1991 1

```
      PROGRAM AREA
C
C Computes area, given latitude, longitude,
C and included part (SQUSE) of grid square surrounding each node.
C (because some nodes are at corners & do not contribute whole elements).
C Reads an input file: N, M, beginning indices (GFDL Grid--
C start top left) and N row by M column matrix of area fractions.
C       units: area fractions are in eigths. (0,1,2,3,4...8)
C Computes an estimate of the total area defined by the grid.
C Note: "estimate" means that the area (dy)x(dx) is estimated as
C dA = (R*dPhi)(R*dLam*cos(PhiNode)), PhiNode is the latitude at
C the node, i.e. the center of the grid element.
C
C Area is in m^2.
C
      CHARACTER*60 TITLE
      CHARACTER*5 FNSET
      CHARACTER*18 FNSQAR, FNAREA
      REAL PI,PHI,SQUSE(73,73)
      PARAMETER (AR=6.371E6, PI=3.14159)
      DATA DPHI, DLAM / 2.5, -5./
      DATA LATZ / 37 /
C
C Convert to radians
      DPHI=DPHI/180.*PI
      DLAM=DLAM/180.*PI
C
      WRITE (6,*) 'Name of dataset?'
      READ (5,*) FNSET
      FNSQAR=FNSET//'.sq'
      FNAREA=FNSET//'.ar'
      OPEN (UNIT=12,FILE=FNSQAR,STATUS='OLD')
      READ(12,100) TITLE
      READ(12,*) N,M,LATB,LONB
      LATF=LATB-N+1
      LONF=LONB-M+1
      SUM=0.0
      DO 10 ILAT=LATB,LATF,-1
         PHI=REAL(ILAT-LATZ)*DPHI
        COSPHI=COS(PHI)
        WRITE (6,*) PHI,COSPHI
        READ(12,*) (SQUSE(ILAT,JLON),JLON=LONB,LONF,-1)
        WRITE (6,*) (SQUSE(ILAT,JLON),JLON=LONB,LONF,-1)
        DO 20 JLON=LONB,LONF,-1
           TERM=COSPHI*SQUSE(ILAT,JLON)/8.
           SUM=SUM+TERM
 20     CONTINUE
 10   CONTINUE
      CLOSE(12,STATUS='KEEP')
C
      RAREA=SUM*AR*AR*DPHI*ABS(DLAM)
      OPEN(UNIT=13,FILE=FNAREA,STATUS='NEW')
      WRITE(13,500) FNSQAR
      WRITE(13,501) RAREA
      STOP
```

```
 100  FORMAT (A60)
 500  FORMAT (1X,'Area Computation for ',A18,3X,'(m^2)'/)
 501  FORMAT (1X,E11.4)
      END
```

```
      PROGRAM BFLUXW
C
C Computes the net atmospheric vapor flux over a specified boundary
C on the plane (spherical), using GFDL's 73x73 (Lat,Lon) grid.
C Created 7/30/90, KB.  Modified for unix fortran 2/28/91.
C Applies bivariate interpolation (allows diagonal boundary segments).
C The two components of the vector must be specified at each node
C along the boundary, and at all corner nodes of a grid when the
C boundary segment is diagonal.
C The net INflux over an infinitesimal segment of the boundary is
C equal to the dot product of the flux vector and the inward normal
C vector; in this case, with linear boundary segments, each segment's
C contribution is the dot product of inward normal and average flux
C vector for the segment.
C The resulting total over the whole boundary is -divV x A,
C where V is the vector quantity and A is the area of the region.
C Influx and Outflux are both computed.
C
C For the variables, the final index distinguishes between the
C value of the quantity, and its variance (sigma^2), as computed by
C standard propagation of error.  The quantity is then expressed
C as +- 2*sigma.
C
C Components of the vector moisture flux (QPHI, QLAM) have units
C g m^(-1) s^(-1)
C Distances (DELX,DELY,BNX,BNY,BX,BY) have units m
C
      CHARACTER*60 TITLE,CJUNK
      CHARACTER*5  FNSET
      CHARACTER*18 FNBNOD, FNAREA, FNSIGF, FNTXT, FNSGFX
      CHARACTER*3 FNAME(17)
      CHARACTER*30 FNLAM, FNPHI
      INTEGER LAT(100), LON(100)
      REAL QPHI(73,73,2), QLAM(73,73,2), FX(2), FY(2), QIN(2),
     &     QNET(2), SUMIN(2), SUMOUT(2),
     &     BNX(100), BNY(100), SFIN(17), SFOUT(17), SEGFLX(100,17),
     &     SQNET(17)
      REAL PHI1,PHI2
      PARAMETER (AR=6.371E6, PI=3.14159, RHOW=1000.,SECDAY=86400.)
      DATA DPHI, DLAM / 2.5, -5./
      DATA FNAME / 'jan','feb','mar','apr','may','jun',
     &             'jul','aug','sep','oct','nov','dec',
     &             'djf','mam','jja','son','yer' /
C
  100 FORMAT(A60)
  101 FORMAT('1',A60,//,1X,'Month',I3,1X,'(',A3,')'//,
     &16X,'Flux, kg m^-1 s^-1    Scaled inward         Segment flux',/
     &16X,'                      normal vector, m      kg s^-1' ,//
     &' Node K  K+1    F(x)       F(y)       B(x)       B(y)       Qin',/,
     &1X,72('='))
  102 FORMAT (1X,I4,I6,4X,5(E10.3,1X),'+-',1X,E10.3)
  105 FORMAT (7E10.3 )
  106 FORMAT (/,1X,'Area   = ',E10.3,' m^2',//
     &1X,'<Qin>  = ',E10.3,' mm/day ','+-',1X,E9.3,
     &              12X,'Qin  = ',E10.3,1X,'+-',1X,E10.3,/,
```

```
     &1X,'<Qout> = ',E10.3,' mm/day ','+-',1X,E9.3,
     &               12X,'Qout = ',E10.3,1X,'+-',1X,E10.3,//,
     &1X,'<Qnet> = ',E10.3,' mm/day ','+-',1X,E9.3,
     &               12X,'Qnet = ',E10.3,1X,'+-',1X,E10.3,/)
 600  FORMAT (1X,'Boundary Flux Computation for ',A18,3X,'(kg s^-1)'/)
 601  FORMAT (1X,12E10.3)
 606  FORMAT (1X,4(E10.3,20X))
 602  FORMAT (/,1X,'Boundary Flux Computation for ',A18,3X,
     &        '(mm mo^-1)'/)
 603  FORMAT (1X,12F10.1)
 607  FORMAT (1X,4(F10.1,20X))
 604  FORMAT (17(1X,F5.1))
 605  FORMAT (/)
 500  FORMAT (A60,/)
 501  FORMAT (1X,E11.4)
C
C Additional conversion factor
      SECMON=30.4*SECDAY
C Convert to radians
      DPHI=DPHI/180.*PI
      DLAM=DLAM/180.*PI
C
C Input job data. FNBNOD has boundary node specifications.
C FNAREA has region's area.
      WRITE (6,*) 'Name of Data Set?'
      READ (5,*) FNSET
      FNBNOD=FNSET//'.bn'
      FNAREA=FNSET//'.ar'
      FNTXT=FNSET//'.txt'
      FNSIGF=FNSET//'.flx'
      FNSGFX=FNSET//'.seg'
      OPEN (UNIT=8,FILE=FNBNOD,STATUS='OLD')
      READ (8,100) TITLE
      N=0
  10  IF (N .GE. 999) GOTO 11
        NPTS=N
        READ (8,*) N, LAT(N), LON(N)
        GOTO 10
  11  CONTINUE
      CLOSE (8, STATUS='KEEP')
      OPEN (UNIT=8,FILE=FNAREA,STATUS='OLD')
      READ (8,500) CJUNK
      READ (8,501) SAREA
      CLOSE (8, STATUS='KEEP')
C
C == BOUNDARY LOOP =======================================================
C
      DO 60 K=1,NPTS-1
C Get delta x, delta y for bdy segment K to K+1.
           KP1=K+1
           I1=LAT(K)
           I2=LAT(KP1)
           J1=LON(K)
           J2=LON(KP1)
           PHI1=DPHI*(I1-37)
```

```
            PHI2=DPHI*(I2-37)
            PHIAV=(PHI1+PHI2)/2.
            DELX=(J2-J1)*DLAM*AR*COS(PHIAV)
            DELY=(I2-I1)*DPHI*AR
C Components of the inward normal vector.
            BNX(K)=-DELY
            BNY(K)= DELX
 60    CONTINUE
C
C == End boundary loop ==========================================
C
      OPEN (UNIT=8,FILE=FNTXT,STATUS='NEW')
C
C == MONTH LOOP =================================================
C
      DO 70 IMON=1,12
C Load component arrays.
      FNLAM=FNAME(IMON)//'_qlam.dat'
      FNPHI=FNAME(IMON)//'_qphi.dat'
      OPEN (UNIT=9, FILE=FNLAM,STATUS='OLD')
      OPEN (UNIT=10,FILE=FNPHI,STATUS='OLD')
      DO 75, K=1,2
      DO 75 I = 1,73
         READ(9,105)   (QLAM(I,J,K),J=1,73)
         READ(10,105) (QPHI(I,J,K),J=1,73)
 75   CONTINUE
      CLOSE (9, STATUS='KEEP')
      CLOSE (10, STATUS='KEEP')
C
      SUMIN(1)=0.
      SUMIN(2)=0.
      SUMOUT(1)=0.
      SUMOUT(2)=0.
      WRITE (8,101) TITLE,IMON,FNAME(IMON)
C Compute and record influx for each bdy segment.
         DO 71 K=1,NPTS-1
           KP1=K+1
           I1=LAT(K)
           I2=LAT(KP1)
           J1=LON(K)
           J2=LON(KP1)
C Averaged flux vector components. divide by 1000 to convert g to kg
           FX(1)= (QLAM(I1,J1,1)+QLAM(I2,J2,1)) / 3. +
     &          (QLAM(I1,J2,1)+QLAM(I2,J1,1)) / 6.
           FX(2)= (QLAM(I1,J1,2)+QLAM(I2,J2,2)) / 9. +
     &          (QLAM(I1,J2,2)+QLAM(I2,J1,2)) / 36.
           FX(1)= FX(1)/1000.
           FX(2)= FX(2)/1000./1000.
           FY(1)= (QPHI(I1,J1,1)+QPHI(I2,J2,1)) / 3. +
     &          (QPHI(I1,J2,1)+QPHI(I2,J1,1)) / 6.
           FY(2)= (QPHI(I1,J1,2)+QPHI(I2,J2,2)) / 9. +
     &          (QPHI(I1,J2,2)+QPHI(I2,J1,2)) / 36.
           FY(1)= FY(1)/1000.
           FY(2)= FY(2)/1000./1000.
C Dot product. Sums.
```

```
            BX=BNX(K)
            BY=BNY(K)
            QIN(1)=BX*FX(1) + BY*FY(1)
            QIN(2)=BX*BX*FX(2)+BY*BY*FY(2)
            IF(QIN(1).GE.0.) THEN
                SUMIN(1)=SUMIN(1)+QIN(1)
                SUMIN(2)=SUMIN(2)+QIN(2)
            ELSE
                SUMOUT(1)=SUMOUT(1)+QIN(1)
                SUMOUT(2)=SUMOUT(2)+QIN(2)
            ENDIF
C Output
            WRITE (8,102) K,KP1,FX(1),FY(1),BX,BY,QIN(1),2.*SQRT(QIN(2))
            SEGFLX(K,IMON)=QIN(1)/1E+6
   71     CONTINUE
C Unit conversion. m to mm; kg water to m^3, sec to days.
C Divide by area to get <Q>.
       UCONV=1000./RHOW*SECDAY
       RFACT=UCONV/SAREA
       QNET(1)=SUMIN(1)+SUMOUT(1)
       QNET(2)=SUMIN(2)+SUMOUT(2)
       SUMOUT(1)=ABS(SUMOUT(1))
       WRITE (8,106) SAREA,
      &               SUMIN(1)*RFACT, 2.*SQRT(SUMIN(2))*RFACT,
      &               SUMIN(1), 2.*SQRT(SUMIN(2)),
      &               SUMOUT(1)*RFACT, 2.*SQRT(SUMOUT(2))*RFACT,
      &               SUMOUT(1),2.*SQRT(SUMOUT(2)),
      &               QNET(1)*RFACT, 2.*SQRT(QNET(2))*RFACT,
      &               QNET(1), 2.*SQRT(QNET(2))
       SFIN(IMON)=SUMIN(1)
       SFOUT(IMON)=SUMOUT(1)
       SQNET(IMON)=QNET(1)
   70 CONTINUE
C
C == END MONTH LOOP ================================================
C
       CLOSE (8,STATUS='KEEP')
C
       UCONV=1000./RHOW*SECMON
       RFACT=UCONV/SAREA
C Write to data file for balance comps.
       OPEN (UNIT=10,FILE=FNSIGF,STATUS='NEW')
       WRITE (10,600) FNBNOD
       WRITE (10,601) (SFIN(I),I=1,12)
       WRITE (10,601) (SFOUT(I),I=1,12)
       WRITE (10,601) (SQNET(I),I=1,12)
       WRITE (10,605)
       WRITE (10,606) (SFIN(I),I=13,16)
       WRITE (10,606) (SFOUT(I),I=13,16)
       WRITE (10,606) (SQNET(I),I=13,16)
       WRITE (10,605)
       WRITE (10,606) SFIN(17)
       WRITE (10,606) SFOUT(17)
       WRITE (10,606) SQNET(17)
       WRITE (10,602) FNBNOD
```

```
      WRITE (10,603) (SFIN(I)*RFACT,I=1,12)
      WRITE (10,603) (SFOUT(I)*RFACT,I=1,12)
      WRITE (10,603) (SQNET(I)*RFACT,I=1,12)
      WRITE (10,605)
      WRITE (10,607) (SFIN(I)*RFACT,I=13,16)
      WRITE (10,607) (SFOUT(I)*RFACT,I=13,16)
      WRITE (10,607) (SQNET(I)*RFACT,I=13,16)
      WRITE (10,605)
      WRITE (10,607) SFIN(17)*RFACT
      WRITE (10,607) SFOUT(17)*RFACT
      WRITE (10,607) SQNET(17)*RFACT
      CLOSE(10,STATUS='KEEP') .
C Write to segment flux file for barplotting.
      OPEN (UNIT=10,FILE=FNSGFX,STATUS='new')
      DO 65 K=1,NPTS-1
         WRITE (10,604) (SEGFLX(K,IMON),IMON=1,17)
   65 CONTINUE
      CLOSE(10,STATUS='keep')
C
      STOP
C
C
      END
```

```
      PROGRAM QEFF
C
C 3/12/91  KB
C Given latitude, longitude at nodes;
C and included part (SQUSE) of grid square surrounding each node.
C (because some nodes are at corners & do not contribute whole elements),
C computes areally-averaged values of the moisture flux vector components.
C Output:  <Qlam>,<Qphi>, |<Q>|, and theta.
C Reads an input file: N, M, beginning indices (GFDL Grid--
C start top left) and N row by M column matrix of area fractions.
C       units: area fractions are in eigths. (0,1,2,3,4...8)
C Computes an estimate of the total area defined by the grid.
C Note: "estimate" means that the area (dy)x(dx) is estimated as
C dA = (R*dPhi)(R*dLam*cos(PhiNode)), PhiNode is the latitude at
C the node, i.e. the center of the grid element.
C
C Area is in m^2.
C
C Addition 3/29/91:
C     Computes average components and theta for each GFDL grid element
C     in the region.  (For checking the validity of assuming uniformity)
C
      CHARACTER*60 TITLE
      CHARACTER*5 FNSET
      CHARACTER*18 FNSQAR, FNOUT, FNEOUT, FNLAM, FNPHI
      CHARACTER*3 FN(12)
      REAL PI,PHI,SQUSE(73,73),TERM(73,73), ETERM(73,73),
     &     QLAM(73,73,2), QPHI(73,73,2)
      PARAMETER (PI=3.14159)
      DATA DPHI, DLAM / 2.5, -5./
      DATA LATZ / 37 /
      DATA FN /'jan','feb','mar','apr','may','jun',
     &         'jul','aug','sep','oct','nov','dec'/
C
C Convert to radians
      DPHI=DPHI/180.*PI
      DLAM=DLAM/180.*PI
C
      WRITE (6,*) '>> Name of dataset?'
      READ (5,*) FNSET
      FNSQAR=FNSET//'.sq'
      FNOUT= FNSET//'.qef'
      FNEOUT= FNSET//'.eleqef'
      OPEN (UNIT=12,FILE=FNSQAR,STATUS='OLD')
      READ(12,100) TITLE
      READ(12,*) N,M,LATB,LONB
      LATF=LATB-N+1
      LONF=LONB-M+1
      WASUM=0.0
      DO 10 ILAT=LATB,LATF,-1
         PHI=REAL(ILAT-LATZ)*DPHI
         COSPHI=COS(PHI)
         READ(12,*) (SQUSE(ILAT,JLON),JLON=LONB,LONF,-1)
         DO 20 JLON=LONB,LONF,-1
            TERM(ILAT,JLON)=COSPHI*SQUSE(ILAT,JLON)/8.
```

```
            ETERM(ILAT,JLON)=COSPHI
            WASUM=WASUM+TERM(ILAT,JLON)
 20       CONTINUE
 10    CONTINUE
       CLOSE(12,STATUS='KEEP')
C
       OPEN (UNIT=13,FILE=FNOUT,STATUS='NEW')
       OPEN (UNIT=15,FILE=FNEOUT,STATUS='NEW')
       WRITE (13,200) FNSET
       DO 50 IMON=1,12
          FNLAM=FN(IMON)//'_qlam.dat'
          FNPHI=FN(IMON)//'_qphi.dat'
          OPEN (Unit=14,file=FNLAM,status='old')
          OPEN (Unit=16,file=FNPHI,status='old')
          DO 60 K=1,2
          DO 60 I=1,73
             READ (14,105) (QLAM(I,J,K),J=1,73)
             READ (16,105) (QPHI(I,J,K),J=1,73)
 60       CONTINUE
          CLOSE (14)
          CLOSE (16)
          QLAMSM=0.0
          QPHISM=0.0
          DO 65 ILAT=LATB,LATF,-1
             DO 65 JLON=LONB,LONF,-1
                QLAMSM=QLAMSM+TERM(ILAT,JLON)*QLAM(ILAT,JLON,1)
                QPHISM=QPHISM+TERM(ILAT,JLON)*QPHI(ILAT,JLON,1)
 65       CONTINUE
          QLAMAV=QLAMSM/WASUM
          QPHIAV=QPHISM/WASUM
          QAV=SQRT(QLAMAV*QLAMAV+QPHIAV*QPHIAV)
          THETA=ATAN(QPHIAV/QLAMAV)*180./PI
C ATAN returns theta in range (-90,90)
          IF (THETA.LT.0.AND.QLAMAV.LT.0) THETA=THETA+180.
          IF (THETA.GT.0.AND.QPHIAV.LT.0) THETA=THETA-180.
          WRITE(13,500) IMON,QLAMAV,QPHIAV,QAV,THETA
C
C element-wise averaging
C
          WRITE(15,700) IMON
          DO 75 ILAT=LATB,LATF+1,-1
            DO 75 JLON=LONB,LONF+1,-1
              I1=ILAT
              I2=ILAT-1
              J1=JLON
              J2=JLON-1
              EWSUM=ETERM(I1,J1)+ETERM(I1,J2)+
     &              ETERM(I2,J1)+ETERM(I2,J2)
              ESUMPHI=ETERM(I1,J1)*QPHI(I1,J1,1)+
     &                ETERM(I1,J2)*QPHI(I1,J2,1)+
     &                ETERM(I2,J1)*QPHI(I2,J1,1)+
     &                ETERM(I2,J2)*QPHI(I2,J2,1)
              ESUMLAM=ETERM(I1,J1)*QLAM(I1,J1,1)+
     &                ETERM(I1,J2)*QLAM(I1,J2,1)+
     &                ETERM(I2,J1)*QLAM(I2,J1,1)+
```

```
     &               ETERM(I2,J2)*QLAM(I2,J2,1)
            EAVPHI=ESUMPHI/EWSUM
            EAVLAM=ESUMLAM/EWSUM
            WRITE (15,705) ILAT,JLON,EAVLAM,EAVPHI
 75       CONTINUE
C
 50    CONTINUE
       CLOSE (13)
       CLOSE (15)
       STOP
C
 100   FORMAT (A60)
 105   FORMAT (7E10.3)
 200   FORMAT (1X,'Area Mean Q Vector for ',A18,//,
     &  1X,'Month      <Q(lam)>      <Q(phi)>      |<Q>|       Theta',/
     &  1X,'           ..........  [g/s/m] ..........       [deg]',//)
 500   FORMAT (1X,I5,2X,3(2X,E10.3),F9.1)
 501   FORMAT (1X,E11.4)
 700   FORMAT (/,1X,'IMON=',I3,2X,'Element Averages',//,
     &         1X,'Top LH Node   <Q(lam)>   <Q(phi)>')
 705   FORMAT (1X,I2,1X,I2,5X,2(2X,E10.3))
C
       END
```

```
      PROGRAM WU
C
C Computes the "wu" term for Budyko recyling analysis.
C
C Here, wu = a weighted average of the inward moisture flux vector
C component in the direction of the average moisture flux vector over
C the region.
C
C The unit direction vector is U, with components ULAM, UPHI
C
C Qphi, Qlambda, and Qin,parallel (wu) have units g m^(-1) s^(-1)
C
C This routine works only for rectangular regions.
C
      CHARACTER*18 FNAR,FNQEF,FNSQ,FNWU,FNBN,FNCHK,FNLAM,FNPHI
      CHARACTER*5 FNSET
      CHARACTER*3 FNAME(12)
      CHARACTER*60 TITLE
      INTEGER IK(73),JK(73)
      REAL QLAM(73,73),QPHI(73,73),RL(73),QP(73),DW(73)
      REAL DELY,YREL,YMAX,XMAX,DELX
      PARAMETER (RPI=3.14159, AR= 6.37E+6 )
      DATA FNAME / 'jan','feb','mar','apr','may','jun',
     &             'jul','aug','sep','oct','nov','dec'/
C
 105  FORMAT (7E10.3)
 200  FORMAT (//,1X,E11.4)
 300  FORMAT ('RAREA= ',E10.3,2X,'YMAX= ',E10.3,2X,'XMAX =',E10.3,/
     &        19X,'DELY= ',E10.3,2X,'DELX =',E10.3)
 305  FORMAT (/,'** IMON= ',I4,' **',
     &        //,'QLAMAV= ',E10.3,2X,'QPHIAV= ',E10.3,2X,
     &          'QAV= ',E10.3,2X,'THETA= ',F6.1)
 310  FORMAT (/,'ABCOS= ',F8.4,2X,'ABSIN= ',F8.4)
 500  FORMAT (//////)
 505  FORMAT (8X,3(2X,E10.3),F9.1)
 600  FORMAT ('ULAM=',F6.2,3X,'UPHI=',F6.2)
 601  FORMAT (/,'ILATB=',I3,2X,'IINC=',I3,2X,'ILATF=',I3,4X,
     &          'JLONB=',I3,2X,'JINC=',I3,2X,'JLONF=',I3)
 602  FORMAT (/,'X-segment integration',/,
     &' K  JK    DELW      RLZ       RL1       AREA       QPZ       QP1
     &    WTZ   WT1    QPBAR')
 603  FORMAT (I2,I4,6(E10.3),2(F6.3),E11.3)
 604  FORMAT (/,'CRIT VAL = ',E9.3,2X,'RLMAX= ',E9.3)
 605  FORMAT (/,'Y-segment integration',/,
     &' K  IK    DW(K)     RLZ       RL1       AREA       QPZ       QP1
     &    WTZ   WT1    QPBAR')
 607  FORMAT (/,31X,'ASUM= ',E9.3,27X,'QPSUM= ',E9.3,/
     &/,31X,'IMON= ',I4,6X,'** QPAVG= ',E9.3,' **')
 700  FORMAT (1X,'Weighted Mean Q(Parallel)',
     &        3X,'[g m^(-1) s^(-1)]',3X,A18,//,
     &        1X,'IMON    <Qp>')
 705  FORMAT (1X,I3,2X,E9.3)
C
      WRITE (6,*) '>> Name of dataset?'
      READ (5,*) FNSET
```

```
      FNAR = FNSET//'.ar'
      FNQEF= FNSET//'.qef'
      FNSQ = FNSET//'.sq'
      FNWU = FNSET//'.wu'
      FNBN = FNSET//'.bn'
      FNCHK= FNSET//'.chk'
      OPEN(unit=25,file=FNCHK,status='unknown')
      OPEN(unit=27,file=FNWU,status='new')
      WRITE (27,700) FNSET
      OPEN(unit=10,file=FNSQ,status='old')
      READ(10,*) TITLE
      READ(10,*) N,M,LATB,LONB
      LATF=LATB-N+1
      LONF=LONB-M+1
      CLOSE(10)
      OPEN(unit=10,file=FNAR,status='old')
      READ(10,200) RAREA
      CLOSE(10)
C
C Planar distances.  Xmax is the average longitudinal dimension
C of the spherical-rectangular region.  Xmax*Ymax=Area.
C
      DELY=AR*RPI/180.*2.5
      YMAX=REAL(N-1)*DELY
      XMAX=RAREA/YMAX
      DELX=XMAX/REAL(M-1)
      WRITE (25,300) RAREA,YMAX,XMAX,DELY,DELX
C
      OPEN(unit=12,file=FNQEF,status='old')
      READ(12,500)
C
C == MONTH LOOP ========================================================
C
      DO 100 IMON=1,12
C
C Read the Q vector components for this month.
C
      FNLAM=FNAME(IMON)//'_qlam.dat'
      FNPHI=FNAME(IMON)//'_qphi.dat'
      OPEN (UNIT=20,FILE=FNLAM,STATUS='old')
      OPEN (UNIT=22,FILE=FNPHI,STATUS='old')
      DO 75, I=1,73
         READ (20,105) (QLAM(I,J),J=1,73)
         READ (22,105) (QPHI(I,J),J=1,73)
 75   CONTINUE
      CLOSE (20)
      CLOSE (22)
C
C Read the region-specific direction data for this month.
C Compute components of the unit direction vector.
C
         READ(12,505) QLAMAV,QPHIAV,QAV,THETA
         write(25,305) IMON,QLAMAV,QPHIAV,QAV,THETA
         ULAM=QLAMAV/QAV
         UPHI=QPHIAV/QAV
```

```
         WRITE (25,600) ULAM, UPHI
C
C Determine direction for integration along inward boundary.
C (JLON,ILAT) is the x,y corner at which to start.
C
         If(ULAM.GT.0.) THEN
            JLONB=LONF
            JLONF=LONB
            JINC=1
         Else
            JLONB=LONB
            JLONF=LONF
            JINC=-1
         Endif
         IF(UPHI.GT.0.) THEN
            ILATB=LATF
            ILATF=LATB
            IINC=1
         ELSE
            ILATB=LATB
            ILATF=LATF
            IINC=-1
         ENDIF
         WRITE (25,601) ILATB, IINC, ILATF, JLONB, JINC, JLONF
C
C == Integrate along the X-direction segment first.
C
C Initialize sums
C
         ASUM=0.0
         QASUM=0.0
C
C If THETA is 180 or -180, skip the x-direction segment.
C
         THETA=THETA*RPI/180.
         ABCOS=ABS(COS(THETA))
         ABSIN=ABS(SIN(THETA))
         WRITE (25,310) ABCOS,ABSIN
         IF(ABS(THETA).eq.180.) GOTO 150
C
C Compute Xcrit and fit it into the sequence of nodes for integration.
C
         MCOUNT=M
         XCRIT=YMAX/ABS(TAN(THETA))
         IF (XCRIT.LT.XMAX) MCOUNT=M+1
         RLMAX=YMAX/ABSIN
         WRITE (25,604) XCRIT,RLMAX
         IFLAG=0
         K=1
         KINT=0
         JK(1)=JLONB
         XREL=0.
         RL(1)=0.
         QP(1)=QLAM(ILATB,JK(1))*ULAM + QPHI(ILATB,JK(1))*UPHI
 120     IF(K.eq.MCOUNT) GOTO 121
```

```
            KINT=KINT+1
C            XREL=XREL+DELX
            XREL=REAL(KINT)*DELX
            IF (XREL.LT.XCRIT) THEN
                K=K+1
                JK(K)=JK(K-1)+JINC
                DW(K)=DELX*ABSIN
                RL(K)=XREL/ABCOS
                QP(K)=QLAM(ILATB,JK(K))*ULAM+QPHI(ILATB,JK(K))*UPHI
            ELSE
               IF (IFLAG.LT.1) THEN
                  K=K+1
                  JK(K)=99
                  RL(K)=RLMAX
                  XDIF=XCRIT-XREL+DELX
                  DW(K)=XDIF*ABSIN
                  K=K+1
                  JK(K)=JK(K-2)+JINC
                  RL(K)=RLMAX
                  XDIF=XREL-XCRIT
                  DW(K)=XDIF*ABSIN
                  QP(K)=QLAM(ILATB,JK(K))*ULAM+QPHI(ILATB,JK(K))*UPHI
                  QP(K-1)=QP(K-2)*(XDIF/DELX)+QP(K)*(1-XDIF/DELX)
                  IFLAG=1
               ELSE
                  K=K+1
                  JK(K)=JK(K-1)+JINC
                  RL(K)=RLMAX
                  DW(K)=DELX*ABSIN
                  QP(K)=QLAM(ILATB,JK(K))*ULAM+QPHI(ILATB,JK(K))*UPHI
               ENDIF
            ENDIF
         GOTO 120
 121     CONTINUE
C
         WRITE (25,602)
         DO 110 K=2,MCOUNT
            RLZ=RL(K-1)
            RL1=RL(K)
            QPZ=QP(K-1)
            QP1=QP(K)
            AREA = (RLZ+RL1)*DW(K)/2.
            DENOM = 3*(RLZ+RL1)
            WTZ = (2*RLZ+RL1)/DENOM
            WT1 = (RLZ+2*RL1)/DENOM
            QPBAR = WTZ*QPZ + WT1*QP1
            ASUM=ASUM+AREA
            QASUM=QASUM+AREA*QPBAR
            WRITE(25,603) K,JK(K),DW(K),RLZ,RL1,AREA,QPZ,QP1,WTZ,WT1,
     &                    QPBAR
 110     CONTINUE
 150     CONTINUE
C
C == The Y-direction segment.
C
```

```
C Compute Ycrit and fit it into the sequence of nodes for integration.
C
          NCOUNT=N+1
          YCRIT=YMAX-XMAX*ABS(TAN(THETA))
          RLMAX=XMAX/ABCOS
          IFLAG=0
          IF (YCRIT.LE.0.) THEN
             YCRIT=0.
             RLMAX=YMAX/ABSIN
             NCOUNT=N
             IFLAG=1
          ENDIF
          WRITE (25,604) YCRIT,RLMAX
          K=1
          KINT=0
          IK(1)=ILATB
          YREL=0.
          RL(1)=RLMAX
          QP(1)=QLAM(IK(1),JLONF)*ULAM + QPHI(IK(1),JLONF)*UPHI
 130      IF(K.eq.NCOUNT) GOTO 131
             KINT=KINT+1
C             YREL=YREL+DELY
             YREL=REAL(KINT)*DELY
             IF (YREL.LT.YCRIT) THEN
                 K=K+1
                 IK(K)=IK(K-1)+IINC
                 DW(K)=DELY*ABCOS
                 RL(K)=RLMAX
                 QP(K)=QLAM(IK(K),JLONF)*ULAM+QPHI(IK(K),JLONF)*UPHI
             ELSE
                IF (IFLAG.LT.1) THEN
                   K=K+1
                   IK(K)=99
                   RL(K)=RLMAX
                   YDIF=YCRIT-YREL+DELY
                   DW(K)=YDIF*ABCOS
                   K=K+1
                   IK(K)=IK(K-2)+IINC
                   RL(K)=(YMAX-YREL)/ABSIN
                   YDIF=YREL-YCRIT
                   DW(K)=YDIF*ABCOS
                   QP(K)=QLAM(IK(K),JLONF)*ULAM+QPHI(IK(K),JLONF)*UPHI
                   QP(K-1)=QP(K-2)*(YDIF/DELY)+QP(K)*(1-YDIF/DELY)
                   IFLAG=1
                ELSE
                   K=K+1
                   IK(K)=IK(K-1)+IINC
                   RL(K)=(YMAX-YREL)/ABSIN
                   DW(K)=DELY*ABCOS
                   QP(K)=QLAM(IK(K),JLONF)*ULAM+QPHI(IK(K),JLONF)*UPHI
                ENDIF
             ENDIF
          GOTO 130
 131      CONTINUE
C
```

```
C Y-segment integration Loop.
C
         WRITE (25,605)
         DO 140 K=2,NCOUNT
            RLZ=RL(K-1)
            RL1=RL(K)
            QPZ=QP(K-1)
            QP1=QP(K)
            AREA = (RLZ+RL1)*DW(K)/2.
            DENOM = 3*(RLZ+RL1)
            WTZ = (2*RLZ+RL1)/DENOM
            WT1 = (RLZ+2*RL1)/DENOM
            QPBAR = WTZ*QPZ + WT1*QP1
            ASUM=ASUM+AREA
            QASUM=QASUM+AREA*QPBAR
            WRITE(25,603) K,IK(K),DW(K),RLZ,RL1,AREA,QPZ,QP1,WTZ,WT1,
     &                    QPBAR
 140     CONTINUE
C
C == End inward-boundary integration.
C
         QPAVG=QASUM/ASUM
         WRITE (25,607) ASUM, QASUM, IMON, QPAVG
         WRITE (27,705) IMON,QPAVG
 100  CONTINUE
C
C == End Month Loop ================================================
C
      CLOSE(25)
      CLOSE(27)
      END
```

APPENDIX C

Sample Input and Output

Examples are given for the North American study region (Figure 2.5)

Input Files

1. na001.bn -- Enumeration of the nodes defining the boundary.
2. na001.sq -- The weighting fractions used in area integrals.

Output Files

1. na001.ar -- The area of the region as computed by AREA.
2. na001.qef -- The components, magnitude and direction of the areally–averaged moisture flux vector, as computed by QEFF.
3. na001.wu -- The boundary influx in the direction of $\langle \vec{Q} \rangle$, $(wu)_{eff}$, as computed by WU.
4. na001.txt -- Segment–by–segment and net moisture flux across the boundary, as computed by BFLUXW.

na001.bn **Sat Mar 30 18:10:25 1991** **1**

```
na001
 1   54   58
 2   53   58
 3   52   58
 4   51   58
 5   50   58
 6   50   57
 7   50   56
 8   50   55
 9   50   54
10   51   54
11   52   54
12   53   54
13   54   54
14   54   55
15   54   56
16   54   57
17   54   58
999 999 999
```

na001.sq **Fri Mar 29 13:39:30 1991** **1**

```
na001
5  5    54    58
2 4 4 4 2
4 8 8 8 4
4 8 8 8 4
4 8 8 8 4
2 4 4 4 2
```

na001.ar **Fri Mar 29 15:07:27 1991** **1**

Area Computation for na001.sq (m^2)

0.1959e+13

na001.qef **Fri Mar 29 14:08:07 1991** **1**

Area Mean Q Vector for na001

Month	<Q(lam)>	<Q(phi)> [g/s/m]	|<Q>|	Theta [deg]
1	0.864e+05	0.112e+05	0.872e+05	7.4
2	0.695e+05	0.417e+04	0.696e+05	3.4
3	0.740e+05	0.184e+05	0.762e+05	14.0
4	0.853e+05	0.430e+05	0.955e+05	26.8
5	0.729e+05	0.360e+05	0.813e+05	26.3
6	0.774e+05	0.443e+05	0.892e+05	29.8
7	0.765e+05	0.174e+05	0.784e+05	12.8
8	0.613e+05	0.173e+05	0.637e+05	15.7
9	0.807e+05	0.459e+05	0.928e+05	29.6
10	0.743e+05	0.211e+05	0.772e+05	15.9
11	0.854e+05	0.114e+05	0.862e+05	7.6
12	0.976e+05	0.218e+05	0.100e+06	12.6

na001.wu **Sun May 19 11:34:45 1991** **1**

Weighted Mean Q(Parallel) [g m^(-1) s^(-1)] na001

IMON	<Qp>
1	0.406e+05
2	0.321e+05
3	0.446e+05
4	0.675e+05
5	0.529e+05
6	0.539e+05
7	0.204e+05
8	0.169e+05
9	0.420e+05
10	0.392e+05
11	0.468e+05
12	0.534e+05

1 na001

Month 1 (jan)

Node K	K+1	Flux, kg m^-1 s^-1 F(x)	F(y)	Scaled inward normal vector, m B(x)	B(y)	Segment flux kg s^-1 Qin	
1	2	0.342e+02	-0.114e+02	0.278e+06	0.000e+00	0.951e+07 +-	0.523e+06
2	3	0.320e+02	-0.859e+01	0.278e+06	0.000e+00	0.890e+07 +-	0.510e+06
3	4	0.332e+02	-0.518e+01	0.278e+06	0.000e+00	0.922e+07 +-	0.498e+06
4	5	0.433e+02	-0.160e+00	0.278e+06	0.000e+00	0.121e+08 +-	0.504e+06
5	6	0.635e+02	0.101e+02	0.000e+00	0.469e+06	0.475e+07 +-	0.138e+06
6	7	0.958e+02	0.308e+02	0.000e+00	0.469e+06	0.144e+08 +-	0.188e+06
7	8	0.126e+03	0.478e+02	0.000e+00	0.469e+06	0.224e+08 +-	0.237e+06
8	9	0.140e+03	0.468e+02	0.000e+00	0.469e+06	0.219e+08 +-	0.240e+06
9	10	0.141e+03	0.382e+02	-0.278e+06	0.000e+00	-0.392e+08 +-	0.864e+06
10	11	0.129e+03	0.286e+02	-0.278e+06	0.000e+00	-0.359e+08 +-	0.904e+06
11	12	0.111e+03	0.188e+02	-0.278e+06	0.000e+00	-0.309e+08 +-	0.903e+06
12	13	0.921e+02	0.112e+02	-0.278e+06	0.000e+00	-0.256e+08 +-	0.862e+06
13	14	0.748e+02	0.390e+01	0.000e+00	-0.410e+06	-0.160e+07 +-	0.180e+06
14	15	0.668e+02	-0.377e+01	0.000e+00	-0.410e+06	0.155e+07 +-	0.255e+06
15	16	0.621e+02	-0.120e+02	0.000e+00	-0.410e+06	0.491e+07 +-	0.334e+06
16	17	0.467e+02	-0.147e+02	0.000e+00	-0.410e+06	0.601e+07 +-	0.362e+06

Area = 0.196e+13 m^2

<Qin> = 0.510e+01 mm/day +- 0.542e-01 Qin = 0.116e+09 +- 0.123e+07
<Qout> = 0.587e+01 mm/day +- 0.783e-01 Qout = 0.133e+09 +- 0.178e+07

<Qnet> = -0.770e+00 mm/day +- 0.953e-01 Qnet = -0.175e+08 +- 0.216e+07

1 na001

Month 2 (feb)

Node K	K+1	Flux, kg m^-1 s^-1 F(x)	F(y)	Scaled inward normal vector, m B(x)	B(y)	Segment flux kg s^-1 Qin	
1	2	0.251e+02	-0.106e+02	0.278e+06	0.000e+00	0.699e+07 +-	0.409e+06
2	3	0.257e+02	-0.835e+01	0.278e+06	0.000e+00	0.714e+07 +-	0.417e+06
3	4	0.274e+02	-0.474e+01	0.278e+06	0.000e+00	0.762e+07 +-	0.450e+06
4	5	0.410e+02	0.330e+00	0.278e+06	0.000e+00	0.114e+08 +-	0.518e+06
5	6	0.601e+02	0.788e+01	0.000e+00	0.469e+06	0.369e+07 +-	0.143e+06
6	7	0.821e+02	0.206e+02	0.000e+00	0.469e+06	0.966e+07 +-	0.160e+06
7	8	0.110e+03	0.310e+02	0.000e+00	0.469e+06	0.145e+08 +-	0.184e+06
8	9	0.126e+03	0.328e+02	0.000e+00	0.469e+06	0.154e+08 +-	0.188e+06
9	10	0.120e+03	0.280e+02	-0.278e+06	0.000e+00	-0.332e+08 +-	0.861e+06
10	11	0.104e+03	0.193e+02	-0.278e+06	0.000e+00	-0.288e+08 +-	0.836e+06
11	12	0.880e+02	0.111e+02	-0.278e+06	0.000e+00	-0.245e+08 +-	0.789e+06
12	13	0.718e+02	0.426e+01	-0.278e+06	0.000e+00	-0.199e+08 +-	0.726e+06
13	14	0.607e+02	-0.227e+01	0.000e+00	-0.410e+06	0.930e+06 +-	0.233e+06
14	15	0.546e+02	-0.969e+01	0.000e+00	-0.410e+06	0.397e+07 +-	0.316e+06
15	16	0.473e+02	-0.163e+02	0.000e+00	-0.410e+06	0.668e+07 +-	0.381e+06
16	17	0.338e+02	-0.151e+02	0.000e+00	-0.410e+06	0.621e+07 +-	0.382e+06

Area = 0.196e+13 m^2

<Qin> = 0.416e+01 mm/day +- 0.517e-01 Qin = 0.942e+08 +- 0.117e+07
<Qout> = 0.469e+01 mm/day +- 0.710e-01 Qout = 0.106e+09 +- 0.161e+07

<Qnet> = -0.539e+00 mm/day +- 0.878e-01 Qnet = -0.122e+08 +- 0.199e+07

1 na001

Month 3 (mar)

Node K	K+1	Flux, kg m^-1 s^-1 F(x)	F(y)	Scaled inward normal vector, m B(x)	B(y)	Segment flux kg s^-1 Qin	
1	2	0.259e+02	-0.659e+01	0.278e+06	0.000e+00	0.720e+07 +-	0.422e+06
2	3	0.268e+02	-0.436e+01	0.278e+06	0.000e+00	0.745e+07 +-	0.443e+06
3	4	0.312e+02	-0.130e+01	0.278e+06	0.000e+00	0.867e+07 +-	0.480e+06
4	5	0.478e+02	0.589e+01	0.278e+06	0.000e+00	0.133e+08 +-	0.547e+06
5	6	0.664e+02	0.181e+02	0.000e+00	0.469e+06	0.849e+07 +-	0.162e+06
6	7	0.871e+02	0.355e+02	0.000e+00	0.469e+06	0.167e+08 +-	0.193e+06
7	8	0.112e+03	0.516e+02	0.000e+00	0.469e+06	0.242e+08 +-	0.211e+06
8	9	0.128e+03	0.505e+02	0.000e+00	0.469e+06	0.237e+08 +-	0.199e+06
9	10	0.129e+03	0.410e+02	-0.278e+06	0.000e+00	-0.357e+08 +-	0.798e+06
10	11	0.117e+03	0.335e+02	-0.278e+06	0.000e+00	-0.325e+08 +-	0.780e+06
11	12	0.101e+03	0.240e+02	-0.278e+06	0.000e+00	-0.279e+08 +-	0.730e+06
12	13	0.778e+02	0.154e+02	-0.278e+06	0.000e+00	-0.216e+08 +-	0.661e+06
13	14	0.595e+02	0.102e+02	0.000e+00	-0.410e+06	-0.418e+07 +-	0.175e+06
14	15	0.504e+02	0.604e+01	0.000e+00	-0.410e+06	-0.248e+07 +-	0.204e+06
15	16	0.445e+02	-0.166e+01	0.000e+00	-0.410e+06	0.680e+06 +-	0.255e+06
16	17	0.336e+02	-0.712e+01	0.000e+00	-0.410e+06	0.292e+07 +-	0.272e+06

Area = 0.196e+13 m^2

<Qin> = 0.499e+01 mm/day +- 0.481e-01 Qin = 0.113e+09 +- 0.109e+07
<Qout> = 0.549e+01 mm/day +- 0.667e-01 Qout = 0.124e+09 +- 0.151e+07

<Qnet> = -0.496e+00 mm/day +- 0.822e-01 Qnet = -0.112e+08 +- 0.186e+07

1 na001

Month 4 (apr)

Node K	K+1	Flux, kg m^-1 s^-1 F(x)	F(y)	Scaled inward normal vector, m B(x)	B(y)	Segment flux kg s^-1 Qin	
1	2	0.276e+02	0.638e+01	0.278e+06	0.000e+00	0.767e+07 +-	0.389e+06
2	3	0.298e+02	0.819e+01	0.278e+06	0.000e+00	0.827e+07 +-	0.432e+06
3	4	0.336e+02	0.106e+02	0.278e+06	0.000e+00	0.934e+07 +-	0.482e+06
4	5	0.502e+02	0.200e+02	0.278e+06	0.000e+00	0.140e+08 +-	0.550e+06
5	6	0.722e+02	0.435e+02	0.000e+00	0.469e+06	0.204e+08 +-	0.323e+06
6	7	0.921e+02	0.744e+02	0.000e+00	0.469e+06	0.349e+08 +-	0.320e+06
7	8	0.111e+03	0.863e+02	0.000e+00	0.469e+06	0.405e+08 +-	0.296e+06
8	9	0.120e+03	0.609e+02	0.000e+00	0.469e+06	0.286e+08 +-	0.252e+06
9	10	0.129e+03	0.385e+02	-0.278e+06	0.000e+00	-0.357e+08 +-	0.642e+06
10	11	0.131e+03	0.342e+02	-0.278e+06	0.000e+00	-0.363e+08 +-	0.668e+06
11	12	0.116e+03	0.259e+02	-0.278e+06	0.000e+00	-0.322e+08 +-	0.654e+06
12	13	0.927e+02	0.179e+02	-0.278e+06	0.000e+00	-0.258e+08 +-	0.613e+06
13	14	0.754e+02	0.173e+02	0.000e+00	-0.410e+06	-0.709e+07 +-	0.186e+06
14	15	0.643e+02	0.230e+02	0.000e+00	-0.410e+06	-0.943e+07 +-	0.155e+06
15	16	0.531e+02	0.219e+02	0.000e+00	-0.410e+06	-0.898e+07 +-	0.136e+06
16	17	0.374e+02	0.118e+02	0.000e+00	-0.410e+06	-0.485e+07 +-	0.108e+06

Area = 0.196e+13 m^2

<Qin> = 0.722e+01 mm/day +- 0.489e-01 Qin = 0.164e+09 +- 0.111e+07
<Qout> = 0.707e+01 mm/day +- 0.583e-01 Qout = 0.160e+09 +- 0.132e+07

<Qnet> = 0.143e+00 mm/day +- 0.761e-01 Qnet = 0.323e+07 +- 0.173e+07

1 na001

Month 5 (may)

Node K	K+1	Flux, kg m^-1 s^-1 F(x)	F(y)	Scaled inward normal vector, m B(x)	B(y)	Segment flux kg s^-1 Qin	
1	2	0.285e+02	0.774e+01	0.278e+06	0.000e+00	0.792e+07 +-	0.326e+06
2	3	0.289e+02	0.964e+01	0.278e+06	0.000e+00	0.802e+07 +-	0.326e+06
3	4	0.301e+02	0.114e+02	0.278e+06	0.000e+00	0.837e+07 +-	0.337e+06
4	5	0.412e+02	0.220e+02	0.278e+06	0.000e+00	0.115e+08 +-	0.376e+06
5	6	0.538e+02	0.458e+02	0.000e+00	0.469e+06	0.215e+08 +-	0.283e+06
6	7	0.622e+02	0.630e+02	0.000e+00	0.469e+06	0.295e+08 +-	0.292e+06
7	8	0.683e+02	0.547e+02	0.000e+00	0.469e+06	0.256e+08 +-	0.297e+06
8	9	0.695e+02	0.286e+02	0.000e+00	0.469e+06	0.134e+08 +-	0.282e+06
9	10	0.807e+02	0.158e+02	-0.278e+06	0.000e+00	-0.224e+08 +-	0.383e+06
10	11	0.973e+02	0.181e+02	-0.278e+06	0.000e+00	-0.270e+08 +-	0.427e+06
11	12	0.103e+03	0.162e+02	-0.278e+06	0.000e+00	-0.285e+08 +-	0.462e+06
12	13	0.968e+02	0.117e+02	-0.278e+06	0.000e+00	-0.269e+08 +-	0.485e+06
13	14	0.890e+02	0.146e+02	0.000e+00	-0.410e+06	-0.599e+07 +-	0.192e+06
14	15	0.810e+02	0.234e+02	0.000e+00	-0.410e+06	-0.957e+07 +-	0.188e+06
15	16	0.671e+02	0.237e+02	0.000e+00	-0.410e+06	-0.971e+07 +-	0.177e+06
16	17	0.431e+02	0.136e+02	0.000e+00	-0.410e+06	-0.560e+07 +-	0.134e+06

Area = 0.196e+13 m^2

<Qin> = 0.555e+01 mm/day +- 0.394e-01 Qin = 0.126e+09 +- 0.894e+06
<Qout> = 0.599e+01 mm/day +- 0.418e-01 Qout = 0.136e+09 +- 0.948e+06

<Qnet> = -0.436e+00 mm/day +- 0.575e-01 Qnet = -0.989e+07 +- 0.130e+07

1 na001

Month 6 (jun)

Node K	K+1	Flux, kg m^-1 s^-1 F(x)	F(y)	Scaled inward normal vector, m B(x)	B(y)	Segment flux kg s^-1 Qin	
1	2	0.428e+02	0.189e+02	0.278e+06	0.000e+00	0.119e+08 +-	0.335e+06
2	3	0.400e+02	0.195e+02	0.278e+06	0.000e+00	0.111e+08 +-	0.316e+06
3	4	0.367e+02	0.192e+02	0.278e+06	0.000e+00	0.102e+08 +-	0.293e+06
4	5	0.370e+02	0.287e+02	0.278e+06	0.000e+00	0.103e+08 +-	0.280e+06
5	6	0.347e+02	0.622e+02	0.000e+00	0.469e+06	0.292e+08 +-	0.326e+06
6	7	0.360e+02	0.827e+02	0.000e+00	0.469e+06	0.388e+08 +-	0.360e+06
7	8	0.450e+02	0.574e+02	0.000e+00	0.469e+06	0.269e+08 +-	0.370e+06
8	9	0.490e+02	0.173e+02	0.000e+00	0.469e+06	0.810e+07 +-	0.360e+06
9	10	0.646e+02	0.407e+00	-0.278e+06	0.000e+00	-0.179e+08 +-	0.273e+06
10	11	0.942e+02	0.372e+01	-0.278e+06	0.000e+00	-0.262e+08 +-	0.328e+06
11	12	0.119e+03	0.614e+01	-0.278e+06	0.000e+00	-0.329e+08 +-	0.391e+06
12	13	0.133e+03	0.636e+01	-0.278e+06	0.000e+00	-0.370e+08 +-	0.449e+06
13	14	0.130e+03	0.936e+01	0.000e+00	-0.410e+06	-0.384e+07 +-	0.261e+06
14	15	0.114e+03	0.274e+02	0.000e+00	-0.410e+06	-0.112e+08 +-	0.255e+06
15	16	0.942e+02	0.446e+02	0.000e+00	-0.410e+06	-0.183e+08 +-	0.247e+06
16	17	0.627e+02	0.325e+02	0.000e+00	-0.410e+06	-0.133e+08 +-	0.214e+06

Area = 0.196e+13 m^2

<Qin> = 0.646e+01 mm/day +- 0.413e-01 Qin = 0.146e+09 +- 0.937e+06
<Qout> = 0.709e+01 mm/day +- 0.389e-01 Qout = 0.161e+09 +- 0.882e+06

<Qnet> = -0.630e+00 mm/day +- 0.567e-01 Qnet = -0.143e+08 +- 0.129e+07

1 na001

Month 7 (jul)

Node K	K+1	Flux, kg m^-1 s^-1 F(x)	F(y)	Scaled inward normal vector, m B(x)	B(y)	Segment flux kg s^-1 Qin	
1	2	0.494e+02	0.642e+01	0.278e+06	0.000e+00	0.137e+08 +-	0.330e+06
2	3	0.385e+02	0.777e+01	0.278e+06	0.000e+00	0.107e+08 +-	0.249e+06
3	4	0.220e+02	0.782e+01	0.278e+06	0.000e+00	0.613e+07 +-	0.169e+06
4	5	-0.750e+01	0.141e+02	0.278e+06	0.000e+00	-0.208e+07 +-	0.175e+06
5	6	-0.204e+02	0.420e+02	0.000e+00	0.469e+06	0.197e+08 +-	0.375e+06
6	7	0.475e+01	0.548e+02	0.000e+00	0.469e+06	0.257e+08 +-	0.407e+06
7	8	0.427e+02	0.291e+02	0.000e+00	0.469e+06	0.136e+08 +-	0.427e+06
8	9	0.703e+02	0.714e+01	0.000e+00	0.469e+06	0.335e+07 +-	0.417e+06
9	10	0.903e+02	-0.289e+01	-0.278e+06	0.000e+00	-0.251e+08 +-	0.279e+06
10	11	0.111e+03	-0.928e+01	-0.278e+06	0.000e+00	-0.309e+08 +-	0.325e+06
11	12	0.127e+03	-0.118e+02	-0.278e+06	0.000e+00	-0.352e+08 +-	0.378e+06
12	13	0.138e+03	-0.132e+02	-0.278e+06	0.000e+00	-0.382e+08 +-	0.426e+06
13	14	0.138e+03	-0.124e+02	0.000e+00	-0.410e+06	0.510e+07 +-	0.329e+06
14	15	0.129e+03	-0.303e+01	0.000e+00	-0.410e+06	0.124e+07 +-	0.351e+06
15	16	0.109e+03	0.101e+02	0.000e+00	-0.410e+06	-0.413e+07 +-	0.326e+06
16	17	0.737e+02	0.101e+02	0.000e+00	-0.410e+06	-0.412e+07 +-	0.227e+06

Area = 0.196e+13 m^2

<Qin> = 0.438e+01 mm/day +- 0.461e-01 Qin = 0.993e+08 +- 0.105e+07
<Qout> = 0.616e+01 mm/day +- 0.368e-01 Qout = 0.140e+09 +- 0.834e+06

<Qnet> = -0.178e+01 mm/day +- 0.590e-01 Qnet = -0.404e+08 +- 0.134e+07

1 na001

Month 8 (aug)

Node K	K+1	Flux, kg m^-1 s^-1 F(x)	F(y)	Scaled inward normal vector, m B(x)	B(y)	Segment flux kg s^-1 Qin	
1	2	0.368e+02	0.326e+01	0.278e+06	0.000e+00	0.102e+08 +-	0.254e+06
2	3	0.290e+02	0.491e+01	0.278e+06	0.000e+00	0.808e+07 +-	0.199e+06
3	4	0.183e+02	0.541e+01	0.278e+06	0.000e+00	0.507e+07 +-	0.151e+06
4	5	-0.235e+01	0.929e+01	0.278e+06	0.000e+00	-0.653e+06 +-	0.175e+06
5	6	-0.915e+01	0.396e+02	0.000e+00	0.469e+06	0.186e+08 +-	0.371e+06
6	7	0.645e+01	0.566e+02	0.000e+00	0.469e+06	0.265e+08 +-	0.389e+06
7	8	0.274e+02	0.287e+02	0.000e+00	0.469e+06	0.135e+08 +-	0.407e+06
8	9	0.509e+02	0.593e+01	0.000e+00	0.469e+06	0.278e+07 +-	0.411e+06
9	10	0.751e+02	-0.150e+01	-0.278e+06	0.000e+00	-0.209e+08 +-	0.279e+06
10	11	0.990e+02	-0.724e+01	-0.278e+06	0.000e+00	-0.275e+08 +-	0.323e+06
11	12	0.118e+03	-0.108e+02	-0.278e+06	0.000e+00	-0.327e+08 +-	0.379e+06
12	13	0.131e+03	-0.139e+02	-0.278e+06	0.000e+00	-0.364e+08 +-	0.434e+06
13	14	0.124e+03	-0.160e+02	0.000e+00	-0.410e+06	0.658e+07 +-	0.310e+06
14	15	0.105e+03	-0.575e+01	0.000e+00	-0.410e+06	0.236e+07 +-	0.314e+06
15	16	0.868e+02	0.100e+02	0.000e+00	-0.410e+06	-0.410e+07 +-	0.292e+06
16	17	0.572e+02	0.881e+01	0.000e+00	-0.410e+06	-0.361e+07 +-	0.214e+06

Area = 0.196e+13 m^2

<Qin> = 0.413e+01 mm/day +- 0.429e-01 Qin = 0.937e+08 +- 0.973e+06
<Qout> = 0.555e+01 mm/day +- 0.362e-01 Qout = 0.126e+09 +- 0.822e+06

<Qnet> = -0.142e+01 mm/day +- 0.562e-01 Qnet = -0.322e+08 +- 0.127e+07

1 na001

Month 9 (sep)

Node K	K+1	Flux, kg m^-1 s^-1 F(x)	F(y)	Scaled inward normal vector, m B(x)	B(y)	Segment flux kg s^-1 Qin	
1	2	0.487e+02	0.105e+02	0.278e+06	0.000e+00	0.135e+08 +-	0.359e+06
2	3	0.443e+02	0.133e+02	0.278e+06	0.000e+00	0.123e+08 +-	0.322e+06
3	4	0.372e+02	0.146e+02	0.278e+06	0.000e+00	0.103e+08 +-	0.278e+06
4	5	0.295e+02	0.223e+02	0.278e+06	0.000e+00	0.819e+07 +-	0.251e+06
5	6	0.262e+02	0.438e+02	0.000e+00	0.469e+06	0.205e+08 +-	0.332e+06
6	7	0.250e+02	0.578e+02	0.000e+00	0.469e+06	0.271e+08 +-	0.356e+06
7	8	0.199e+02	0.489e+02	0.000e+00	0.469e+06	0.229e+08 +-	0.375e+06
8	9	0.151e+02	0.272e+02	0.000e+00	0.469e+06	0.128e+08 +-	0.367e+06
9	10	0.327e+02	0.173e+02	-0.278e+06	0.000e+00	-0.909e+07 +-	0.275e+06
10	11	0.746e+02	0.231e+02	-0.278e+06	0.000e+00	-0.207e+08 +-	0.334e+06
11	12	0.111e+03	0.271e+02	-0.278e+06	0.000e+00	-0.308e+08 +-	0.403e+06
12	13	0.133e+03	0.283e+02	-0.278e+06	0.000e+00	-0.368e+08 +-	0.467e+06
13	14	0.145e+03	0.350e+02	0.000e+00	-0.410e+06	-0.143e+08 +-	0.222e+06
14	15	0.140e+03	0.459e+02	0.000e+00	-0.410e+06	-0.188e+08 +-	0.227e+06
15	16	0.115e+03	0.433e+02	0.000e+00	-0.410e+06	-0.177e+08 +-	0.219e+06
16	17	0.749e+02	0.225e+02	0.000e+00	-0.410e+06	-0.924e+07 +-	0.163e+06

Area = 0.196e+13 m^2

<Qin> = 0.563e+01 mm/day +- 0.415e-01 Qin = 0.128e+09 +- 0.941e+06
<Qout> = 0.695e+01 mm/day +- 0.380e-01 Qout = 0.158e+09 +- 0.862e+06

<Qnet> = -0.132e+01 mm/day +- 0.563e-01 Qnet = -0.299e+08 +- 0.128e+07

1 na001

Month 10 (oct)

Node K	K+1	Flux, kg m^-1 s^-1 F(x)	F(y)	Scaled inward normal vector, m B(x)	B(y)	Segment flux kg s^-1 Qin	
1	2	0.373e+02	-0.383e+01	0.278e+06	0.000e+00	0.104e+08 +-	0.352e+06
2	3	0.350e+02	0.350e+00	0.278e+06	0.000e+00	0.973e+07 +-	0.324e+06
3	4	0.325e+02	0.487e+01	0.278e+06	0.000e+00	0.902e+07 +-	0.302e+06
4	5	0.354e+02	0.154e+02	0.278e+06	0.000e+00	0.984e+07 +-	0.303e+06
5	6	0.463e+02	0.271e+02	0.000e+00	0.469e+06	0.127e+08 +-	0.224e+06
6	7	0.541e+02	0.269e+02	0.000e+00	0.469e+06	0.126e+08 +-	0.247e+06
7	8	0.504e+02	0.174e+02	0.000e+00	0.469e+06	0.816e+07 +-	0.262e+06
8	9	0.435e+02	0.109e+02	0.000e+00	0.469e+06	0.509e+07 +-	0.257e+06
9	10	0.538e+02	0.141e+02	-0.278e+06	0.000e+00	-0.149e+08 +-	0.380e+06
10	11	0.763e+02	0.220e+02	-0.278e+06	0.000e+00	-0.212e+08 +-	0.438e+06
11	12	0.917e+02	0.285e+02	-0.278e+06	0.000e+00	-0.255e+08 +-	0.493e+06
12	13	0.102e+03	0.326e+02	-0.278e+06	0.000e+00	-0.283e+08 +-	0.536e+06
13	14	0.106e+03	0.314e+02	0.000e+00	-0.410e+06	-0.129e+08 +-	0.168e+06
14	15	0.101e+03	0.247e+02	0.000e+00	-0.410e+06	-0.101e+08 +-	0.186e+06
15	16	0.873e+02	0.129e+02	0.000e+00	-0.410e+06	-0.531e+07 +-	0.212e+06
16	17	0.577e+02	-0.195e+00	0.000e+00	-0.410e+06	0.799e+05 +-	0.202e+06

Area = 0.196e+13 m^2

<Qin> = 0.342e+01 mm/day +- 0.369e-01 Qin = 0.776e+08 +- 0.836e+06
<Qout> = 0.522e+01 mm/day +- 0.435e-01 Qout = 0.118e+09 +- 0.987e+06

<Qnet> = -0.179e+01 mm/day +- 0.571e-01 Qnet = -0.407e+08 +- 0.129e+07

1 na001

Month 11 (nov)

Node K	K+1	Flux, kg m^-1 s^-1 F(x)	F(y)	Scaled inward normal vector, m B(x)	B(y)	Segment flux kg s^-1 Qin	
1	2	0.383e+02	-0.840e+01	0.278e+06	0.000e+00	0.107e+08 +-	0.445e+06
2	3	0.373e+02	-0.596e+01	0.278e+06	0.000e+00	0.104e+08 +-	0.443e+06
3	4	0.391e+02	-0.239e+01	0.278e+06	0.000e+00	0.109e+08 +-	0.451e+06
4	5	0.532e+02	0.510e+01	0.278e+06	0.000e+00	0.148e+08 +-	0.484e+06
5	6	0.731e+02	0.156e+02	0.000e+00	0.469e+06	0.734e+07 +-	0.159e+06
6	7	0.937e+02	0.275e+02	0.000e+00	0.469e+06	0.129e+08 +-	0.183e+06
7	8	0.109e+03	0.342e+02	0.000e+00	0.469e+06	0.160e+08 +-	0.200e+06
8	9	0.110e+03	0.286e+02	0.000e+00	0.469e+06	0.134e+08 +-	0.193e+06
9	10	0.111e+03	0.228e+02	-0.278e+06	0.000e+00	-0.309e+08 +-	0.659e+06
10	11	0.113e+03	0.213e+02	-0.278e+06	0.000e+00	-0.313e+08 +-	0.680e+06
11	12	0.107e+03	0.181e+02	-0.278e+06	0.000e+00	-0.297e+08 +-	0.672e+06
12	13	0.978e+02	0.143e+02	-0.278e+06	0.000e+00	-0.272e+08 +-	0.650e+06
13	14	0.864e+02	0.736e+01	0.000e+00	-0.410e+06	-0.301e+07 +-	0.166e+06
14	15	0.779e+02	-0.320e+00	0.000e+00	-0.410e+06	0.131e+06 +-	0.207e+06
15	16	0.693e+02	-0.673e+01	0.000e+00	-0.410e+06	0.276e+07 +-	0.250e+06
16	17	0.515e+02	-0.982e+01	0.000e+00	-0.410e+06	0.403e+07 +-	0.257e+06

Area = 0.196e+13 m^2

<Qin> = 0.456e+01 mm/day +- 0.471e-01 Qin = 0.103e+09 +- 0.107e+07
<Qout> = 0.538e+01 mm/day +- 0.591e-01 Qout = 0.122e+09 +- 0.134e+07

<Qnet> = -0.830e+00 mm/day +- 0.756e-01 Qnet = -0.188e+08 +- 0.171e+07

1 na001

Month 12 (dec)

Node K	K+1	Flux, kg m^-1 s^-1 F(x)	F(y)	Scaled inward normal vector, m B(x)	B(y)	Segment flux kg s^-1 Qin	
1	2	0.380e+02	-0.449e+01	0.278e+06	0.000e+00	0.106e+08 +-	0.530e+06
2	3	0.378e+02	-0.149e+01	0.278e+06	0.000e+00	0.105e+08 +-	0.542e+06
3	4	0.386e+02	0.215e+01	0.278e+06	0.000e+00	0.107e+08 +-	0.548e+06
4	5	0.520e+02	0.966e+01	0.278e+06	0.000e+00	0.144e+08 +-	0.569e+06
5	6	0.761e+02	0.219e+02	0.000e+00	0.469e+06	0.103e+08 +-	0.193e+06
6	7	0.108e+03	0.450e+02	0.000e+00	0.469e+06	0.211e+08 +-	0.248e+06
7	8	0.136e+03	0.633e+02	0.000e+00	0.469e+06	0.297e+08 +-	0.279e+06
8	9	0.142e+03	0.557e+02	0.000e+00	0.469e+06	0.261e+08 +-	0.244e+06
9	10	0.145e+03	0.425e+02	-0.278e+06	0.000e+00	-0.403e+08 +-	0.807e+06
10	11	0.144e+03	0.342e+02	-0.278e+06	0.000e+00	-0.399e+08 +-	0.876e+06
11	12	0.126e+03	0.246e+02	-0.278e+06	0.000e+00	-0.350e+08 +-	0.886e+06
12	13	0.104e+03	0.160e+02	-0.278e+06	0.000e+00	-0.288e+08 +-	0.836e+06
13	14	0.873e+02	0.874e+01	0.000e+00	-0.410e+06	-0.358e+07 +-	0.127e+06
14	15	0.766e+02	0.261e+01	0.000e+00	-0.410e+06	-0.107e+07 +-	0.144e+06
15	16	0.654e+02	-0.354e+01	0.000e+00	-0.410e+06	0.145e+07 +-	0.172e+06
16	17	0.488e+02	-0.647e+01	0.000e+00	-0.410e+06	0.265e+07 +-	0.177e+06

Area = 0.196e+13 m^2

<Qin> = 0.606e+01 mm/day +- 0.539e-01 Qin = 0.138e+09 +- 0.122e+07
<Qout> = 0.656e+01 mm/day +- 0.756e-01 Qout = 0.149e+09 +- 0.171e+07

<Qnet> = -0.492e+00 mm/day +- 0.929e-01 Qnet = -0.111e+08 +- 0.211e+07